In-Cycle Control of the Thermoforming Reheat Process

by

Ben Moore

Department of Electrical and Computer Engineering

McGill University

A THESIS SUBMITTED TO THE FACULTY OF GRADUATE STUDIES AND RESEARCH IN PARTIAL FULFILLMENT OF THE REQUIREMENTS OF THE DEGREE OF

Masters in Engineering

May 2002

Abstract

In this thesis, the problem of closed loop control during the thermoforming sheet reheat process is considered. The approach aims to improve the material distribution of a formed thermoplastic part via better sheet temperature control prior to forming. Improved control of material distribution will increase part quality and result in fewer part rejects, thereby increasing production efficiency.

A process model consisting of individual components describing sensor, heater, and sheet heating dynamics has been developed. Recommendations for improvements to the process model, particularly for the sheet heating model, are also made. An in-cycle control strategy is proposed and the feasibility of in-cycle sheet reheat temperature control is examined based on simulation results for multivariable H_∞ control is examined based on simulation results for multivariable H_∞ and MPC controller designs.

Résumé

Cette dissertation traite du problème de commande rétroactive du procédé de chauffe d'une feuille de polymère pour le thermoformage. Notre approche a pour but d'améliorer la distribution de matière dans une pièce formée en thermoplastique à l'aide d'une meilleure commande de température de la feuille avant l'opération de formage. Une meilleure distribution de masse sur la pièce finie améliore sa qualité et permet de diminuer le nombre de pièces rejetées, ce qui augmente la productivité.

On développe un modèle du procédé composé de modèles du capteur, du système de chauffage par radiation, et de la dynamique de chauffe de la feuille. On donne des recommandations pour l'amélioration du modèle du procédé, en particulier pour le modèle de température de la feuille. Une stratégie de commande en-cycle est proposée, et la faisabilité d'une commande de température de la feuille est examinée sur la base de résultats de simulation de compensateurs multivariables (H-infinity) et à commande prédictive (MPC).

Contents

List of Tables

List of Figures

List of Symbols

Symbol	Description	Units
T, θ	temperature	K, ^{o}C
T_{emb}	embedded heater temperature	K, ^{o}C
T_{surf}	surface heater temperature	K, ^{o}C
τ	embedded heater model time constant	1/s
Q	heat flow	kJ
A	surface area	m^2
k	thermal conductivity[*]	W/m^{2}K
α	thermal diffusivity	m^2/s
h	convection heat transfer coefficient	W/m^{2}K
h_upper, h_u	convection heat transfer coefficient for upper side of sheet	W/m^{2}K
h_lower, h_l	convection heat transfer coefficient for lower side of sheet	W/m^{2}K
θ_∞	ambient oven air temperature	K, ^{o}C
σ	Stephan-Boltzman constant	W/m^{2}K^4
$Fview$	radiation view factor	-
ε_{eff}	effective emissivity	-
ε_h	heater emissivity	-
ε_s	sheet emissivity	-
q_{rad}	radiation heat flow	kJ
q_{conv}	convection heat flow	kJ
Δh	distance between sheet model nodes	m
L	length of square sheet zone sides	m
V	volume	m^3
$f_{correction}$	radiation correction factor	-
a	constant component of radiation correction factor	-
b	temperature dependent component of radiation correction factor	-
ρ	density	kg/m^3
N	number of nodes/layers	-
ω	frequency	rads/s
Np	length of prediction horizon	-
Nu	length of control horizon	-
$\hat{y}$	predicted sheet temperatures	K, ^{o}C
Δu	control moves (i.e. heater temperatures)	K, ^{o}C
y_m	measured sheet surface temperatures	K, ^{o}C
y_r, y_d	desired sheet surface temperature	K, ^{o}C
f_i	notation used for linearized equations	-

---

[*] unless denoted otherwise

1. Introduction

Thermoforming is a process in which useful tub-shaped plastic parts are manufactured from a flat sheet of plastic material. The thermoforming process is composed of three basic phases: 1) sheet heating, 2) forming, and 3) cooling. In the first stage a flat plastic sheet is heated in an oven until the material is soft and pliable. The sheet is then formed to a mold using pressure and/or vacuum forces in order to achieve the desired part shape. Finally, the formed part is left to cool in the mold until the material solidifies and is rigid enough to be removed from the mold.

This thesis focuses only on the details of the heating stage, which is often referred to as sheet reheat in industry. The goal of the research is to develop a control strategy that is capable of tracking desired sheet temperature profiles throughout the reheat cycle. The sheet temperature is altered by manipulating the temperatures of heating elements within the oven. Proper control of sheet temperature will allow for an overall improvement of the thermoforming process. The specific objectives of a control system for thermoforming reheat are defined by considering the motivations for process improvement. The most basic motivation is improved part quality. Higher quality parts can be achieved through better control of material distribution before the actual forming of the sheet via close control of sheet temperature distribution. Close temperature control and disturbance rejection will also result in a reduction in the number of rejected parts for a given production cycle. As a result, production efficiency will increase and material costs can significantly decrease. This is particularly important for producers of products manufactured from very expensive plastic materials.

Production efficiency can also be improved by decreasing the time it takes to make each individual part. Control during sheet reheat will allow for more aggressive sheet temperature trajectories, and thus shorter heating times for some thermoforming operations. In other words, control during the reheat stage can lead to an increase in production rates.

It is also possible for reheat temperature control to result in a decrease in energy consumption by generating optimal (in terms of energy) control signals that will achieve the desired sheet temperature profile. This should be a significant motivation for the

application of sheet reheat control since thermoforming is generally an energy intensive process. Energy, or heating, costs are often the most significant operating expenses for a thermoforming operation.

Finally, control of sheet reheat can potentially result in reduced machine maintenance. As the oven heating elements age, their performance can deteriorate. Also, individual heating elements can deteriorate at different rates. This results in non-uniform sheet heating which can subsequently affect part quality. A control system can effectively extend the life of heating elements by compensating for uneven sheet heating. The end result is an increase in production efficiency over time.

There are two opportunities to take corrective control action for the thermoforming reheat process: in-cycle, and cycle-to-cycle. A cycle-to-cycle control strategy involves updating heater temperature settings at the end of each reheat cycle such that the next part that is made is improved in some sense. The role of cycle-to-cycle control is to iteratively improve part quality via better sheet temperature distribution and to correct for gradual drift of machine operating parameters. An in-cycle control strategy involves manipulating heater temperatures during the actual heating of the sheet. The role of in-cycle control is to provide corrective action for the purposes of reference trajectory tracking and short-term disturbance rejection.

The in-cycle control problem is the subject of this thesis. Although it appears to be quite a simple process, in-cycle sheet temperature control of the thermoforming reheat process is a very challenging control problem in which a number of factors contribute to the overall difficulty of the problem. First, the thermoforming reheat process is highly nonlinear and time-varying. Second, thermoforming reheat is a distributed parameter system governed by a set of partial differential equations, not ordinary differential equations. Control during sheet reheat is also complicated by the fact that there is a high level of uncertainty surrounding the process, particularly with the material properties. The fact that this is a multi-input, multi-output (MIMO) problem with a high degree of coupling between inputs and outputs also introduces additional complexity. Finally, there are a number of hard constraints that must be taken into consideration such as maximum allowable sheet and heater temperatures.

Another factor that contributes to the overall difficulty in developing an effective in-cycle control strategy for the thermoforming reheat process is the overwhelming lack of information on closed-loop control of thermoforming available in the literature. In fact, not a single article specifically addressing in-cycle control of thermoforming reheat could be found; however, one paper by Michaeli and van Marwick, [16], was found. They proposed ideas for a closed-loop cycle-to-cycle control strategy as well as techniques for online measurement of part wall thickness.

The fact that there has been very little work done on the in-cycle control of the thermoforming reheat process is a direct result of the historical conservative nature of the thermoforming industry. In comparison, much more work on process modeling and control has been done for blow molding, and in particular, injection molding. Simulation software has long been used to improve and speed up the development of injection molded parts. Advanced model based control techniques, such as the work done by Dubay in [17], have also been used to improve the injection molding process. In a similar work, DiRaddo and Garcia-Rejon, [25], demonstrate the effectiveness of in-cycle control of extrusion blow molding.

The thermoforming industry is, however, catching up. Although the application of closed-loop control is not yet established, the use of thermoforming simulation software during product design is increasing. A number of simulation packages are now commercially available. T-Sim from Accuform is recognized as one of the first simulation packages available to thermoformers. C-Mold, which offers the popular Moldflow injection molding simulation software, also has a thermoforming simulation package. Other simulation packages are offered by Fluent Inc. and ESI Group. Sherwood Technologies is in the process of developing Java based programs for the simulation of sheet heating and cooling only. Finally, IMI's FormSim software package allows users to simulate the various stages of the thermoforming process.

As the demand for thermoforming simulation software increases, so too will the demand for increased accuracy of the simulated predictions. The work of Yousefi *et al.* in [15] addresses the issues related to the improvement of sheet temperature prediction during the sheet reheat stage. The approach aims to improve the quality of predictions through more accurate evaluation of simulation input parameters. Results indicate that

3

prediction accuracy can be greatly improved by using more accurate[1], and in some cases, time-varying model parameters. Continued improvements in thermoforming simulation modeling will only help to increase the effectiveness of future closed-loop control strategies that may be applied to improve the thermoforming process. Modeling improvements will also improve the effectiveness of open-loop control strategies such as the strategy presented in [24] by Alaeddine and Doumanidis, which involves the solution of the inverse heat conduction problem.

Fortunately, the application of advanced model based control strategies to similar thermal processes are quite well documented in the literature, and the information that is available can be adapted to the thermoforming reheat process.

The manufacturing of advanced engineering materials through the used of multi-zone furnaces is one such similar process. In [11], Gopinathan *et al.* discuss the modeling and control of hot isostatic pressing (HIP) furnaces used for the processing of advanced aerospace materials. The authors demonstrate the effectiveness of a fault tolerant model predictive control (MPC) design and stress its superiority over existing PID control of HIP furnaces. A projective control design for a multi-zone crystal growth furnace was developed by Srinivasan *et al.* in [21]. The projective controller has a structure similar to a MIMO proportional-plus-integral controller, and it exhibits reasonable transient behavior and good steady state error performance. The authors indicate that the projective control approach is particularly appealing for furnaces having a large number of heating zones because the projective control approach allows for the systematic increase in controller order until the desired performance criteria are satisfied, thus yielding a satisfactory controller of minimal complexity.

Rapid thermal processing (RTP) of semiconductor materials is another thermal process that is very similar to thermoforming reheat. RTP involves the heating of semiconductor wafers via high temperature radiation heating lamps. Strict wafer temperature control is the determining factor in achieving desired material properties. A significant amount of work has been done on the modeling and control of RTP systems.

---

[1] More accurate model parameters were determined via a series of identification experiments.

Cho and Kailath, in [14], compare black box and first principles modeling approaches for RTP systems. In [23], Lee *et al.* propose a robust controller design for an RTP system using the structured uncertainty approach. A model based feed-forward, feedback controller structure with gain scheduling is presented in [13] by Park *et al.* Similarly, Kamali and Kosut, in [19], present a time-varying feed-forward, feedback control design. The authors state that due to the time-varying nature of the linearized model around a reference trajectory, a time-varying LQR design is superior to controller designs with constant parameters. It is important to mention, however, that the performance of this design was evaluated based on single-input, single-output (SISO) simulations. The development of a time-varying MIMO controller is a much more difficult problem.

MPC designs have also been proposed for RTP systems. In [20], Dekeyser and Donald III document the successful application of an MPC design to an actual RTP system. The model used for the prediction of wafer temperatures consisted of a number of locally linearized models that describe the RTP reactor over its entire operating range. A fuzzy logic based combination of the individual linear model outputs led to the actual nonlinear model output used in the prediction strategy.

In [12], Schaper *et al.* used a multivariable internal model control (IMC) approach to improve the uniformity and repeatability of wafer temperatures in RTP systems. The authors also address a number of practical controller implementation issues. Their goal was to design a generalized control strategy that could be applied to any RTP machinery, and therefore, allow for flexible manufacturing.

It was mentioned earlier that efforts are being made to improve the accuracy of thermoforming simulation predictions. Even with accurate predictions, complex simulation software has the drawback of being just that, complex. The software uses large time dependant and often three-dimensional finite element models for the prediction of sheet temperatures. Even when run on high performance computers, simulations can take hours, even days, to execute. Regardless of accuracy, this makes these large finite element models virtually useless for real-time applications. A great deal of research work has been done recently on the reduction of large simulation models. It is worthwhile to

briefly discuss the details of one of the more popular model reduction techniques as well as potential uses for reduced order models.

Banerjee *et al.*, in [18], discuss the proper orthogonal decomposition (POD) model reduction approach for RTP systems. The modeling equations are solved by the Galerkin finite element method, which approximates the temperature fields by using expansions in piecewise, low order polynomials. This approach has the advantage of being general and flexible, but the large number of coefficients required leads to large nonlinear matrix problems. The number of coefficients could be reduced, in principle, if the approximating functions were similar in form to the actual solution. One approach for obtaining better approximating functions is the POD method, which involves obtaining empirical eigenfunctions from experimental data or detailed model predictions of temperature fields, or snapshots, for the entire RTP reactor at discrete time intervals. The eigenfunctions then form an optimal basis set for the given series of snapshots. The eigenfunctions can be viewed as a set of ideal fitting functions. The actual model reduction is achieved by considering only a few dominant eigenfunctions that describe most of the temperature field data.

The result is a nonlinear, low order model that is obtained without approximating the physical equations that govern the process. These equations are therefore more accurate over a wider range of conditions as compared to conventional reduced order, linearized models. An order of magnitude reduction in simulation execution time was achieved with the reduced order model as compared to the full order finite element RTP model. The authors suggest that a well designed reduced order model could help in cutting down the number of experiments required in designing a process recipe and thus reduce the transition time in bringing a process from the research to the manufacturing stage. It is also suggested that a reduced order POD model could be used in real-time, advanced model based control strategies. A reduced order POD model could potentially be obtained from thermoforming simulation software and used to predict sheet temperatures in an MPC controller design.

A brief description of thermoforming, as well as a problem definition, was given in this section. A summary of relevant work in the literature was also presented. A more

detailed description of the thermoforming process is given in Section 2. Section 3 details the development of the process models used for controller design. The controller design and simulation results are given in Section 4. A summary and conclusion are given in Section 5.

2. Process Description

2.1 Introduction and Historical Review

Thermoforming is a generic term used to categorize the many different techniques for producing useful articles from a flat thermoplastic sheet. The name thermoforming suggests the application of heat. Although this is generally true, there are specialized forming techniques that do not require heat; however, for simplicity, the application of heat will be assumed throughout the remainder of this discussion. The idea behind the thermoforming process is not new. Even early man used heat to shape various organic materials into useful tools. Nevertheless, the real roots of thermoforming came with the development of synthetic rubber during WWII. Various thermoplastic materials soon followed and subsequently the thermoforming industry was born. The commercial success of thermoforming began in the late 1940's and early 50's with the development of the packaging industry. By the 60's blister packaging developed into a high volume market. The 60's also saw new advancements and trends in the industry as well as the establishment of separate thin and thick sheet sectors. During this time resin manufactures became more involved and offered technical support and expert knowledge of material properties to thermoformers. By the 70's thermoforming machine manufacturers also began to support the advancement of thermoforming technology. Demand had risen significantly in a few short years, which prompted machine manufacturers to develop high output equipment. As the production volume increased in many thermoforming operations, the desire to cut costs prompted machine manufacturers to make advancements in production and quality controls which led to more automated operations. The desire to stay competitive and decrease costs also prompted improvements in scrap handling. Minimization of material costs and recycling suddenly became important issues. The 80's saw an even greater demand for more cost effective, automated operations. This led to further advancements in thermoforming technology and allowed thermoformers to introduce new product lines that were previously not possible. The 80's also saw the introduction of new pellet-to-product equipment as well as major advancements in process controls. The advancement of thermoforming

technology has not been continuous however. The industry saw a significant slowdown in the early 90's as a result of the economic slowdown in North America as well as the repercussions of rising environmental concerns, which led to many fast food organizations discontinuing the use of certain types of takeout food containers. As a result, some product lines were discontinued and many thermoforming operations were left idle and a good number had to shut down completely.

Today, the thermoforming industry is seeing growth once again. The relatively low capital costs associated with the thermoforming process has spurred interest in the possibility that advances in technology may allow new thermoforming techniques to produce many common parts traditionally manufactured by other more expensive processes.

Although many advancements have been made since thermoforming's early years, the industry, as a whole, has been relatively conservative in terms of the application of new technologies when compared to other polymer processing industries. For example, the injection molding industry has long used established FEM simulation software in the design and production of new parts. Because thermoforming is still considered to be a process of high craftsmanship and experience, it is regarded as the polymer processing area with the highest growth potential. Advances in materials and process controls (specifically for sheet heating) will allow more complex parts to be made. For example, twin-sheet thermoforming is now becoming the process of choice for manufacturing gas tanks that meet the strict Partial Zero Emissions Vehicle (PZEV) mandates that have been introduced recently in California. Also, it has been suggested that the forming of very strong, lightweight foamed material will continue to increase. As was the case with injection molding, thermoforming will likely see more automation and shorter product development times with the aid of various CAE tools. As heating costs continue to rise it is reasonable to believe that strides will be taken towards improved, energy efficient thermoforming processing. Similarly, rises in material costs will see a continued effort to reduce the amount of waste associated with thermoforming. No one can say for certain exactly where the thermoforming industry will be 10 years from now; however, one can be confident in saying that the future definitely looks quite

promising. The timeline shown in figure 2.1 summarizes the historical progression of the thermoforming industry.
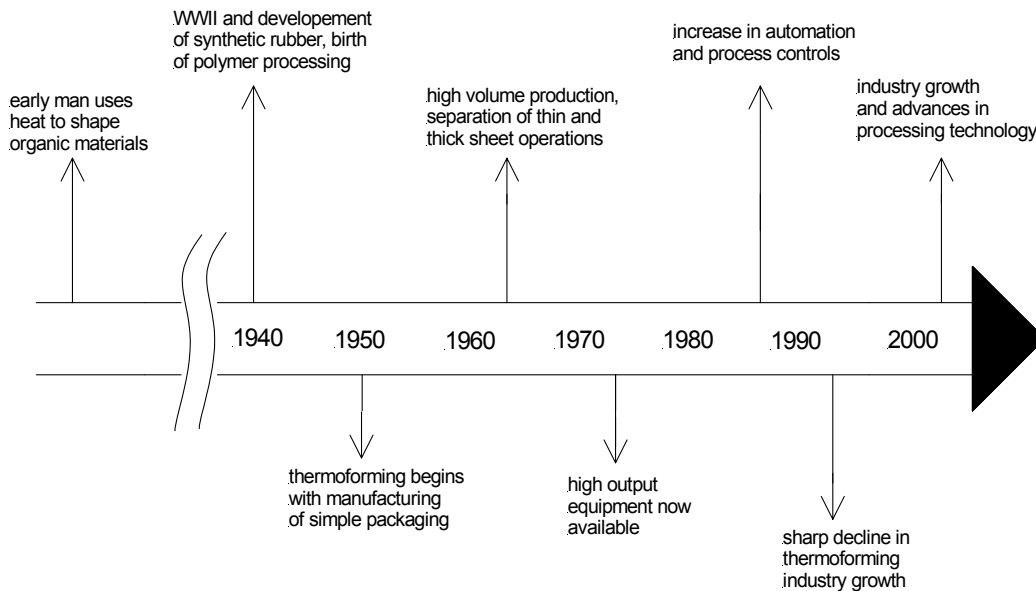
Figure 2.1: historical timeline of thermoforming industry

2.1.1 Advantages and Disadvantages

While introducing a new manufacturing process it is useful to note the advantages and disadvantages as compared to competing processes. Obviously some products can only be produced by one particular method but there are many products in the polymer processing industry that can be manufactured by a number of different processes. Thermoforming has a number of competitive advantages. Most importantly, the tooling and equipment costs are quite low when compared to other processes. In particular, the molds used for thermoforming are relatively simple, and therefore, they are not overly expensive. Another advantage is that thermoforming can handle multi-layered materials, foams, printed, and coated materials which can reduce the amount of post-forming processing time. Finally, thermoforming can allow for the production of much larger parts than for many other processes. Thermoforming also has distinct disadvantages. Primarily, the complexity of a thermoformed part is limited. Second, the thermoforming process is a high waste process, which means higher material costs. Fortunately, some, but not all, of the waste can be recycled. Finally, another one of the major drawbacks is

the fact that only certain materials can be used with the thermoforming process. This last point will be elaborated on in the discussions to follow.

2.1.2 Parts Made by Thermoforming

Early on, the thermoforming industry was dominated by the production of very simple tub-shaped parts for the packaging industry. Today, numerous different parts of varying complexity are produced using thermoforming techniques.   Many thermoformed parts that are in use today have been made to replace earlier forms of the same products that were made from different materials. Usually, plastic is much more durable, or it has other desirable material characteristics (i.e. thermal, electrical, chemical, etc.) The table shown below highlights the diversity of today's thermoforming industry. Examples of thermoformed products categorized by industry or sector have been given as a general reference.

Table 2.1: *list of products made by thermoforming*

Industry	Products and Comments
packaging	- for use with retail products including food items - highest volume of thermoformed parts - blister packs are most popular - includes product display units
fast food	- still uses many thermoformed containers although decomposable cardboard containers are becoming more widely used
automotive and transportation	- both interior and exterior parts used - roof liners, door panels, dashboards, trunk liners, floor covers, pickup truck bed liners - bus and train seats - aircraft seat backing, armrests, fold-down trays, many other interior airplane components
sings	- large pieces of acrylic used to make sturdy one-piece signs with raised lettering
home appliances	- refrigerator interior linings, refrigerator door liners - dishwasher linings, clothes dryer linings, home air-conditioner components, personal computer casings, radio and television cabinets and components
institutional food services	- food serving trays and disposable dishes
medical	- various types of medical equipment and tools are stored in sterile disposable containers - use of recycled materials not acceptable because integrity of packaging very important - surgical tables, dental chairs

horticulture	- trays for seedlings
recreational products	- small fishing boat hulls, canoes, sailboats, paddle boats - windshields for boats, snowmobiles, motorcycles, etc. - children's pools
housing and construction	- skylights - bathtubs, shower enclosures - garage door face panels
luggage	- suitcase and briefcase bodies and linings
photography	- developing trays
food processing	- tubs and vats for storage and processing
funeral	- casket liners and components
shipping	- more durable plastic pallets are quickly replacing their wooden counterparts
miscellaneous	- dunnage containers, gas tanks, light fixtures, amusement park rides

2.2 Physical Description of the Process

As mentioned earlier, a good understanding of the process at hand is a prerequisite for successful control design. Thorough process knowledge can prevent inappropriate designs and nearly always result in shorter design time. For this reason, the process is described here in a fair amount of detail. When viewed from a distance, thermoforming appears to be a simple, almost primitive process. In general, five basic steps are involved: *clamping, heating, forming, cooling,* and *trimming*. Actually, clamping cannot be considered as an individual step. It simply refers to the mechanism used to secure the sheet during heating, forming, and cooling. The heating stage involves heating the sheet in an oven to a specified temperature known as the forming temperature. Once the sheet is heated it is then formed to a mold using pressure and\or vacuum forces. Next, the formed sheet is left to cool until it is rigid enough to be removed from the mold. The formed sheet is then transferred to a trimming station for the removal of any excess material.

There is, however, more than meets the eye when considering the details of thermoforming. The discussions to follow will elaborate on the basic steps mentioned above. Section 2.2.1 will describe the key components of the thermoforming process. Section 2.2.2 will introduce some of the different types of thermoforming machines that are used and section 2.2.3 will evaluate, in more detail, each of the thermoforming steps.

2.2.1 Components of Thermoforming

2.2.1.1 Sheets

The thermoplastic sheet is the most important component of the entire thermoforming process. Its role is obvious. Upon forming, the sheet is transformed into a useful article. The molecular composition of the sheet is a determining factor in both the processing steps and final part quality. The name, "poly-mer" indicates that sheets are composed of many (poly) interconnected units (mer) that form carbon-hydrogen chain structures. The length and entanglement of these chains are key factors in the thermoforming process. Long molecular chains will have large molecular weights, and will therefore be stronger than polymers consisting of short molecular chains, which tend to be more brittle. In fact, one of the most basic requirements of a formable thermoplastic sheet is that it has a high melt strength (high molecular weight), which means that upon softening, the material is capable of supporting its own weight. In contrast, a material with a low melt strength (low molecular weight) will soften once the glass transition temperature is reached and easily tear away from the clamping mechanism as the sheet succumbs to gravity.

Thermoplastic materials can be either amorphous or partially crystalline. As with molecular weight, the degree of crystalinity is a determining factor in the thermoforming process. Generally, a material with a higher degree of crystallinity requires a higher forming temperature than for an amorphous thermoplastic. On the other hand, amorphous materials are usually crystal clear which can be an important issue depending on the heating mechanism used. The last point will become clear later on in the discussion.

Now that we know material properties are key factors in the thermoforming process, it is useful to briefly discuss how the various sheet manufacturing methods can affect some material properties. Thermoplastic resins, which are primarily derived from crude oil, coal, and natural gas, are manufactured into pellet form. Thermoplastic sheets are then manufactured from these small pellets. There are a number of different ways in which sheets can be produced, however, three methods dominate.

1. Calendaring

Calendaring is a similar method to paper making. First, the small pellets are fed into large feed rolls. The pellets are then melted and forced into sheet form as the material passes through subsequent sets of rollers. This method of sheet manufacturing generates no molecular orientation in the sheet, which results in slightly weaker sheets that will be subject to increase sagging during the heating process. Calendaring is also subject to the problem of pinholes, which are tiny voids in the sheet caused by an insufficient supply of feed pellets. Pinholes allow air to escape through he sheet, which complicates the forming and can sometimes render a sheet useless. Fortunately, newer manufacturing equipment has reduced the occurrence of pinholes. Nevertheless, it is still a problem that can surface from time to time.

2. Casting

Casting involves pouring a liquid plastic into a mold and then letting the material cool and harden to form a solid plastic sheet. For some materials casting is the only method suitable for the production of sheet forms of the material. As with calendaring, casting does not result in any molecular orientation. Sheets made by the casting method are typically free of pinholes. They also have no hidden residual strains and have equal strength in all directions. The casting method can produce tiny bubbles of trapped air within the sheet. This can sometimes affect further sheet processing as well as the appearance of sheets that are designed to be completely transparent.

3. Extruding

Extruding is the most popular method for manufacturing thermoplastic sheets. The pellets enter the extruder barrel through a feed hopper. The pellets melt and the liquid material is then squeezed through a die into sheet form. The sheet is then pressed through a series of rollers that are spaced to give the sheet its proper thickness. Unlike the previous two methods, extrusion results in a sheet that can contain biaxial orientations as a result of extrusion through the die and stretching between the rollers. This orientation results in a stronger sheet that is more resistant to sag during heating.

Sheet Sizes and Materials

Each of the three sheet producing methods is capable of producing a wide range of sheet sizes. As calendaring and extrusion operations produce wound rolls of thermoplastic materials, the sheet thickness for these operations is limited. Casting on the other hand can produce much thicker sheets. Generally sheet thickness can range from 0.05 mm to 15 mm and up to 60 mm for some foams. Sheet sizes for thermoforming operations range from small sheets ($< 30 \text{ cm}^2$) to sheet sizes in the range of 3 m x 3 m and larger. It is important to note that part sizes and thus sheet sizes are only limited by the size of the machine, keeping in mind that the larger the part, the greater the forming force that is required.

There are now many different types of materials that are used with thermoforming. All materials possess their own distinctive qualities and behave differently throughout the thermoforming process. The selection of thermoformable materials is now so varied that the choice of part material has become one of the most important thermoforming design steps. Some of the more common materials include: Polystyrene (PS), Toughened Polystyrene (HIPS), Acrylonitrile-Butadiene-Styrene (ABS), Low and High Density Polyethylene (LDPE and HDPE), Polypropylene (PP), and Polyvinylchloride (PVC). A more detailed list of thermoforming materials including material properties can be found in [2].

Material Properties and How They Relate to Thermoforming

As previously mentioned, material properties can have a direct effect on part formability as well as final part quality. Some of the more important properties and their effects will be identified in this section.

1. Moisture Absorption

Some thermoplastic materials are hydroscopic (ie. they have the ability to absorb moisture). Moisture is predominantly retained on the sheet surface, and when a damp material is heated, small bubbles will form on the sheet surface. At the very least, retained moisture will affect heating times. In more severe cases moisture can damage the appearance of the part or even affect the structural properties of the part. In these

cases the part is often rejected. It is easy to see why some thermoforming operations include sheet drying as an important pre-processing step.

2. Frictional Behavior

The frictional properties of a sheet are normally only a concern when using plug-assist techniques to further stretch certain areas of the sheet. The frictional behavior depends on the sheet and tool (i.e. the plug) material and surface finish. If there is insufficient friction the tool will tend to want to push directly through the sheet, which will result in an uneven part wall thickness distribution. Conversely, too much friction will cause the sheet to stick to the tool upon contact, which will also result in uneven thickness distribution. It is very tricky to obtain the proper amount of frictional forces. Slight changes to the tooling surface as well as the tooling and sheet temperatures are required to obtain the desired results.

3. Shrinkage

Shrinkage of polymer materials is an important issue in all polymer processing operations. Shrinkage, and particularly warpage, is important because the integrity of the part is directly affected (i.e. strict repeatable part dimension tolerances are desirable). In severe cases, parts can be rejected due to shrinkage and warpage. In thermoforming, shrinkage can affect the performance of downstream processes such as trimming operations. Some degree of shrinkage is generally unavoidable in polymer processing operations and it is considered in the part design.

4. Orientations

As mentioned earlier molecular orientation affects the strength of a material. The level of orientation is determined by the material, and the way in which it was produced. If a material is stretched in one direction the material generally becomes stronger in that direction and weaker in the opposite direction. Material strength not only comes into play during heating (i.e. resistance to sag), it also is important for the final formed part. The forming process stretches the material and this causes a further degree of orientation

which will affect the strength of the final part. All of this must be considered in the overall part design.

5. Static Charging

Except for electrically conductive materials, thermoplastic sheets become electrostaticly charged during material handling and processing. As a consequence, small particles such as plastic saw chips can become attached to the surface and subsequently embed themselves into the surface during forming resulting in parts of lower aesthetic quality. Care must therefore be taken to ensure a clean production environment.

Thermoformable Materials and Types of Thermoplastic Sheets

As mentioned before, one of the advantages of thermoforming is that a number of different types of sheets can be used. Table 2.2 lists types of thermoplastic sheets that are available.

Table 2.2: *types of thermoplastic sheets used for thermoforming*

Sheet Type	Comments
Natural	- made from resins without fillers of additives - usually crystal clear - can transmit infrared heat energy
Oriented	- very sensitive to heat as loss of orientation is very close to softening temperature - requires precise and fast heating
Tinted	- sheets with dye additives - sometimes slight improvement in heat absorption
Pigmented	- uniform colored sheets
Filed	- additives added to sheet for purposes of reduced cost or an improvements in physical characteristics
Foamed	- much lighter material - when colored foams are desired only light colors are possible
Textured	- sheets with patterns imprinted by textured rollers
laminated	- multi-layered sheets usually for economic reasons
co-extruded	- multi-layered sheets - usually fast and easy to manufacture
printed	- sheets with pre-printed text or images
flocked	- sheets with soft velvet like finish on one side
metallic	- sheets with metallic coatings can be made but these are not popular
specialty	- many other kinds of specialty sheets are possible

2.2.1.2 Clamping Mechanisms

The clamping mechanism provides the following functions: 1) support of the sheet during sheet heating; 2) transporting heated sheet to forming area; 3) firmly holds sheet during forming and cooling; 4) implementation of part removal; 5) transfer from forming to trimming stations. There are two basic types of clamping mechanisms: 1) clamp frame, and 2) transport chain mechanisms.

The clamp frame is capable of handling a single sheet at a time. The sheet is clamped between two matching frames. One frame is usually stationary (lower) while the other frame (upper) is hinged to allow insertion of the sheet. The frame can be operated manually or automatically for more sophisticated higher volume machines. One important consideration is the grip the frame has on the sheet. It is vital that the sheet does not slip during heating or forming. Often matching grooves and even pins are required to hold the sheet in place.

The other type of clamping mechanism is the transport chain, which is used for continuously fed machines (see section 2.2.2). The transport chains function as the two parallel sides of a clamp frame and carry the sheet through the oven and then on to the forming station. Again it is important that the sheet be properly secured with the use of high pressure forces and sometimes pins as well.

One important consideration for both types of clamping setups is the heating of the clamping mechanism. In operations where production rates are high, clamping mechanisms will repeatedly enter the oven and eventually heat up over time. If this heating is significant, sheet heating will be affected as the heat from the clamping mechanisms will be transferred to the sheet. Also, care must be taken to ensure that the heat build up is not excessive as the clamping mechanism may actually melt the plastic sheet. Excessive heating can sometimes be avoided in radiation heating ovens by applying reflective paint to the clamping components.

2.2.1.3 Heating Systems

The heating system is a key element of the thermoforming process. Regardless of the heat source, the application of heat must be relatively precise and repeatable in order to have predictable cycle-to-cycle results. The heating system is also a key factor when

examining the economics of a thermoforming operation because thermoforming is an energy intensive process and heating of the sheet accounts for up to 80% of the energy consumption. Two basic energy sources are available for sheet heating: gas and electricity. Gas is much less expensive than electricity but the latter offers much better temperature control. Although there is a wide variety of specific heating methods and heater types available, there are only three basic heating methods applied to thermoforming.

The first is gas fired convection ovens. These ovens are usually very large to accommodate the heating of large, extra thick sheets. Cycle times for these larger sheets tend to be measured in hours as opposed to seconds; therefore, it is obvious that electrical heating is not economically feasible. The sheet itself is actually heated by hot air that is forced over the sheet surfaces by large blowers. Although these gas fired ovens offer less controllable heating, the size and bulk of these larger sheets does not warrant such close temperature control.

The second method is contact heating. This setup consists of heated metal plates that directly contact the sheet to heat it. The metal plates can be heated by either a gas flame or by electrical strip heaters either embedded or mounted to the opposite surface of the plate. In this type of heating it is important to ensure proper contact with the sheet. Uneven contact can trap air between the plate and the sheet and cause uneven heating. This method is limited to uniform heating (no zoning) of thinner thermoplastic sheets. Because this method of heating is quite slow, the sheet is sometimes preheated with other heating methods to increase production speed.

The final method of heating is radiant heating. Radiant heating methods are definitely the most popular because of their controllability and efficiency. No contact is needed in this method. The sheet surface absorbs infrared energy from the heaters, and heat is then conducted from the sheet surfaces to the interior of the sheet. Gas fired radiant heaters are sometimes used but electrical radiant heaters are much more common. Electrical radiant heaters can operate over a very wide temperature range; however, the best electrical to radiation conversion efficiency occurs when the heaters operate at temperatures that produce infrared energy concentrated at wavelengths of between 3 to 3.5 μm. More will be said later about the infrared spectrum. Since electrical heaters are

the most widely used a list of the different types and their properties has been assembled in table 2.3 below.

Table 2.3: electrical radiant heater types

Heater Type	Comments
tubular or rod	- similar to heating elements found in electric ovens and stove top burners - low cost - very uneven temperature distribution - requires reflectors since energy is radiated in all directions
flat strip	- similar to rod heaters but formed into a flat strip - can be placed in many different patterns - inefficient due to lost heating through backing
ceramic	- consists of wound element wires embedded in ceramic material - very popular - more expensive but good temperature control - even surface temperatures - periodic cleaning required - slow dynamics
Pyrex	- electro-conductive film backing covered by Pyrex glass - usually come in panel form - highly efficient source - provides uniform heat over entire surface - slow dynamics and very fragile
quartz	- consists of conductive element covered with quartz - can be in tubular or flat panel form - very fast dynamics as quartz easily transmits infrared energy - requires reflectors but can be built in
flat panel	- flat panel heaters with many different coverings are available - even surface temperatures
heat lamp	- seldom used for thermoforming applications

2.2.1.4 Process Controls

It was mentioned in the historical review of thermoforming that there have been great advances in thermoforming process controls over the years. Today, process controls should be considered as a key component of the thermoforming process. This is true, however, it is important to differentiate between automation related controls (i.e.

material handling, cycle timers, heater controls, etc.) and feedback control of process parameters. The improvements have been with machine automation whereas the application of feedback control, such as control of sheet temperature, has been virtually nonexistent.

Feedback control of the heater settings is nearly universal on modern machines so it is worth mentioning here. There are basically two types of temperature controllers available. The first type uses switched, or on-off control, to regulate the heater temperatures. In this type of control, full power is intermittently sent to the heaters. The second type of control is slightly more sophisticated. It uses power electronic devices to supply varying power levels to the heaters in order to maintain the setpoint. Both types of control result in oscillations about the setpoint with the on-off control oscillations being more prominent. Oscillations are rarely a problem, however, when heaters have a relatively high thermal mass. This is the case with the popular ceramic heater, which is designed to maintain a constant surface temperature without responding to small power fluctuations. Machine automation procedures and equipment vary extensively. Because there are so many different types of machines available a full discussion of machine automation is beyond the scope of this work.

2.2.1.5 Molds

Occasionally molds are not required to form a sheet, as is the case with "free-blow" forming methods used to make skylight windows for homes. The vast majority of forming operations do require molds for shaping the plastic sheet. The primary purpose of the mold then is to transform its shape to the heated, flat plastic sheet. The sheet is either forced into or drawn over a mold. Three different types of molds exist. All have different qualities and will leave distinctive characteristics implanted into the formed part. All three molds can be found in single or multi-up forms. A single mold uses a single sheet to form one individual part. A multi-up mold forms an array of multiple parts from the same plastic sheet. A number of considerations are important for all mold types. For example, part shrinkage considerations and mold venting are important design issues. Mold material is also an issue that requires some thought. Thermoforming molds are usually made from aluminum. Epoxy materials are sometimes used, and even wood

can be used to construct a mold. The mold material is generally dictated by the intended use and life expectancy of the mold.

Female molds

For the female mold shown in figure 2.2a the heated sheet is drawn into the mold cavity by either pressure or vacuum forces, or a combination of both. A female mold results in less characteristic evidence of the mold on the part, which means that female molds are often not used where intricate details are required on the part surface. Since the part will shrink during cooling the part will actually begin to pull away from the mold walls which results in easy part removal. As can be seen in figure 2.2b, most of the stretching occurs at the bottom of the sheet whereas the flange areas remain close to the original part thickness. This suggests that even material distribution before forming does not result in a part with even wall thickness.
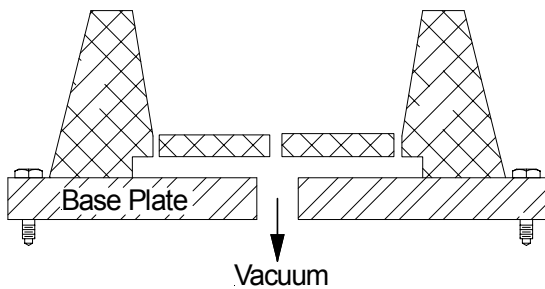
Figure 2.2a: *basic female mold*

Figure 2.2b: *material distribution for female molded part*

Male Molds

The male mold is basically an inverse form of the female mold. An operation that uses a male mold is often referred to as drape molding. Indeed, this is an accurate description as the forming is performed by draping the sheet over the mold, and then drawing it tight with vacuum and/or pressure forces. The male mold results in a complete reversal from the female case in terms of material distribution. The top of the part contacts the mold first; therefore, it cools first and stretches less. One advantage of the male mold is that it is much less expensive to manufacture than the female mold. The male mold also has disadvantages. For starters, part removal becomes much more of an issue with male molds because shrinkage causes the part to wrap around and "grip" the

mold. Pressurized air is often used for part removal. Another disadvantage is that it is much more difficult to implement multi-up molds. Spacing is more critical than with female molds since the majority of the stretching and material thinning will take place between the molds and not over the mold area. Figure 2.3a shows a basic male mold.
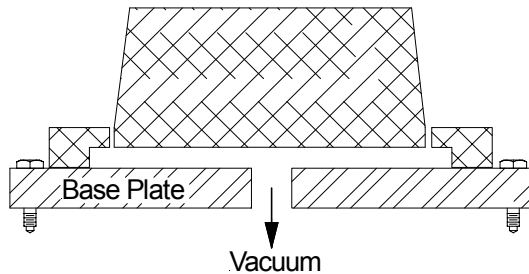
Figure 2.3a: basic male mold

Figure 2.3b: material distribution for male molded part

Matched Molds

In its purest form matched molding sees a sheet being mechanically forced into a female mold by a matching male mold. Variations also exist where air pressure and/or vacuum forces are also used. Mold alignment is a very important issue in matched molding. Small misalignment will result in rejected parts. On advantage of matched molds is that it is possible to get different surface features on opposite sides of the part.

Mold Temperature

The second, and equally important, function of the mold is to absorb heat from the sheet. For high volume productions a mold will heat up to a point where its temperature will match that of the sheet; therefore, some form of auxiliary cooling is generally required. Thermoforming molds can be cooled simply by airflow over their surfaces or internal liquid cooling channels. The mold must not be cooled so much as to cause poor forming detail or possibly uneven stretching of the sheet. Some operations do not require mold cooling as enough heat is dissipated to the ambient environment. Some low volume productions actually require auxiliary mold heating because some thermoplastic materials require elevated mold temperatures for proper forming. Mold heating can be achieved via electrical heating or circulation of heated fluids (usually water or oil) through the

interior of the mold. Proper mold temperatures are critical for the production of a successful part. Sheet manufacturers usually give an ideal mold temperature range but there is always a certain level of fine-tuning involved.

2.2.2 Thermoforming Machines

Thermoforming machines come in a wide variety of shapes and sizes. Machines are often specially designed for the purpose of making a particular part. Some machines can be considered to be more general purpose but these machines often lack the high-speed production capabilities of their specialized cousins. Much could be said about the many thermoforming machine variants but is does not really add to this discussion. Only the basics will be discussed in the remainder of this section.

Thermoforming machines come in two basic types: sheet fed and roll fed. Both types can have varying levels of sophistication and automation. A wide range of sizes are also available for both types. The size of a machine is generally measured by the mold size that can be accommodated and the amount of forming force that is available.

2.2.2.1 Sheet Fed

The sheet fed machine can generally accommodate only one sheet at a time except for twin sheet thermoforming machines which process two sheets simultaneously. The simplest sheet fed machine is the stationary machine, where the sheet is heated and formed in the same location. Shuttle thermoforming machines such as the one shown in figure 2.4 are more common. The basic feature of the shuttle machine is that the clamped sheet is shuttled in and out of the sheet heating area. A number of variations can be found but the basic operating principle remains the same. One variation that is worth mentioning is the rotary shuttle thermoforming machine. For this machine the sheet is still shuttled from station to station but the stations are arranged in a compact circular arrangement, which improves speed and efficiency.

2.2.2.2 Roll Fed

Roll fed machines are high volume, in-line machines that draw the thermoplastic material from large rolls at the end of the machine. The process is much more efficient since it is not necessary to continuously load and unload material in and out of the machine. It is important to note that roll fed machines can only work with thin gauge materials since it is not possible to wind thicker materials into roll form. Variations of the roll fed machine include in-line trimming machines and even in-line sheet production equipment giving complete, pellet-to-product operations.
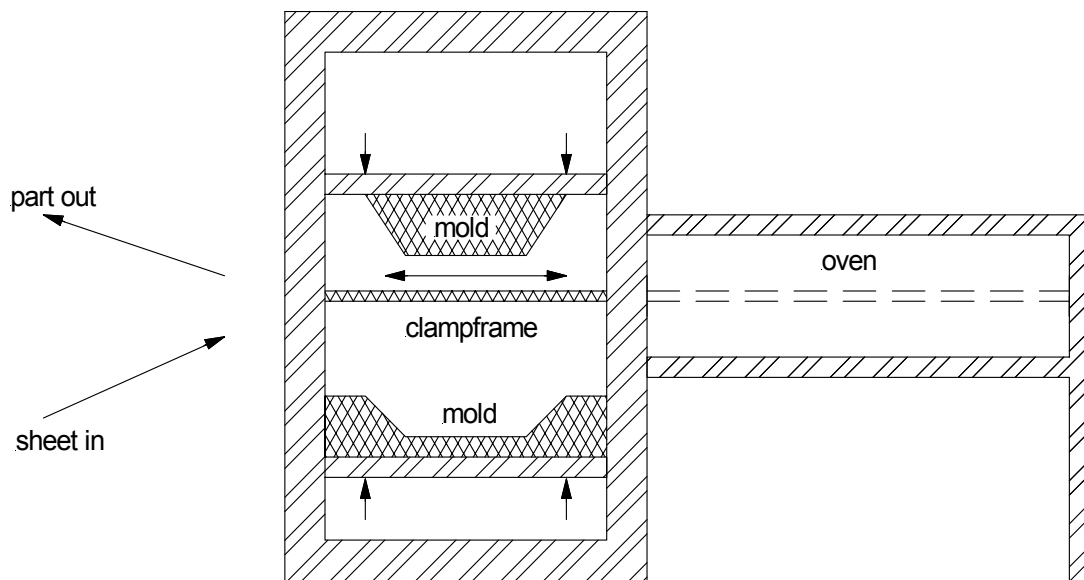
Figure 2.4: Basic single station shuttle machine.

2.2.3 Process Steps

2.2.3.1 Sheet Handling

Sheet handling refers to all of the pre-heating processes. To begin, the thermoforming process the sheets (or roll) are removed from storage and dried in a drying oven if necessary. (note that wound rolls cannot be dried only individual sheets) The sheet is then fed into the transport chain mechanism or clamp frame. The thermoforming process is now ready to begin.

2.2.3.2 Sheet Heating

Sheet heating, or reheat, is probably the single most important step because the results of sheet reheat can affect all subsequent processing steps. The focus of this work is almost exclusively on the reheat stage. One of the main motivating factors for developing an in-cycle control strategy is the fact that the reheat stage has been essentially untouched by advances in process control technology. Also, the reheat stage is the only step in which it is even possible to make any significant improvements through the application of model based control techniques.

The two controlling factors for the sheet reheat stage are heater temperature settings and heating time. The goal of sheet reheat is to bring the sheet centerline temperature up to the minimum forming temperature as quickly as possible. For radiation heating, the sheet surface temperature will increase very rapidly, and it will continue to rise so long as the sheet remains in the oven. It is very important to set the heater temperatures such that the sheet surface temperature does not rise above the maximum allowable temperature. If the sheet surface temperature does become too high there is a strong possibility of material degradation and even scorching of the sheet surface, which will result in a rejected part. It is also important to limit the heating rate for some materials. A heating rate that is too fast can cause loss of molecular orientation, surface degradation, and for foamed materials, foam breakdown due to poor material expansion. The maximum allowable heating rate will be dictated by the application of the part and the type of thermoplastic sheet.

The curve shown in figure 2.5 shows the typical heating profile of a thermoplastic sheet. The forming window (minimum and maximum allowable sheet temperatures) is generally specified by the material manufacturer. The fact that the sheet centerline lags behind the sheet surface temperature suggests that temperature gradients will appear through the sheet thickness, which is indeed the case. Figure 2.6 shows the temperature gradients that appear through the thickness of the sheet during the heating cycle. The level of temperature variation through the sheet depends on the thickness of the material. Thicker sheets will see larger temperature variations whereas thinner sheets will see very little variation. It is important to note that a minimal amount of temperature variation

26

through the sheet thickness is desired. Smaller temperature gradients result in parts that
have superior mechanical properties and parts that are generally easier to mold.
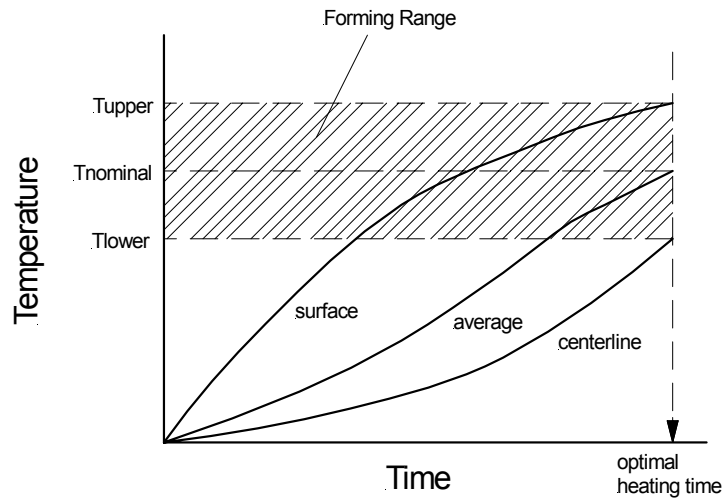
Figure 2.5: *example sheet heating profile with forming window*

Temperature gradients can also appear across the surface of the sheet due to
uneven heating. Uneven heating occurs naturally in radiation heating systems even if the
heat source is maintained at a constant, evenly distributed temperature. If the radiation
source is held at a uniform temperature, the center of the sheet will become hotter than
the edges and corners.   This is due to the nature of radiation heating. The center of the
sheet will "see" more radiation energy than the edges and corners, thus it will become
hotter. Modern thermoforming machines typically have ovens with multiple, individually
controlled heating zones so it is possible to adjust the heating zones for even sheet
heating; however, even sheet heating is not necessarily desirable in all applications. For
some cases it may be desirable to set the heater temperatures to yield hot spots on the
sheet for the purpose of material transfer. For example, basic forming using a female
mold results in thinner wall thicknesses towards the bottom center of the part. This was
established in Section 2.2.1.5. Now, with heater zoning it is possible to heat the sheet
more in the center so that material will flow towards the center of the sheet so that, after
forming, the part wall thickness will be more uniform than without zoned heating. It
should now be clear that setting the heater temperatures is tricky business, and by no
means is an optimally formed part automatic.
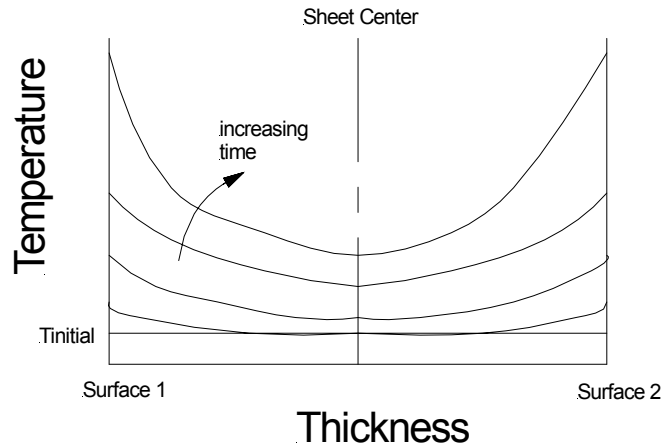
Figure 2.6: *example sheet heating profile: temperature gradient through sheet thickness*

It is interesting to briefly discuss the typical behavior of a thermoplastic sheet during reheat. First, two facts about material behavior should be mentioned. Sheets made from the same material but with different manufacturing techniques will not behave in the same manner when subjected to the same heating conditions. Also, the same thermoplastic materials produced in the same manner should theoretically lead to identical behavior in the heating and forming processes. In practice slight differences will exist. To begin the heating process, some sheets actually undergo transient wavelike movements due to initial high temperature gradients within the sheet. Usually, this phenomenon is quite rapid and goes unnoticed. After further exposure to heat the sheet tends to temporarily tighten up. This behavior also goes unnoticed most of the time. Upon further heating the sheet will soften once the glass transition temperature has been reached. It will eventually yield to gravity and begin to sag. This is the first noticeable sheet behavior. Generally sag is undesirable and it should be reduced as much as possible. Sometimes sag can be advantageous if used for pre-stretching of the sheet in an attempt to achieve better wall thickness distribution. It is also important to note, however, that sag is very difficult to control and uneven stretching due to sag will subsequently lead to uneven part wall thickness. Of course, if the sheet is left in the oven too long, it will eventually overheat and rupture.

2.2.3.3 Forming

Once the sheet is heated it is ready to be formed. Forming is necessary in order to transfer the shape of the mold to the sheet. As mentioned earlier, nearly all thermoforming operations use either male, female, or matched molds. Forming can be classified based on whether pressure or vacuum forces are used. Vacuum forming is more widely used but the application of pressure forming forces is growing since it is possible to obtain higher part definition with the larger pressure forces than with the smaller vacuum forces. Many different forming methods exist. The most popular are explained well in [3]. One common goal that all of these forming methods have is even material distribution, which can be generalized as the ultimate goal of the thermoformer.

2.2.3.4 Cooling

The next step in the thermoforming process is part cooling. The material must cool until it is completely rigid before it can be ejected from the mold. The cooling is performed by the mold itself and sometimes auxiliary fans are used to blow ambient air over the part to cool it more quickly. Sometimes, misting equipment is also used in conjunction with fans to cool the part even faster. As with the heating rate, the cooling rate must also be considered since the cooling rate affects material crystallization, which can be a determining factor in the mechanical properties of the part. Factors that affect the cooling time include: 1) sheet material; 2) sheet thickness; 3) forming temperature; 4) mold material; 5) mold temperature; 6) contact intensity between the mold and sheet.

2.2.3.5 Trimming

Once the part is formed and cooled it is removed from the mold and transferred to a trimming station. For a single part made from a single sheet, the sheet material that was used for clamping usually needs to be removed. This material is often referred to as flash material in the polymer processing industry. For multiple parts made from a single sheet of material the flash material includes the clamping material as well as the material between the molds. Trimming can be performed manually using hand held knives or power tools but this technique is usually reserved for operations that produce a small

number of parts. Usually automated equipment such as punch and die sets, or even robotic cutting systems are used.

This section provided a description of the thermoforming process in a level of detail that will allow the reader to comfortably move through the remainder of this thesis with sufficient background information. This section was, however, only an introduction to thermoforming. Many good works are available in the literature, including [1], if a deeper knowledge of the subject is required.

2.3 IMI Equipment Description

An industrial scale thermoforming machine located at the IMI facility was used for all experimentation and testing that was required for completion of this project. The original machine is actually quite old, but it has been retrofitted over the years. It can now be considered a suitable "research" or "experimental" machine.

The IMI machine is a simple, single oven, single forming station shuttle thermoforming machine capable of sheet sizes up to approximately 60 x 90 cm. The sheet heating is performed by an upper and lower radiation heating oven, each with six individually controlled heater zones (figure 2.7) for a total of twelve heater zones. The center heater in each zone has an embedded thermocouple for temperature feedback measurements. It is common practice not to have temperature feedback for all individual heater elements since it is not economically feasible to control each individual element. The temperature control (figure 2.8) is performed via PID controllers that are tuned using their convenient auto-tune feature.

The timing of the processing steps are controlled by a rather old mechanical thumbwheel system where the process steps are selected by inserting pegs into appropriate slots in the "wheel". The timing for each step is adjusted using a series of thumbwheel switches.

The typical process contains the following steps:

1. The heater band settings are selected on the PID controllers and the mechanical control system (i.e. the timing) is appropriately configured.

2. The sheet is loaded into the clamp frame at the forming station.

3. The sheet is carried into the oven by the clamp frame.

4. The sheet is heated for the specified amount of time.

5. The sheet is returned to the forming station by the clamp frame.

6. The mold is raised into its proper position just underneath the heated sheet.

7. The plug (for plug assisted forming) is lowered down into the sheet for pre-stretching.

8. The vacuum forces are activated and the part is formed.

9. The plug is returned to its original position.

10. A cooling fan is activated. The fan forces ambient air over the part.

11. After the specified cooling time the mold is returned to its original position and the part is ejected.

12. The formed sheet is removed from the clamp frame.
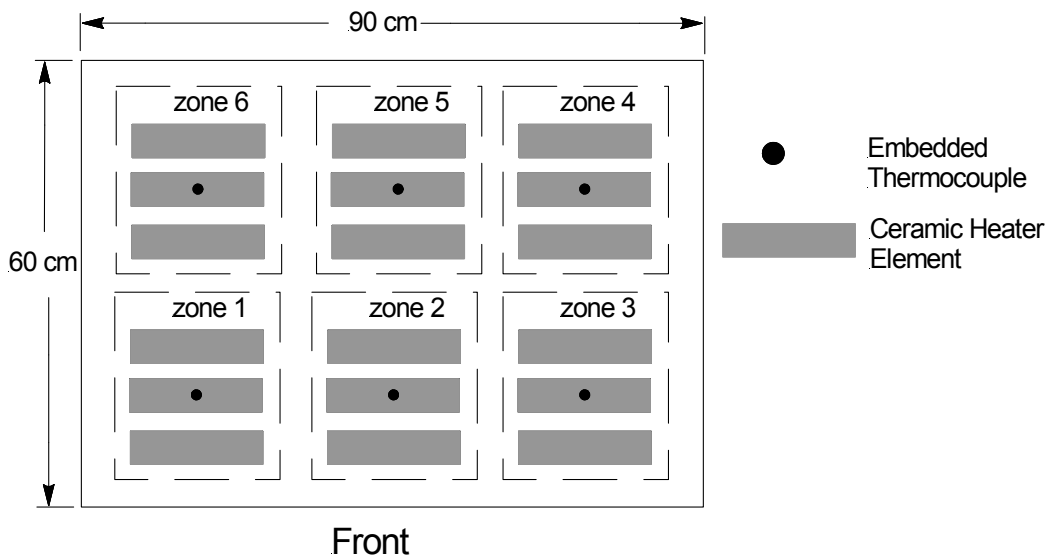
Figure 2.7: Oven layout for IMI thermoforming machine

Material Selection

Two different materials were used for testing and experiments. One of the materials chosen was HIPS, which was selected because of its high melt strength and large forming window. HDPE was also selected as a test material. Although it is slightly more difficult to form than HIPS, it was chosen because of its widespread popularity and use in related research initiatives at IMI.

31

Table 2.4: *IMI AAA Thermoforming Machine Data*

Machine type	Single station shuttle
Oven size	60 x 90 cm
Sheet size	30 x 45 cm
Heater size	650 W, ceramic
Heater controls	PID control
Sheet material	HIPS, HDPE
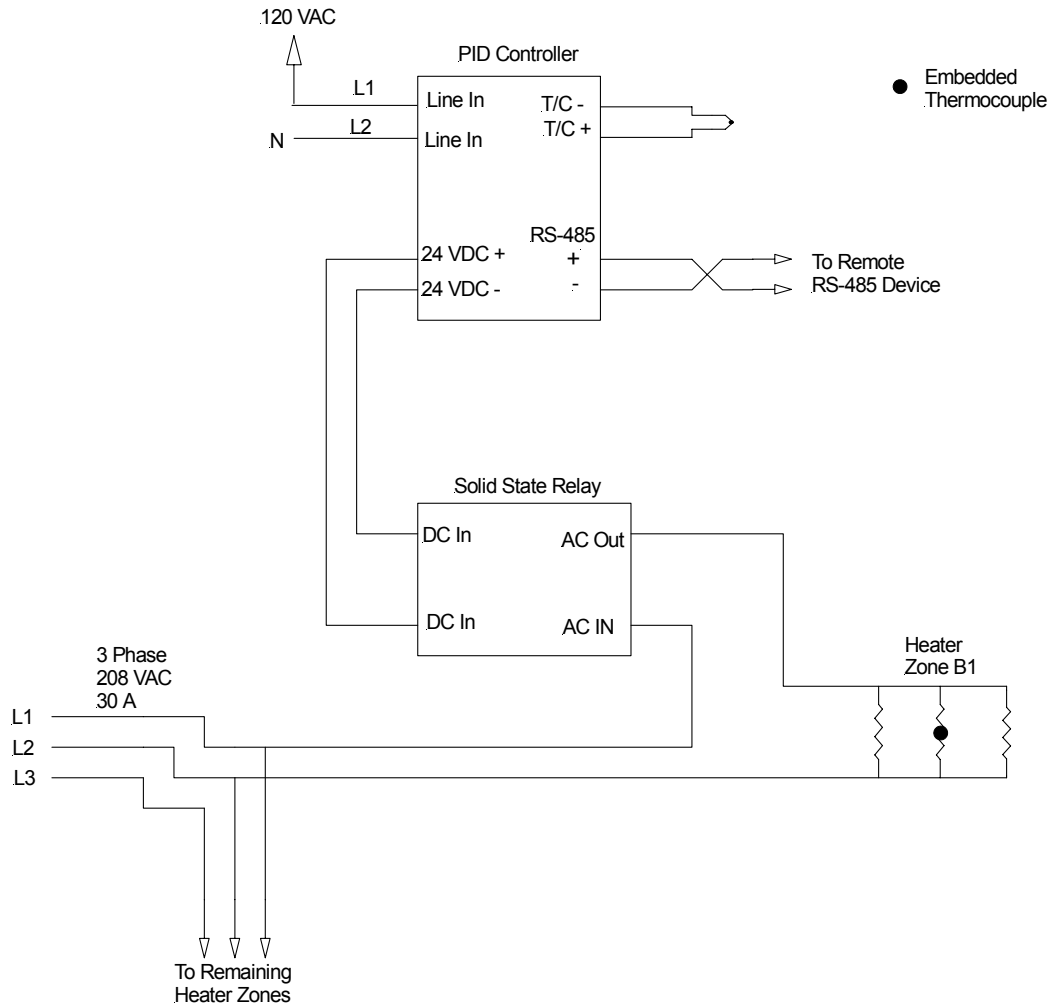
Figure 2.8: *Simplified control circuit diagram for heater zone B1*

3. Process Modeling

3.1 Introduction

Developing deterministic process models is usually the first step in any model based control design project. This project was no different. A full order, finite element simulation model of the thermoforming process had been previously developed by research associates at IMI; however, this large, very complex model is not suitable for the design of implementable, low order controllers. Development of a low order, process model, is therefore required.

Generally there are two basic methodologies that are available for process modeling. The first is the direct, first principles approach which utilizes in depth knowledge of the system and various laws of physics (i.e. conservation of mass, energy, etc.) to obtain mathematical equations which describe the system's behavior. The second approach is commonly referred to as the "black box" modeling approach. This approach uses system identification techniques to obtain mathematical models from experimental input-output data.

The first principles approach has some distinct advantages. To start, the mathematical equations that are derived have physical meaning. Each of the terms in the equations relates to a specific physical phenomenon which yields greater insight into system behavior. As a result, it is possible to tune the parameters in the model so that the model better represents the actual physical system. This also leads to a more flexible design since it is possible to simplify or expand upon the model as required. Another advantage is the fact this approach generally does not require as many model validation and identification experiments. Finally, the first principles approach usually results in better extrapolation performance. This means that the model will often describe, quite well, the behavior of the system in operating ranges that are outside of the range in which the identification and validation experiments were performed.

Of course there are also drawbacks of the first principles approach. One important drawback, which is of major concern, is the fact that a lot of time and effort is usually required to develop a suitable model. The model parameters can sometimes be

difficult to obtain, particularly when there are many uncertain parameters within the model. This will also increase the design time. Inaccurate models are also a major disadvantage. Modeling errors can occur when unmodeled, higher order dynamics are left out, or when very complex physical phenomena are described by over simplified mathematical relationships.

Like the first principles approach, the black box approach also has its own distinct advantages and disadvantages. One advantage is that a black box model, depending on its structure, can often better describe the behavior of the system within a certain operating range even though the modeling equations hold no physical meaning. Another advantage is the fact that this approach is very versatile and can be applied to a wide range of systems. This accounts for the method's popularity. One final advantage is the fact that an in depth understanding of the system dynamics is not necessarily required. As a result, the black box approach is often a practical, less labour intensive modeling strategy.

One of the disadvantages of black box modeling is the fact that "plant friendly" inputs are not always possible. This means that some systems may not be suitable for the application of system identification techniques that require relatively large input perturbations, which can subsequently bring the system out of its normal operating range and cause a defective product or even damaged equipment. Sometimes small signal PRBS (Pseudo Random Binary Signal) analysis is used to extract process models from processes that are sensitive to large perturbations. Unfortunately, this technique is not directly applicable to thermoforming due to the slow response of the heating elements. Also, if the process is time-varying, most black box models will not be capable of capturing the time-varying dynamics of the process. Finally, the black box approach can sometimes require many identification experiments, which can be time consuming and costly depending on the process. Table 3.1 summarizes the key attributes of the first principles and black box modeling methodologies. One must ultimately choose the appropriate modeling approach for the process at hand upon considering all of the advantages and disadvantages of each modeling approach.

Table 3.1: comparison between modeling approaches

	Advantages	Disadvantages
First Principles	- greater insight into system behavior - fewer experiments required - better extrapolation	- significant time and effort - difficult to obtain model parameters - modeling errors common
Black Box	- better description of system behavior possible - nearly universal approach - in-depth system understanding not required	- "plant-friendly" inputs not always possible - problems capturing time-varying dynamics - many experiments often required

The goal here was not only to develop a single process model for the AAA thermoforming machine at IMI, but also to produce a modeling strategy that is applicable to any thermoforming machine. One requirement was that the modeling approach needed to be relatively simple so that a thermoforming machine operator would feel comfortable with the process modeling and would not require a great deal of assistance from a professional with modeling and control expertise. It is for this reason that the black box modeling approach was chosen first. Recalling the advantages discussed earlier, the approach can be applied to any machine, and expert knowledge of thermoforming reheat dynamics is not necessarily required.

The goal then, of the black box approach is to obtain input-output models for the configuration shown in figure 3.1. To simplify the procedure, only heater zones 2 and 5 (for both upper and lower heater banks)[2] were considered along with sheet surface temperatures at the top and bottom center of the sheet; therefore, a 4-input, 2-output system was considered. The order of this system requires a total of eight input-output models in the form of transfer functions. The number of transfer functions can be reduced to four by making the assumption of symmetry. In other words it was assumed that the effect on sheet surface temperature from heater zone T2 (B2) would be the same as that from heater zone T5 (B5). It is important to mention that it is not reasonable to assume that there is symmetry between the upper and lower ovens since the heating mechanisms above and below the sheet are quite different throughout the heating cycle. This will become clearer during the discussions on sheet modeling in Section 3.3.

---

[2] refer to figure 2.7

Inputs:
- B2 setpoint
- B5 setpoint
- T2 setpoint
- T5 setpoint

Heater Dynamics → Sheet Dynamics

Outputs:
- top center sheet surface temp.
- bottom center sheet surface temp.

Note: model combines heater and sheet heating dynamics
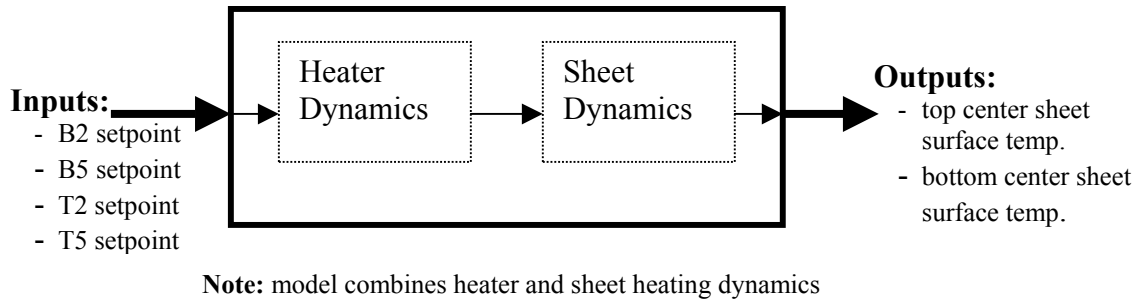
Figure 3.1: black box modeling configuration

Unfortunately, black box modeling of thermoforming is not a straightforward procedure. Standard system identification techniques would involve bringing the process up to a steady state, perturbing an input (e.g. a step), and measuring the output until the process reaches its new steady state. This input-output data would then be used to obtain a model describing the output due to its corresponding input change. The problem with thermoforming is sheet sag. The sheet cannot be brought up to its forming temperature and held there for any length of time since the sheet will continue to sag and eventually fall apart. One could apply standard step like system identification inputs while operating at much lower temperatures (no sag) but the input-output models obtained would not be valid within the normal operating temperatures. As a result, there is no traditional "static" steady state to speak of.

To overcome this problem, a "dynamic" steady state is employed. The dynamic steady state is considered to be the nominal response of the system for constant heater band settings of 350 ^{o}C. In order to isolate the effect of the particular step input, the output data for the system identification then becomes a temperature differential of the form:

Output = T_{surf_step} - T_{surf_nom}

where: T_{surf_step} is the perturbed sheet surface temperature (i.e. with step input)

T_{surf_nom} is the nominal sheet surface temperature

In order to fully examine the dynamics, the effects from step inputs of different magnitude, direction, and time were observed. Figures 3.2 to 3.5 illustrate the most

important aspects of the reheat dynamics that were observed. Figure 3.2 shows the step response for a step from 350 ^{o}C to 400 ^{o}C on heater zone B2 at 45 seconds into the cycle time.   The first thing that is noticed about figure 3.2 is the fact that the curves do not start at time zero. This is because of the experimental setup that was used. The data acquisition was performed using an Agilent 34970A digital multi meter with accompanying data acquisition software running on a laptop computer.   The data acquisition program had to be restarted manually for each of the individual experiments. The sheet also needed to be manually inserted into the oven for each experiment. Because it was virtually impossible to start the data acquisition software and insert the sheet into the oven at exactly the same time, the data acquisition software was started 10 seconds prior to inserting the sheet into the oven.   This method produced the most consistent and repeatable results.

The second most prominent aspect of the plot in figure 3.2, as well as the plots in figures 3.3 to 3.6, is the fact that there are significant offsets at the beginning of the cycles.   This was not originally expected considering the fact that the initial heater temperature settings were the same for all experiments.   There are two probable causes for this offset. The first is the fact that the experiments were performed over the course of several hours. Over this time period the machine operating conditions such as ambient and oven air temperatures as well as the temperature of machine components, such as the clamp frame, will change. These changes in operating conditions subsequently have an effect on the sheet heating.   The second cause is much more significant.   It was mentioned above that the sheet was inserted into the oven 10 seconds after starting the data acquisition software; however, because the sheet was inserted manually, the sheet did not reach its final position in the oven at exactly the same instant every time. Furthermore, the sampling rate of the data acquisition program was set to one second. This means that there can actually be up to two seconds difference between the first sampling instants of different experiments. Since the sheet surface heats up very quickly during the first one to two seconds, there can be significant discrepancies between the first measurements of different experiments.

From figure 3.2 it can be seen that the bottom surface response closely resembles that of a first order system with a lag time. On the other hand, it is unclear exactly how

the top surface will respond since the curve never levels out to its steady state value. The top surface temperature is still rising quite sharply towards the end of the cycle time. This is because the additional energy from the step on the bottom heater does not have sufficient time within the cycle to fully pass through to the top surface of the sheet. There is, therefore, a significant lag time between the energy input from one heater and its effect on the opposite side of the sheet. It should be noted that figures 3.2 through 3.6 represent responses due to steps on the lower heater bands. The step responses for the upper heater bands are not shown here because they did not clearly show the behavior that is exhibited in these five figures. The step responses (both top and bottom surfaces) for the steps on the upper heater bands never quite approached steady state. It was expected that the bottom surface response would not reach a steady state due to the slow energy transfer through the sheet; however, it was not expected that the top surface responses would still not level out towards the end of the heating cycle. Possible causes of this include effects from sheet sag and the varying convection heating mechanisms on the upper side of the sheet.

Figure 3.3 shows the effects on the step response due to heater step inputs of different magnitudes. As expected, the larger step sizes result in increased sheet temperatures, but only towards the end of the heating cycle. This is a direct result of the dynamics of the ceramic heater elements, which will be discussed further in Section 3.3.
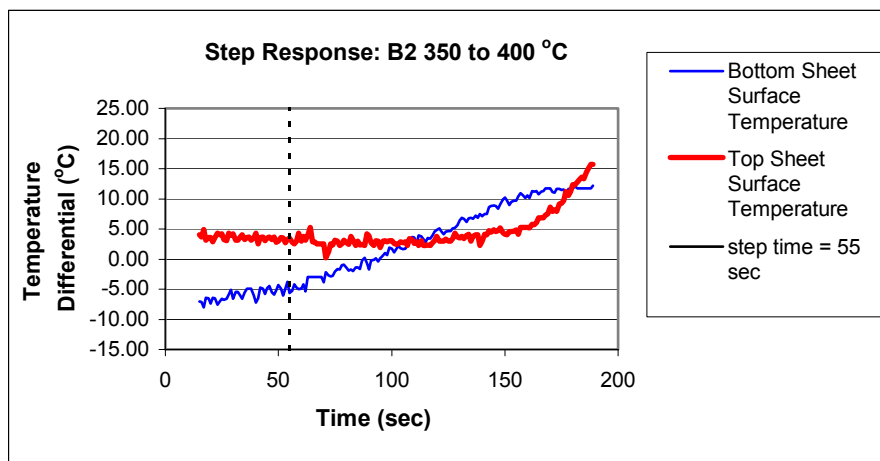
Figure 3.2: response for a step from 350 to 400 °C on heater zone B2
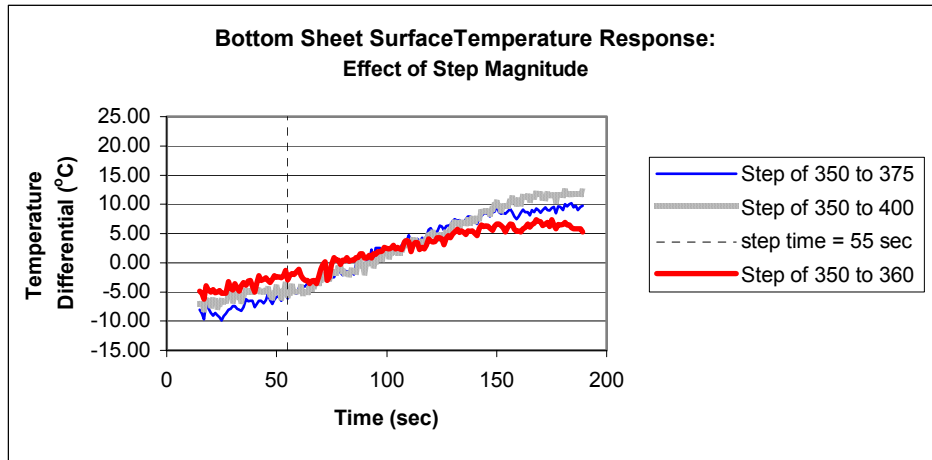
Figure 3.3: *effects on bottom sheet surface temperature response due to different input step magnitudes for heater zone B2*
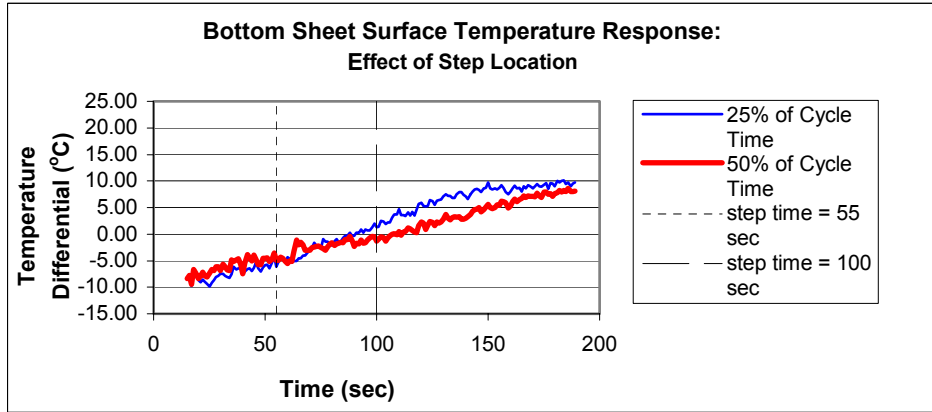
Figure 3.4: *effects on bottom sheet surface temperature response due to different input step times for heater zone B2*

Figure 3.4 shows the effects of input step time on the bottom surface temperature response. As was the case for different magnitudes, there is not a significant difference in the two responses. The small effects that were observed for different step input times were as expected. The earlier step input brings the response closer to the steady state as is evidenced by the leveling off of the upper curve in figure 3.4.

Figure 3.5 shows the sheet surface temperature response for a negative step on heater zone B2. Aside from the very large initial offset for the top surface temperature,

the most prominent feature of this plot is the nearly constant slope of the curve after the negative step has been applied. This is also a direct result of the dynamics of the heating elements.   Because the heaters cool very slowly, they never actually reach the new setpoint of 300 ^{o}C and there is no visible "step like" response characteristics in the sheet surface temperature curves.   Finally, figure 3.6 is used to validate the symmetry assumption that was made earlier. As can be seen in the figure, the responses due to a step on heater zone B2 and heater zone B5 are practically identical, which supports the symmetry assumption.

Figure 3.5: response for a step from 350 to 400 ^{o}C on heater zone B2

Figure 3.6: bottom sheet surface temperature response for step inputs on heater zones B2 and B5

System Identification

The first black box system identification attempt was not successful. Matlab's system identification toolbox was used and numerous model structures were tried. A model structure and order could not be found such that the resulting model had good prediction capabilities and stability properties. We believe that the primary rea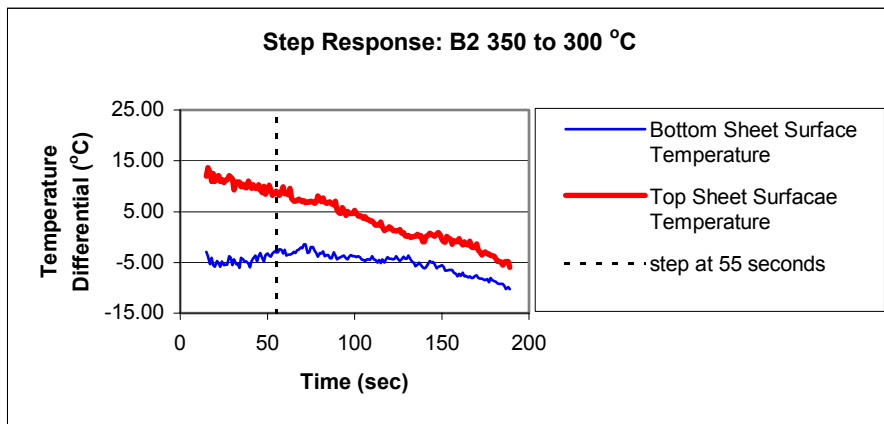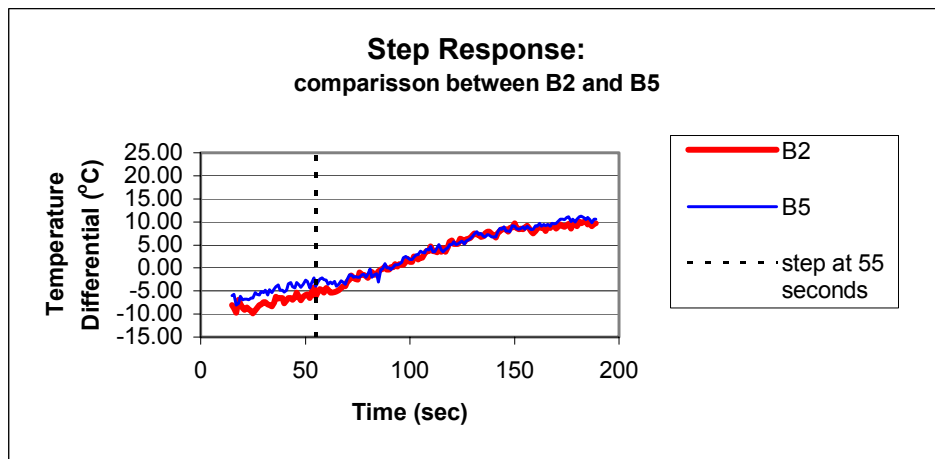son for this failure is the fact that the experimental data that was collected was not suitable for good system identification results. As mentioned earlier, the step responses did not fully reach steady state; therefore, the system identification algorithms had difficulty fitting a model to the data. One way to fix this problem would be to apply the step inputs earlier in the heating cycle so that a full response could be obtained. Another problem was the offset issue. This could have been avoided by using a more sophisticated experimental setup. For example, an automated data acquisition system could be implemented whereby data collection begins the moment a proximity switch is triggered by the entry of the sheet into the oven. This would ensure that the data collection started at precisely the same moment for each experiment. The other problem that needs to be overcome is the soak time issue (i.e. the slow energy transfer to opposite side of the sheet). One way to tackle this problem may be to use earlier step inputs of larger magnitudes so both sides of the sheets would better approach steady state.

After reviewing the results of the system identification experiments a decision was made not to act upon the recommendations made above and continue with the black box modeling method. The first principles approach was chosen as the new modeling methodology. There were two reasons for this decision. The first is the fact that not all of the experimental observations could be fully explained with a high level of confidence. Taking a first principles approach would help to obtain a deeper understanding of the dynamics involved, and any further phenomena that were observed, either experimentally or through simulation, could be related back to the actual modeling equations. The second, and probably most influential, motivation for the switch in methodology was the fact that the black box modeling approach would not be practical on larger thermoforming machines. For example, a machine with 25 heater zones in both the top and bottom ovens, and 5 sheet zones of interest, would require, at minimum, one experiment for each heater-sheet zone combination. This would result in extensive

experimental time and material costs just to obtain a working model for controller design. Then even more experiments would need to be performed for controller tuning. All of this experimentation time adds up to lost production, which may be detrimental to some thermoforming operations. The first principles approach, however, does not require nearly as many as identification and validation experiments in order to obtain a functioning control design. This being said, the first principles modeling approach seems to be the most appropriate solution to the modeling problem.

First Principles Design

The central idea behind the first principles approach is that separate independent models are obtained for each of the system components shown in figure 3.7. The modeling of each of these components: sensors, heater, and sheet, is discussed in the next three sections.
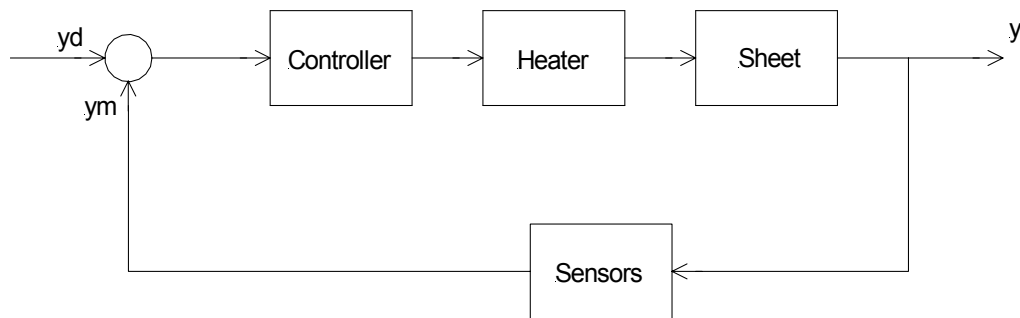
Figure 3.7*: individual system components*

3.2 Sensors

Instrumentation is a critical component of any feedback control system. Without proper measurement of process signals it is impossible to accurately control the system as desired. It is very important that all sensing equipment be properly calibrated and that the measurement dynamics are accounted for. Before discussing sensor calibration and dynamic modeling, however, it is worthwhile to describe the sensing system and some of the related issues.

3.2.1 Thermoforming Instrumentation

Numerous instrumentation and control devices can be found on modern thermoforming machines. There are, however, only three measurements available for in-cycle temperature control that are of importance. These are: sheet surface temperature, oven air temperature, and heater temperature. It is also possible to incorporate airflow measurements in and around the oven using a hot wire anemometer, but airflow instrumentation tends to be very complex and fragile, attributes that are not well suited for industrial applications. Furthermore, the cost of airflow instrumentation, and the amount of time required to develop an advanced control scheme that incorporates airflow measurements, does not justify its use. A more practical approach is to limit airflow in and around the thermoforming equipment.

The heater temperatures are obtained using thermocouples that are embedded into the ceramic material by the manufacturer. Heater temperature measurements are integrated into the heater modeling procedure so no further discussion is necessary here.

The oven air temperature measurements can be found using either RTD's (Resistance Temperature Detectors) or thermocouples. RTD's are generally much more reliable and are used more often in harsh industrial environments. They are also quite accurate (usually within +/- 1 ^{o}C). They also have the advantage of the capability of being used in applications where the actual sensing element and sensing electronics are separated by long distances. RTD's are, however, quite expensive. Thermocouples, on the other hand, are cheaper, less accurate (+/- 1 ^{o}C at best), and they are more difficult to install. Care must be taken to ensure that the installation is not susceptible to electrical noise since thermocouple signal levels are very small.

After examining the pros and cons of each type of device the thermocouple was chosen for the IMI machine because of its low cost and slightly faster response. The use of a thermocouple for oven air temperature measurements is not automatic. The measurement is complicated by the fact that the thermocouple is within a radiation environment and is susceptible to heating from the heater elements, which would result in erroneous measurements. Two solutions are possible. The first is to limit the radiation heating effects by coating the thermocouple with a low emissivity, reflective paint. The

second approach is to use a sheathed sensor. This was accomplished at IMI by placing the thermocouples within small lengths of aluminum tubing open at both ends to allow air movement around the sensor. Pre-fabricated thermocouples with perforated sheathing are also commercially available.

Sensor placement is also an issue. The IMI setup consisted of two thermocouples for oven air temperature measurement, one above the sheet and one below. Each sensor was located at the center of the sheet midway between the heater elements and the sheet. The number of sensors and their placement will depend on the thermoforming equipment because the oven air temperature can be highly non-uniform as was reported by Yousefi in [15].

The sheet surface temperatures are found using non-contact IR (infrared) sensors. A number of different IR sensor types are commercially available and their cost and complexity can vary. See table 3.2 for cost comparisons. The simplest design is commonly referred to as an IR thermocouple. The sensing element receives IR energy from the measurement target and transforms this energy into a standard thermocouple voltage signal. This type of sensor costs as little as $200 and it requires no external power supply since there are no "on board" electronics. The actual temperature measurement is obtained using separate instrumentation such as a digital multi-meter configured for thermocouple measurements. The repeatability and interchangeability of IR thermocouples is similar to regular thermocouples. Other more sophisticated IR sensors contain their own electronics and can allow the user to specify the emissivity of the target and configure the output signal to be in the form of an RS-232, 0-5 V, or $4-20$ mA signal. Most IR sensors require an air-cooling jacket for operation in elevated temperature environments such as in an oven of a thermoforming machine; however, some models are configured with a remote pick-up element connected to the main sensor unit via a fiber optic cable. These types of sensors can be operated in very harsh environments. The IR sensors that were used for the IMI setup were the Raytek RAY-MID 10-4 IR sensors which cost approximately $1200 each. They can be configured to output various thermocouple signals as well as a standard 4-20 mA signal.

Table 3.2: *IR sensor cost comparisons*

IR Sensor Type	Approx. Cost
IR thermocouple	$200 to $500
IR sensors with transmitter	$600 to $2000
IR Camera/Imaging system	> $10 000

Two IR sheet surface temperature measurements were used for the basic IMI setup, one for the top surface and one for the bottom surface. Each sensor was focused towards the center of the sheet. The type, number, and placement of sensors that are used is an economic decision that has to be made prior to implementing a control design. One has to determine whether or not the benefits of using additional sensors justifies their added cost. The issue of observability also needs to be considered if some form of state estimation is used to estimate sheet surface temperatures at additional locations across the sheet surface.

3.2.2 Sensor Modeling

Fortunately, sensor modeling for this particular application is very easy. A typical thermocouple, and especially an IR sensor, have fast measurement dynamics. Because thermoforming is a slow processes, the sensor dynamics become negligible. This means that the sheet surface and oven air temperatures will not change fast enough for the measurements to be affected by any measurement lag. The mathematical equation describing sensor behavior simply becomes:

$$y_m(t) = e(T)y(t) + n(t) \tag{3.1}$$

where: $y_m(t)$ is the measured signal
$n(t)$ is the measurement noise
$e(T)$ is a sensor calibration function
$y(t)$ is the un-calibrated measurement signal

3.2.3 Calibration and Maintenance

The $e(T)$ function in (3.1) represents a sensor calibration function. For the thermocouple oven air temperature measurements, $e(T) = 1$, which simply means that it is

assumed that the thermocouple is properly calibrated and the only source of error is the measurement noise *n(t)*.

Unfortunately the IR measurement is not so straightforward. IR sensors are typically calibrated by the manufacture using a precision controlled, black body temperature source. The user can then make adjustments to account for the emissivity of the target area at hand. This works well for most applications but thermoforming is somewhat of a special case in which there are many different sources for measurement error. First, most IR sensors are accurate only within a relatively small temperature range. Thermoforming requires accurate measurements over a wide range of approximately 25 to 200 $^{\circ}$C. Measurement error is then unavoidable if the sensor is called upon to operate outside of its operating range. Emissivity of polymer materials changes with temperature, which will also result in measurement errors since almost all IR sensor models assume a constant emissivity. Changes in ambient air temperature may affect the electronics in less expensive models and result in further measurement error. Reflected radiation from the heater elements is probably the most significant source of measurement error however. Many of the models do have optical lenses, which are intended to filter out any ambient radiation sources. Nevertheless, additional radiation will be picked up by the sensor and cause measurement error. Further complicating the situation is sheet sag, which will cause the level of reflected radiation to change as the shape of the sheet surface changes.

Given all of the possible sources for measurement error, the only way to properly calibrate the sensors is to use thermocouples as a true reference temperature. Thin foil thermocouples were adhered to the sheet surface with a flexible, highly conductive silicone paste and a strip of high temperature adhesive tape. The temperature dependant calibration function, *e(T)*, is in the form of a polynomial and is written as:

$$e(T) = \frac{T_{T/C}}{T_{sensor}} \tag{3.2}$$

where: $T_{T/C}$ is the thermocouple measurement

T_{sensor} is the IR sensor measurement

It is important to note that proper bonding between the sheet surface and the foil thermocouple is essential. Thermocouple cement is not appropriate for bonding the thermocouple to the sheet surface because the cement hardens and becomes rigid. As the sheet sags the bonded thermocouple will actually begin to pull away from the sheet surface, and the thermocouple measurement will not reflect the true surface temperature, thus resulting in improper calibration.

Proper instrument maintenance is key in maintaining the performance level of any control system. The IR sensors will need to be periodically recalibrated. The maintenance schedule would depend upon the factory specifications for the particular sensor model that is being used. Ideally, the sensors should be recalibrated before the start of every new production run using the procedure described above.

3.3 Heater Modeling

The purpose of the heater modeling is to capture the dynamic behavior of the heater elements. As mentioned in the process description, there are many different kinds of heating systems available for thermoforming. The IMI machine uses ceramic heating elements to heat the sheet. The basic structure and dimensions of these elements are shown in figure 3.8. The actual resistive heating element is a thin wire that is embedded in the ceramic material. The purpose of the ceramic material is to create a stable, relatively even temperature source.

Since the geometry of the heaters is quite complex, it would be extremely difficult to develop an analytical model for the heaters. Furthermore, the material properties are not well known, and the exact positions of the heating coil and embedded thermocouple are unknown. It is, therefore, not reasonable to use a first principles approach for heater modeling. Unlike the heater-sheet combination, the black box approach is well suited for heater modeling since standard system identification techniques can be applied. A number of different system identification experiments were performed for the heater modeling. Figures 3.9 and 3.10 will be used to explain the heater modeling methodology.
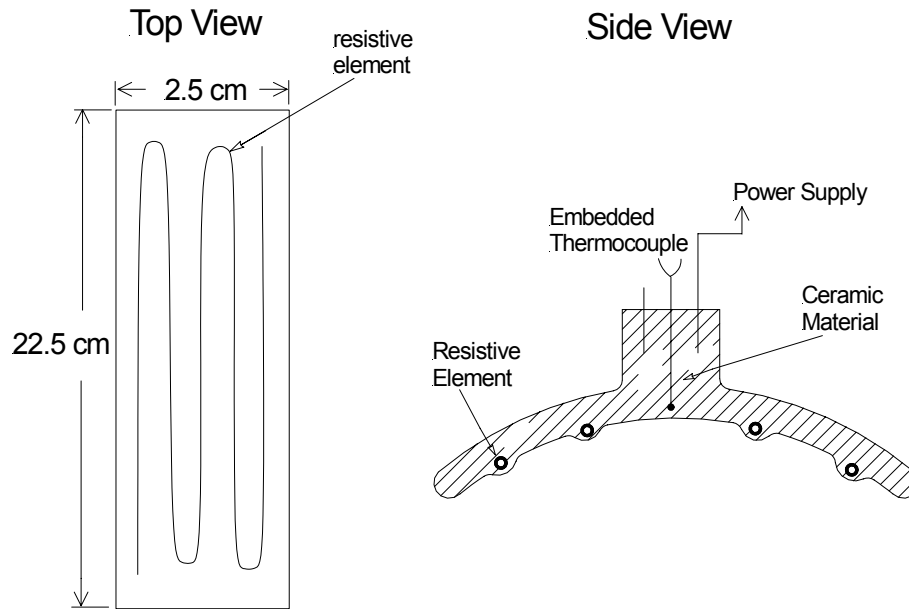
Figure 3.8: *physical dimensions of heating elements*

Figure 3.9 shows a sample step response of the heating elements. The lower curve represents the embedded thermocouple measurement and the upper curve represents the surface temperature of the heater element as measured by a thin film cement-on thermocouple. The relationships between the components named in figure 3.10 and the step response shown in figure 3.9 are explained in the discussions below.
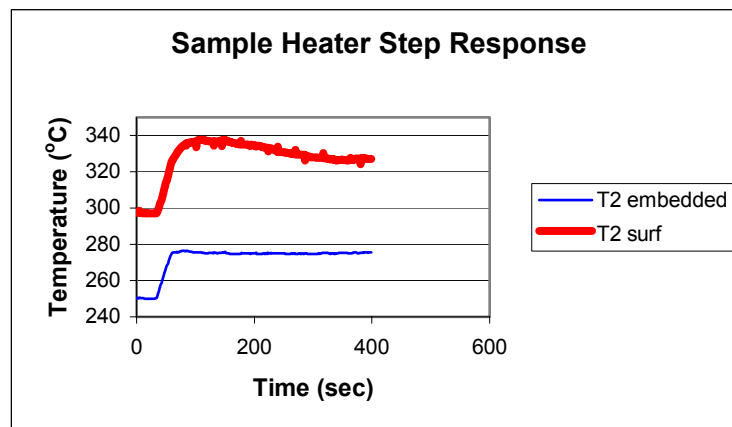
Figure 3.9: *sample heater step response*
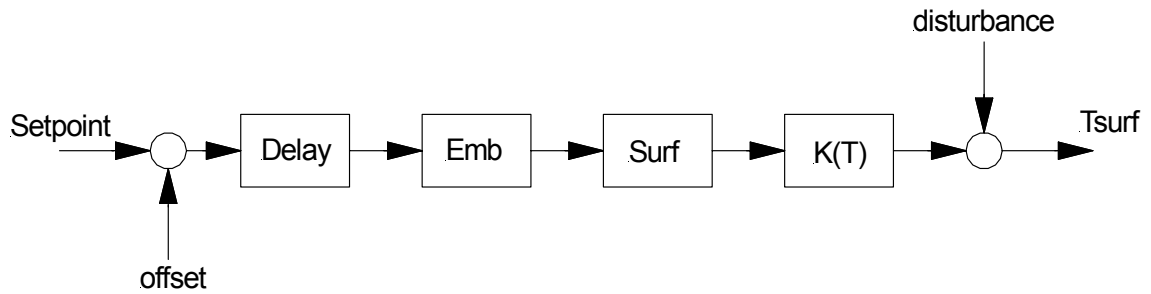
Figure 3.10: *configuration of heater model*

Setpoint

The setpoint is the desired heater temperature. The PID controllers regulate the power supplied to the heaters in order to maintain the setpoint value. It is important to note that the PID controllers control the heater temperature via the embedded thermocouple measurements. The heater surface temperature is not controlled. This distinction will become clearer throughout the discussions to follow.

Tsurf

Tsurf represents the heater surface temperature. The heater surface temperature is not readily available. As mentioned above, an additional thermocouple had to be bonded to the heater surface in order to obtain this measurement.

Offset

The large offset between the embedded thermocouple measurement and the surface measurement was unexpected. As can be seen in figure 3.9, the difference between the embedded and surface temperature is in excess of 40 $^{\circ}$C during a typical step response. It was originally thought that this large temperature differential was due to radiation heating effects from the opposite heater bank (i.e. the bottom heaters were heating the surface of the top heaters and vice versa). This explanation was discredited after additional experiments were performed. Identification experiments on a single heater zone, with all other zones turned off, still resulted in large offsets. In the absence of a valid explanation, the only way to deal with the temperature offset was to account for it in the heater model. Figure 3.11 shows the steady state offset at different temperature

levels. As can be seen from the figure, the offset is temperature dependant. A first order polynomial fit gave the following results:

$$\text{Upper heater offset} \ = \ 31.51 + 0.0662 * T_{emb} \qquad (3.3)$$
$$\text{Lower heater offset} \ = \ 35.51 + 0.04252 * T_{emb} \qquad (3.4)$$

The "offset" signal in figure 3.10 represents the constant component in equations 3.3 and 3.4. Similarly, the K(T) block in figure 3.10 represents the temperature dependent component of the offset in equations 3.3 and 3.4.
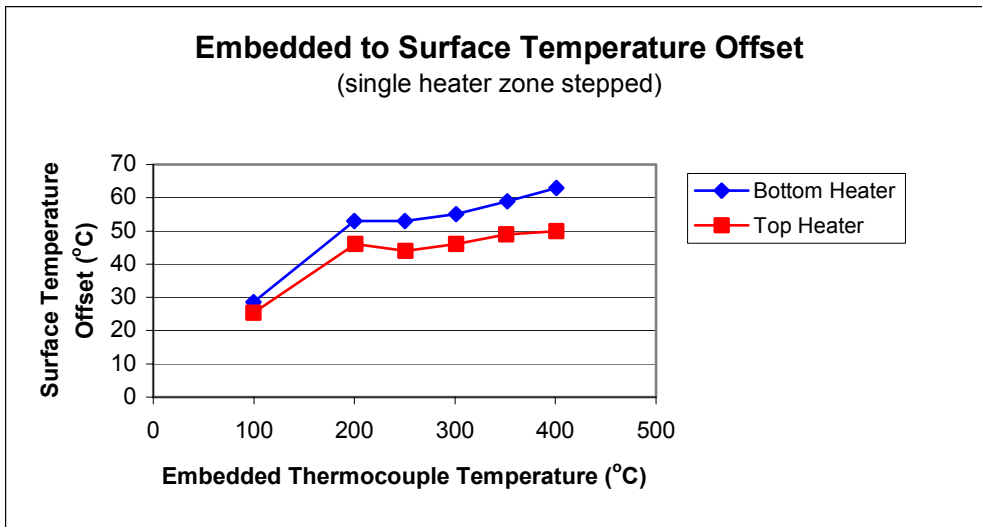
Figure 3.11: heater embedded to surface temperature offset temperature dependency

It is worthwhile mentioning some of the other heater designs that may be less susceptible to the surface temperature offset problem. The placement of the thermocouple used for feedback control is the central issue. There are some designs that have the thermocouple embedded very close to the surface of the heater. These designs claim superior surface temperature control; however, this is not necessarily the case. A ceramic heater from Salamander Inc. was purchased and tested on the IMI machine. This heater element used what was termed a replaceable thermocouple. The thermocouple was not actually embedded into the ceramic material. It sat close to the surface in a thermo-well and was held in place by a spring mechanism. Unfortunately, the heater was

hand made and of poor quality. Needless to say it did not offer good temperature control. It is not possible to comment on the performance of some of the other designs that claim good surface temperature control without actually testing them first.

Delay

The "Delay" block in the heater model configuration represents the delay that was observed in the heater step response data. The delay was found to be anywhere between 3 and 7 seconds so a value of 5 seconds was used. The difference in delay times between step responses was a consequence of the experimental setup. The data acquisition and step inputs were both initiated manually. For similar reasons as were outlined in the discussion of initial offsets in Section 3.1, slight differences in the timing of each experiment resulted, thus the difference in delay times. The total delay time is a combination of the response of the PID controllers and the lag time between an increase in supplied heater power and the corresponding temperature change within the heater element at the location of the embedded thermocouple. The delay is represented by a first order Padé approximation.

Emb

The "Emb" block in the heater model configuration represents the dynamics of the embedded temperature response as measured by the embedded thermocouple (i.e. the lower curve in figure 3.9). At lower operating temperatures, the embedded response resembles that of a first order system. Figure 3.12 shows, however, that the response becomes less linear at elevated temperatures as indicated by the upper curve. The form of the embedded model is a fist order transfer function resembling:

$$Emb(s) = \frac{k}{s\tau + 1}$$

(3.5)

where: k is the gain
τ is the time constant

The gain, k, of the embedded model is always 1. This is because the embedded temperature is under PID control; therefore, it will always settle at the desired setpoint

51

value. The time constant, τ, was recorded by visually inspecting the step response data. As can be seen in figure 3.13, the time constant changes with operating temperature.
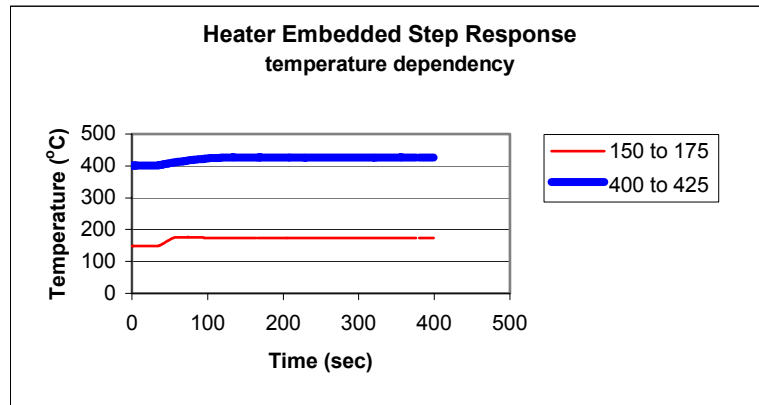
Figure 3.12: Temperature dependency of embedded heater step response. Step on heater zone T2 from 150 to 175 °C and 400 to 425 °C
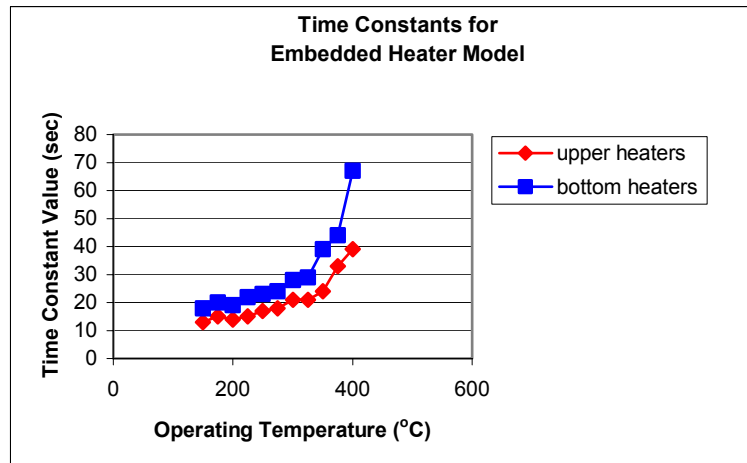
Figure 3.13: temperature dependent time constant for first order embedded heater model

Surf

The "Surf" block in the heater model configuration diagram represents the measured surface temperature dynamics. The offset between the heater embedded and surface temperatures has already been presented above. The upper curve in figure 3.8 also suggests that the heater embedded to surface temperature offset is dynamic in nature

as evidenced by the overshoot in the surface temperature response. The first attempt to capture the surface temperature dynamics involved visually inspecting the step response data to obtain the parameters for a second order model of the following form:

$$T_{surf}(s) = \frac{a_1 s + a_0}{b_2 s^2 + b_1 s + b_0}$$

(3.6)

Unfortunately, the results were not satisfactory. The second approach employed Matlab's system identification toolbox. An appropriate model was obtained using the input-output (heater embedded and surface temperatures respectively) data from the step experiments. A number of different model structures were applied with the best performance given by a second order state space model[3].

The application of the system identification methods was not immediately successful. Various data conditioning steps needed to be performed first. The first step was to normalize the input and output data. This was accomplished by subtracting the initial value of each data set from the remaining values in the corresponding data set. This resulted in initial input and output values of zero. Next, the time delay was removed from the step response data, and then outliers were removed. Finally, the temperature dependant offset between the embedded and surface temperatures was removed from the output (surface temperature) data. When combined, these conditioning operations led to good system identification results.

One block is omitted from figure 3.10 in order to avoid confusion. This block is the PID controller. The PID controller is actually embedded in the 'Emb' block of the heater model, because the input-output data that was used for the system identification was the actual closed loop response of the heater elements. In effect, the heater model captures the dynamics of the heater elements as well as the closed loop PID control. This configuration was used because the relationship between applied heater power and heater temperature is highly nonlinear and not well known. Separation of the PID controller and heater dynamics is unnecessary as it does not add any value to the design. Such a separation would also be quite difficult and introduce added complexity.

---

[3] All model parameters are given in the Appendix.

3.3.1 Disturbances and Modeling Errors

Although a detailed study of disturbances acting on the heater system was not performed, it is worthwhile mentioning the important disturbance sources. One of the main sources of heater disturbances is air movement in and around the oven. Any cooler air that enters the oven area will pass over the heater surfaces, which will have a cooling effect. There is also air movement within the oven during a regular heating cycle caused by natural convection currents within the oven. The fact that hot air rises is well known. This suggests that the effects from air movement will be different for the upper and lower ovens respectively. Furthermore, it is extremely difficult to predict airflow within the oven. The only reasonable way to predict airflow within the oven and capture its effects on heater temperature is through the use of artificial neural networks. This approach to disturbance modeling would, however, require time and a significant amount of experimental data to train the neural network. It is for these reasons that disturbance modeling was not considered in this project.

Another source of heater disturbance is supply voltage fluctuations. A power source with higher frequency fluctuations, or higher order harmonic content, will not adversely affect heater performance. This is accomplished without the addition of any power regulation electronics. The high thermal mass of the ceramic material naturally results in a low bandwidth; therefore, higher frequency disturbances will be easily attenuated. Very low frequency fluctuations on the other hand, can affect heater temperatures. Since these types of disturbances are actually power quality issues and beyond the scope of this thesis, no further investigation into power supply related disturbances was made.

It is also important to identify modeling errors and future improvements that can be made. The major source for modeling error is the fact that the temperature across the surface of the heaters was found to be very uneven. Measured temperature differences across the surface are in excess of 50 $^{\circ}$C for some individual heater elements. This automatically becomes a source for modeling error since the heater models were found using measured input-output data. The output data, heater surface temperature, was recorded using a small, cement on thermocouple, which for all intents and purposes is a

point source measurement that does not reflect the true average surface temperature of the heater. An attempt was made to assess the accuracy of the measured output data using thermal images of the heater elements taken with an IR camera. The images were not consistent enough, however, to make a proper assessment, or adjustment, of the output data. As a result, the large surface temperature differentials were simply treated as an uncertainty for controller design.

An important fact that was discovered only towards the very end of this project is that the voltage level supplied to the heaters was incorrect. The heaters were operated under a 208 VAC supply upon completion of this project. At this voltage level, temperature differentials in excess of 50 ^{o}C were measured across the heater surface. It was later learned that the heaters were supposed to be operated at 240 VAC. A test was performed in which 240 VAC was supplied to a single heater element and the temperature differential across the heater was measured to be less than 10 ^{o}C. Modeling error would be greatly reduced if new heaters were used of if the existing heaters were operated at their specified voltage levels. Unfortunately, time and economic constraints meant that results for this project were obtained using these very uncertain heater elements. More importantly, however, is the fact that the overall heater modeling methodology presented here can be applied to any thermoforming oven using electrical radiant heaters.

3.3.2 Model Validation

After constructing the overall heater model from its individual components, the heater model was validated using experimental data that was different from the original data that was used to identify the model components. Figure 3.14 shows that the model performs quite well over a wide temperature range. Figure 3.15 shows the response of the heater model, found using step response data for heater zone T2, against experimental data for a step test on heater zone B2. The plots suggest that a single model can be used to describe the behavior of both the upper and lower heater banks. For simplicity, a single heater model was used, but separate models for the upper and lower heaters, respectively, could be used if desired.
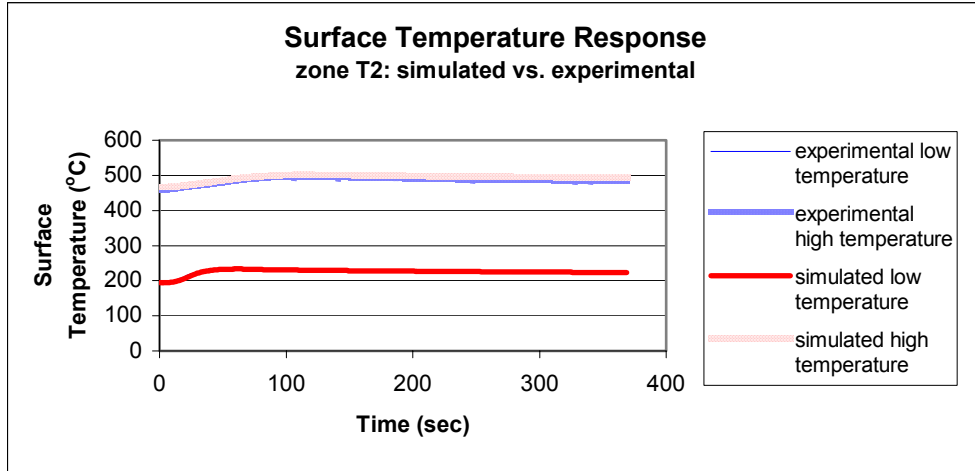
Figure 3.14: *Model validation results for heater zone T2*
(heater zone T2 data used for system identification)
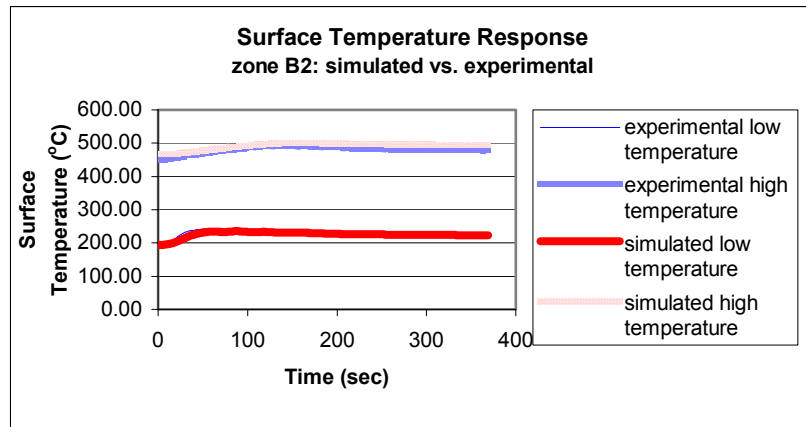
Figure 3.15: *Model validation results for heater zone B2*
(heater zone T2 data used for system identification)

3.3.3 Additional Heater Dynamics

There are additional heater dynamics that require attention before concluding the heater modeling discussion. The first is the settling time of the heaters. Figure 3.16 shows that the total settling time of the heaters is approximately 700 seconds. This indicates that the overshoot, which may be characterized by second order surface dynamics, lingers for quite some time after a setpoint change. 400 seconds worth of data

was collected for the system identification experiments. As a guideline, this should be the minimum amount of time used for system identification of ceramic heating elements.
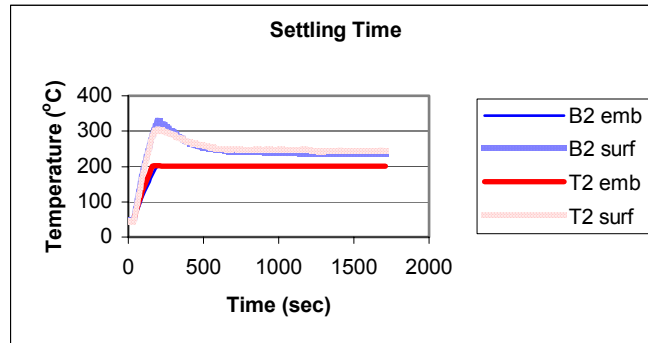
Figure 3.16: *Heater settling time*

The coupling between heater zones was also examined as part of the heater modeling procedure. It was assumed that all heater zones were decoupled from one another. In other words, the assumption is that a change in setpoint in one zone does not affect the temperature of any of the remaining zones. This is an important assumption. Any significant coupling between heating zones, the actuators, would make multivariable control of the sheet temperature extremely difficult. After reviewing the results shown in figure 3.17, it was decided that the decoupling assumption was valid. The plot was obtained under the following experimental conditions:

1) heater zones T2 and B2 were held at a setpoint of $200\,^{\circ}\text{C}$

2) all other remaining zones in the oven were stepped from room temperature to $400\,^{\circ}\text{C}$

As can be seen from the figure the effects on heater zones T2 and B2 are relatively small under the conditions of extreme temperature differentials between heater zones. Under normal operating conditions, the temperature differentials between heater zones will be much less; therefore, the decoupled assumption holds.

The most significant aspect of the heater dynamics can be observed by viewing the negative step response shown in figure 3.18. The shallow slope of the curves in the figure indicates that heater cooling is much slower than heating. This is true because the

heaters can only cool at their natural rate. Negative power input to the heaters is not possible. The significance of this behavior will become very obvious in the discussions on controller performance.
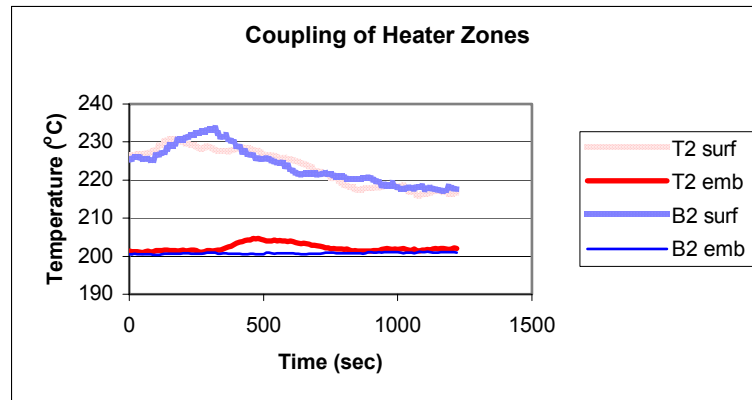
Figure 3.17: heater zone coupling

Figure 3.18 shows that the second order surface dynamics (i.e. the 'Surf' block from figure 3.10) do not change under cooling. This figure shows the simulated response of the second order surface model for actual experimental embedded heater temperatures as an input. As can be seen from the figure the results are still quite good. The same cannot be said for the results of the first order embedded model. Figure 3.19 shows the simulated response of the overall heater model (i.e. embedded and surface dynamics) to a negative step input. As can be seen from the figure, the overall model predicts much faster cooling. The source of this behavior is in the first order embedded heater model. This problem was addressed by adding a rate limiter in the full Simulink thermoforming simulation model.
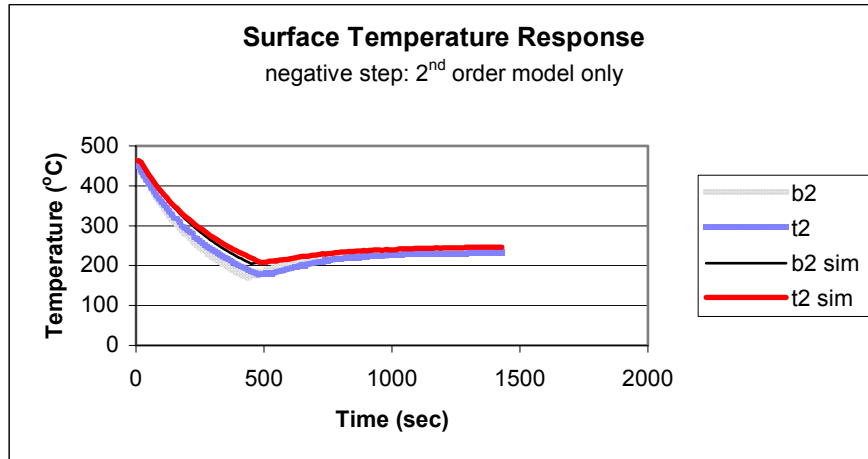
Figure 3.18: *negative step response of second order surface model with actual experimental data as input*
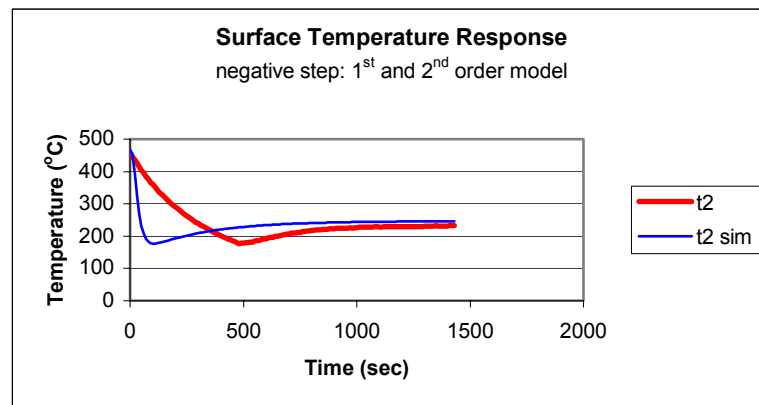
Figure 3.19: *negative step response of first order embedded model with a negative step input*

3.4 Sheet Modeling

The sheet heating model is the final, and most complex, component of the thermoforming model. For reasons presented earlier in Section 3.1, a first principles modeling approach was employed for sheet modeling. The ultimate goal is a set of analytic equations that describe the input-output behavior of the block diagram in figure 3.20. The inputs to the model are heater surface temperatures that are generated by the heater model discussed in the previous section. The outputs of the sheet model are sheet

surface temperatures at specified locations on the sheet surface. The states of the model represent internal sheet temperatures at specified locations.

Figure 3.20: conceptual block diagram for sheet heating model

3.4.1 Heat Transfer Theory

Before discussing the development of the sheet modeling equations in detail, it is necessary to establish some basic heat transfer theory. The simple diagram in figure 3.21 depicts the basic energy movement that the heat transfer theory tries to explain. The theory describes how energy transfer to and from the sheet surfaces is accomplished as well as the three-dimensional transfer of energy within the sheet material itself. To begin, the presentation of a number of concepts is useful.
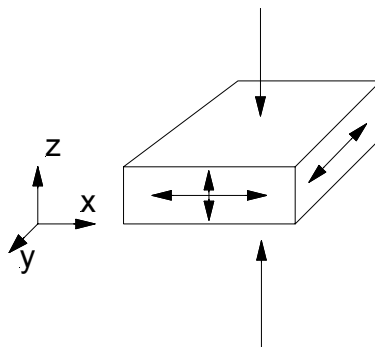
Figure 3.21: coordinate system and direction of energy transfer

Entropy: Entropy is basically a term used to quantify the degree of molecular disorder within a system, or similarly, a measure of how close a system is to an equilibrium state.

Heat: Heat is the energy that is transferred within a system as a result of a temperature differential. Heat always flows from a high to a low temperature region.

1st Law of Thermodynamics: The 1st law of thermodynamics is basically a statement of the law of conservation of energy. It is usually written as $\Delta E = q + w$ which states that the change in energy within a system (ΔE) is equal to the net heat flow (q) and work (w) done on the system.

2nd Law of Thermodynamics: The 2nd law of thermodynamics is not as straight forward as the first law. It is often stated in different forms but the main idea remains the same. Through the concept of entropy, the 2nd law places restrictions on a thermal process and leads to determination of the direction of heat flow and the maximum amount of work that can be obtained from a thermal system.

Heat Capacity: Heat capacity is a property that is indicative of a material's ability to absorb heat energy. The heat capacity of a material can be assessed by the effectiveness in which the two modes of thermal energy can be introduced into a system:
1. vibrational heat capacity: refers to molecular vibration caused by wave energy
2. electric heat capacity: refers to kinetic energy of free electrons

Specific Heat: The specific heat of a material represents the heat capacity per unit mass of material. Specific heat is defined as the amount of heat energy required to raise the temperature of a unit mass of a substance by one degree. It is important to note that specific heat values for polymers are generally quite temperature dependant. Specific heat can be measured experimentally in a lab with the appropriate equipment.

Thermal Conductivity: Thermal conductivity is a measure of the efficiency of energy transfer (by molecular interaction) within a material. Thermal conductivity is very difficult to measure accurately. It is somewhat temperature dependant, but because of the level of uncertainty, constant thermal conductivities are defined for most polymers.

Thermal Diffusivity: Thermal diffusivity is similar to conductivity in some respects. Thermal conductivity can be considered to be a measure of the extent of energy transmission through a substance whereas thermal diffusivity is a measure of the rate at which the energy transfer occurs.

Thermal Expansion Coefficient: The thermal expansion coefficient is a measure of how much a material will expand when heated. One of the main causes for expansion of polymers is the temperature dependency of the material's density.

Infrared Spectra: Infrared spectra refers to the fact that polymers tend to selectively absorb, transmit, and reflect radiation energy of different wavelengths. This project used relatively thick, opaque materials, and it was assumed that all of the radiation energy was absorbed by the material (i.e. no reflection/transmission). This is not the case with all materials and spectral response can be an important thermoforming issue. Transmission spectra for various polymers are given in [1].

Heating Mechanisms

There are three energy exchange mechanisms involved in the thermoforming process: conduction, convection, and radiation.

Conduction

The conduction heating mechanism is a solid phase heat transfer phenomenon that occurs within a solid body or between two bodies in contact with one another. The energy transfer, or heat flow, occurs as a result of the transfer of vibrational molecular wave energy as well as the movement of free electrons within a body. Conduction heat transfer is governed by Fourier's Law, which states that energy transfer occurs when temperature gradients exist within a body, and that the rate of energy transfer is proportional to the normal of the temperature gradient. Fourier's Law can be written as:

$$\frac{q}{A} = -k\frac{d\theta}{dx} \tag{3.7}$$

where q/A is the heat flow rate per unit area

k is the thermal conductivity

$\dfrac{d\theta}{dx}$ is the temperature (θ) gradient in the direction of heat flow, x

The general three-dimensional heat conduction equation can be written in Cartesian coordinates as:

$$\frac{d^2\theta}{dx^2}+\frac{d^2\theta}{dy^2}+\frac{d^2\theta}{dz^2}+\frac{\dot{q}}{k}=\frac{1}{\alpha}\frac{d\theta}{dt} \qquad (3.8)$$

where $\dfrac{d^2\theta}{dx^2}+\dfrac{d^2\theta}{dy^2}+\dfrac{d^2\theta}{dz^2}$ represents the temperature gradients within the body

$\dfrac{\dot{q}}{k}$ is a term that represents any energy that may be generated internally within the body

α is the thermal diffusivity

$\dfrac{d\theta}{dt}$ is the time rate of change in temperature within the body

Equation (3.8) describes the temperature distribution within a body over time. Solving this equation requires several boundary conditions. Two of the boundary conditions are governed by the two remaining heat transfer mechanisms: convection and radiation.

Convection

Convection is a fluid phase contact heat transfer mechanism. For thermoforming, this means that energy is transferred between the sheet surface and a thin fluid (air) layer above the sheet surface. It is important to note that convection heat transfer is actually a conduction process. At the sheet surface, the velocity of the air surrounding the sheet is zero, and the energy transfer is between the sheet surface and stationary air molecules in contact with the sheet surface. The net rate of heat flow is given by the equation:

$$\frac{q}{A}=h(\theta_\infty-\theta_{sheet}) \qquad (3.9)$$

where q/A is the flow rate per unit area

θ_∞ is the temperature of the air surrounding the sheet

θ_{sheet} is the sheet surface temperature

h is the convection heat transfer coefficient

At first glance, equation (3.9) looks very similar to Fourier's Law. As mentioned above, the similarity is because convection is actually a conduction process. The differences lie with the proportionality constants k and h. In Fourier's Law, k, is more or less a constant for most polymers. The convection heat transfer coefficient, h, in equation (3.9) is dependent upon many variables including the thermal properties of the fluid (thermal conductivity, specific heat, density, etc.) and the viscous behavior of the fluid. The fact that the viscous behavior of the fluid affects the heat transfer is evidenced by the fact that fast moving air over the sheet surface will have a greater impact on the sheet surface temperature than will slow moving, or quiescent air.

It is important to mention the direction of heat flow as a result of the notation in equation (3.9). A typical thermoforming application will see a reversal in convection heat transfer over the heating period. At the beginning of the heating cycle, the oven air temperature will usually be greater than the sheet surface temperature. The air movement around the sheet will then tend to heat the sheet during the beginning of the cycle. Towards the end of the heating cycle, the sheet temperature will rise above the oven air temperature, which increases very little during the heating cycle. At this point, the oven air movement around the sheet will then begin to cool the sheet rather than heat it.

Radiation

Unlike the previous two heating mechanisms, radiation heat transfer is a non-contact heat transfer mechanism. Radiation heat transfer is the dominant heating mechanism in the thermoforming process. Electromagnetic energy is emitted by the oven heaters and absorbed at the sheet surface. The absorbed energy at the sheet surface is then conducted towards the center of the sheet. It is important to note that the radiation energy transfer does not directly depend on the distance between the source (heaters) and the sink (sheet).

The Stephan-Boltzmann Law of radiation states that the maximum total energy emitted by an ideal source, termed a *black body*, is given by the equation:

$$E_b = \sigma\theta^4 \tag{3.10}$$

where E_b is the radiation energy emitted by the black body

θ is the temperature, in degrees Kelvin, of the black body

σ is a proportionality constant called the Stephan-Boltzmann constant

Obviously the concept of a black body is only theoretical. To account for the fact that realistic temperature to radiation energy conversion efficiency is less than 100 percent, we need to introduce the concepts of emissivity and absorptivity. Emissivity is a scaling factor which indicates the fraction of black body radiation emitted by a non-ideal source called a *gray body*. Similarly, absorptivity is a scaling factor which indicates the fraction of radiation absorbed by a gray body as compared to an ideal black body that absorbs all radiation it is exposed to. In general, emissivities and absorptivities of materials are considered to be equal. As such, the term emissivity is used interchangeably to describe both the absorption and emitting properties of a material. Emissivities are usually wavelength dependant, reflecting the fact that most materials tend to absorb radiant energy preferentially in specific wavelength ranges of the infrared spectrum. As mentioned earlier, infrared spectra were not considered in this project.

Using the Stephan –Boltzmann Law, the energy exchange that takes place during the thermoforming heating cycle is written as:

$$\frac{q}{A} = \sigma F_{view} \mathcal{E}_{eff} (\theta_{heater}^4 - \theta_{sheet}^4) \tag{3.11}$$

where q/A is the heat flow into the sheet surface per unit area

σ is the Stephan-Boltzmann constant

F_{view} is the radiation view factor

$\mathcal{E}_{eff}$ is the effective emissivity

θ_{heater} is the heater surface temperature

θ_{sheet} is the sheet surface temperature

As can be seen from the above equation, the energy absorbed by the sheet is proportional to the difference between the 4th powers of the heater and sheet temperatures. Two new terms appear in this equation. The first is the effective emissivity ($\mathcal{E}_{eff}$), or efficiency, of

the total energy exchange between the heaters and the sheet. The effective emissivity is a function of the sheet and heater emissivity values and is calculated using:

$$\varepsilon_{eff} = \left[\frac{1}{\varepsilon_h} + \frac{1}{\varepsilon_s} - 1 \right]^{-1} \tag{3.12}$$

where ε_{heater} is the heater emissivity

ε_{sheet} is the sheet emissivity

The second new term to appear in equation (3.11) is the radiation view factor (F_{view}). The view factor is a dimensionless scaling factor to account for the fact that a body only absorbs radiation energy that it "sees" from the source. In other words, all of the radiation energy emitted from a source may not hit the target body; therefore, a fraction of the radiation energy is lost to the surrounding environment. This lost energy is accounted for by the radiation view factor. The view factors for this project were calculated using a formula obtained from a catalogue of view factors for various geometric configurations.[4]

3.4.2 Sheet Model

The development of the thermoforming sheet heating model begins with the generalized three-dimensional conduction equation (3.8). An analytical solution to these types of three-dimensional partial differential equations is often quite elusive, therefore, a few simplifying assumptions are required. The first assumption is that the conduction will only occur through the sheet thickness in the z direction. In other words, it is assumed the transfer of energy in the x-y direction will be negligible. This assumption is valid since the temperature gradients across the sheet surface in the x-y direction will be relatively small as compared with the temperature gradients through the sheet thickness. Coupled with the fact that thermoplastic materials are generally poor heat conductors, the dominant energy transfer will occur in the z direction.

---

[4] Consult [5] for generalized view factor calculations

We are now left with a one-dimensional heat conduction equation. A one-dimensional equation is far more manageable than a three-dimensional one; however, the simplified equation still contains partial derivatives. This partial differential equation gives the sheet temperature at an infinite number of locations. Because the ultimate goal is a finite dimensional controller, an additional simplification assumption is necessary. The second assumption is that the system can be discretized into a finite number of isothermal sheet zones. The discretization is shown in figure 3.22.

Top View   Side View
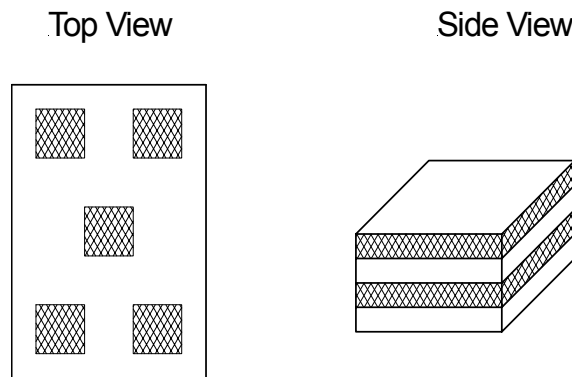
Figure 3.22: discretization of sheet into isothermal zones

In effect, the sheet is broken down into a number of sections in the *x-y* plane (top view figure 3.22), and within each of these sections, or zones, the sheet is broken down further into a number of isothermal layers (side view figure 3.22). The choice of discretization is somewhat arbitrary. A five zone rectangular configuration was chosen for its simplicity; however, one must address the issue of controllability before settling on a sheet zone configuration. For example, circular zoning may be desirable to reflect the fact that sheets tend to heat more towards the center and less around the edges. One must keep in mind, however, the oven configuration. A loss in controllability will occur when the heater-sheet zoning is such that it is physically impossible to heat one area (zone) of the sheet differently than another area of the sheet. Controllability will be more of an issue for ovens with a small number of large heating zones. Ovens with numerous smaller heating zones will prove to be much more versatile.

3.4.2.1 Modeling Equations For a Single Sheet Zone

The modeling equations for a single sheet zone will be developed in this section. Each sheet layer is considered to be an isothermal entity, or node as shown in figure 3.23. The convention is to locate each node in the middle of each isothermal layer. The interaction between nodes constitutes the sheet heating model. The model is constructed by performing an energy balance on each node. The result is a set of finite dimensional, ordinary differential equations.
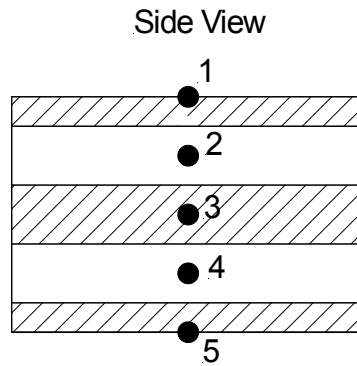
Figure 3.23: *sheet discretization: node numbers*

The modeling equation for node 1 is written as:

$$\rho V C_p \frac{d\theta_1}{dt} = q_{in} - q_{out} \tag{3.13}$$

Equation (3.13) states that the rate of change in energy for the top layer, node 1, is equal to the energy flow rate into the layer minus the energy flow rate out of the layer. Expanding, this equation becomes:

$$\frac{d\theta_1}{dt} = \frac{1}{\rho V C_p}\left[q_{rad} + q_{conv} - \frac{kA}{\Delta h}(\theta_1 - \theta_2)\right] \tag{3.14}$$

where $V = \dfrac{l^2 \Delta h}{2}$ is the volume of the top layer

The $\dfrac{kA}{\Delta h}(\theta_1 - \theta_2)$ term represents the conduction heat transfer from node 1 to 2.

The convection and radiation heat transfer is represented by the equations:

$$q_{conv} = Ah(\theta_\infty - \theta_1) \tag{3.15}$$

$$q_{rad} = A\sigma\mathcal{E}_{eff} f_{correction} \sum_{i=1}^{6} \left(\theta_{heater_i}^4 - \theta_1^4\right) F_{view_i} \tag{3.16}$$

where $f_{correction} = a + b\theta_1$ is a radiation correction factor that is explained in the discussion on model validation

The modeling equations for the interior nodes are somewhat simpler since conduction is the only mode of heat transfer within the sheet itself. The equations for the interior nodes are simply written as:

$$\rho V C_p \frac{d\theta_i}{dt} = Q_{in} - Q_{out}$$

$$= \frac{kA}{\Delta h}\left(\theta_{i-1} - \theta_i\right) - \frac{kA}{\Delta h}\left(\theta_i - \theta_{i+1}\right)$$

$$\therefore \frac{d\theta_i}{dt} = \frac{1}{\rho V C_p}\left[\frac{kA}{\Delta h}\theta_{i-1} - \frac{2kA}{\Delta h}\theta_i + \frac{kA}{\Delta h}\theta_{i+1}\right] \tag{3.17}$$

where $V = l^2\Delta h$ is the volume of the interior layers

The derivation of the equations for the bottom surface, node N, where N is the number of layers/nodes, is the same as that for the top surface. The equation for the bottom layer is given as:

$$\frac{d\theta_N}{dt} = \frac{1}{\rho V C_p}\left[q_{rad} + q_{conv} - \frac{kA}{\Delta h}(\theta_N - \theta_{N-1})\right] \tag{3.18}$$

where $V = \frac{l^2\Delta h}{2}$ is the volume of the bottom layer

The equations for the convection and radiation heat transfer are the same for the bottom layer as those for the top layer with one minor change: $\theta_1 = \theta_N$.

3.4.2.2 Model Validation

Model validation was a multi-step process. To begin the model validation process, the performance of a model with fictitious parameters and material properties was examined. Two basic characteristics were sought after. The first was the ability of the model to predict the basic, U-shaped, temperature distribution through the sheet as shown in figure 3.24. As shown by the curves, the model met this basic requirement. The second characteristic was model stability. The simulated step response of the model for various Matlab integration algorithms was observed and it was found that *ode15s* performed best. The popular *ode45* algorithm resulted in severe oscillatory behavior. It is important to note that the time step size is also important when determining simulation stability. It is important to keep the time step sufficiently small so that the 2nd Law of Thermodynamics is not violated.[5]
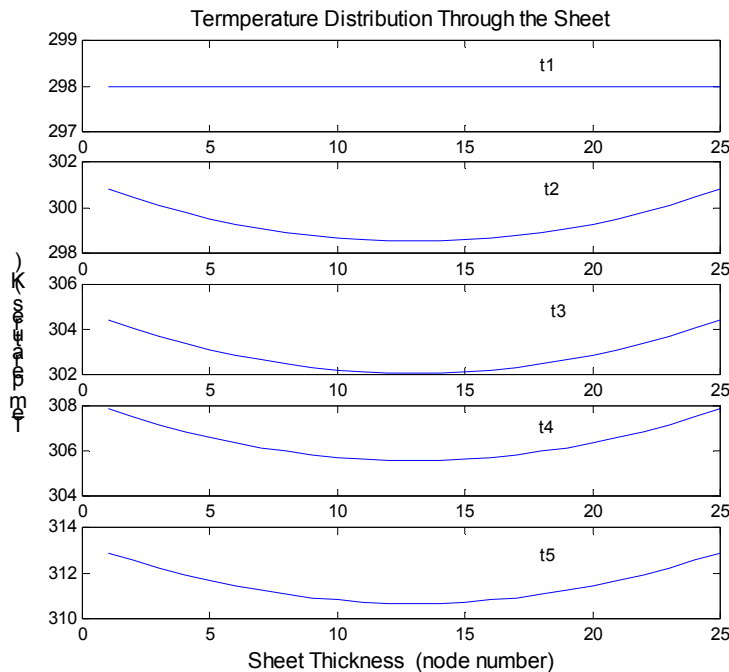

Figure 3.24: *simulated temperature distribution through the sheet at various time instants*

The next step in the model validation process was to determine the number of layers, or nodes. Obviously it is desirable to have a large number of nodes since the true temperature distribution through the sheet will be better represented, but an increase in

---

[5] see[4] for details

70

the number of nodes brings added complexity to the model. After performing a number of simulations, the value for N, the number of nodes, was chosen to be 5.

The final model validation step involved estimating model parameters. Many of the parameters within the sheet heating model are quite uncertain. For example, the material properties, including specific heat, thermal conductivity, and density, have a certain level of uncertainty associated with them. These values are temperature dependant and known to only a certain degree of accuracy.

Similarly, there is a great deal of uncertainty associated with the radiation heat transfer. The effective emissivity is really only an estimate of the level of efficiency of radiation energy exchange. The emissivities of the sheet and heater elements area not well known. Other effects such as reflected radiation energy and energy absorbed by the clamping mechanism only add to the level of uncertainty surrounding the radiation heat transfer. The exact level of convection heat transfer is also not well known. In fact, the convection heat transfer coefficient is the most uncertain parameter within the model. The heat transfer coefficient can range from 2 to 5 for the lower side of the sheet and anywhere from 5 to 30 for the upper side of the sheet depending on air movement.

All of this model uncertainty results in poor model performance when nominal parameters are used. A better estimate of these parameters is then required in order to predict sheet temperatures that are close to measured experimental values. This is the goal of parameter estimation.

It is quite a daunting task to adjust all of the individual model parameters. As a compromise, only a few key parameters were chosen. The upper and lower convection heat transfer coefficients were chosen as adjustable parameters since they are the most uncertain. The radiation correction factor shown in equation (3.16) was also chosen for the parameter estimation procedure. The radiation correction factors simply represent a temperature dependant scaling on the effective emissivities for the upper and lower sides of the sheet. The temperature dependant terms were included in an attempt to account for a number of known temperature dependant phenomena that were left unmodelled (i.e. temperature dependant material properties, sheet sag, etc.)

Three different parameter estimation methods were tested. The first is a basic, unconstrained least squares algorithm. As can be seen from figure 3.25 the results are

very good. The simulated response fits the experimental data (the same T_{surf_nom} data that was used for the black box modeling in Section 3.1) perfectly; however, there is a catch. The parameters that the algorithm converged to were physically unrealizable. For example, the values for both the upper and lower radiation correction factors had large negative terms, which would result in the heaters actually cooling the sheet. Obviously, this is not physically possible.
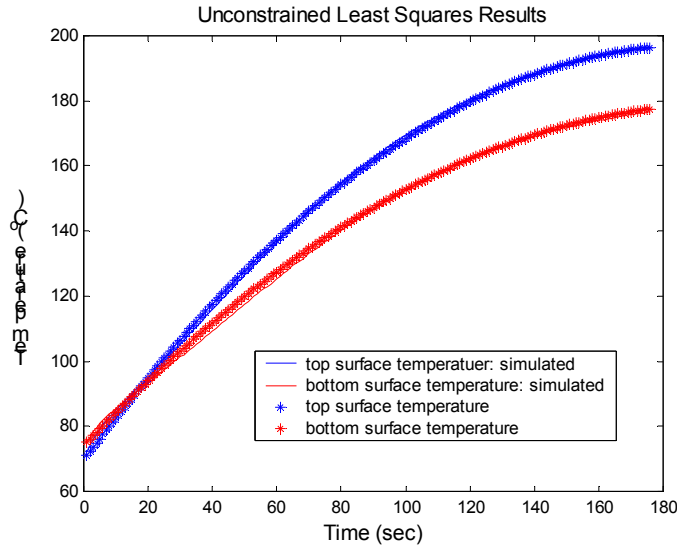
Figure 3.25: *parameter estimation results from unconstrained least squares algorithm*

The second algorithm that was tested was Matlab's nonlinear least squares algorithm *lsqnonlin*. This is a constrained optimization algorithm in which upper and lower bounds can be placed on the estimated parameters. The results were much better in that the estimated parameters fell within a physically realistic range. The fit to the experimental data, however, was not nearly as good as the previous algorithm. Even when very large bounds on the estimated parameters were used, the fit was still not as good as the simple least squares algorithm. The nonlinear least squares algorithm was not easy to apply. Since the system is multivariable and highly nonlinear, slight differences in the initial conditions produced very different results.

The final method of parameter estimation was manual tuning. The model parameters were adjusted manually until the simulation results closely matched the experimental data. The plot shown in figure 3.26 shows the results of the manual tuning. These results were actually better than the sophisticated nonlinear least squares algorithm

results. Also, the time required to perform the manual tuning was not significant. Only a few adjustments had to be made before the results shown were obtained. The final estimated parameters can be found in the Matlab code given in the Appendix. The fact that the radiation correction factors were quite large suggests that the initial estimates of the effective emissivities were way off. This may not necessarily be the case. It is believed that the large correction factors are a result of the discretization of the system. Parameter estimation of this scale is not a trivial process. New techniques and/or "correction functions" could easily be the subject of future work. Additional parameter estimation and model validation results will be given in [26].

3.4.2.3 Disturbances

Sheet heating is subject to a number of disturbances. The most notable is air movement in and around the oven. As mentioned earlier, airflow over the sheet surface can have a drastic effect on the convection heat transfer coefficient. The other important disturbance acting on the system is machine drift. The machine operating parameters can change significantly with time. These changes subsequently result in alterations to the sheet heating dynamics. Due to time constraints, the stochastic properties of the process were not studied in detail. This will be the subject of future work most likely related to cycle-to-cycle control design.
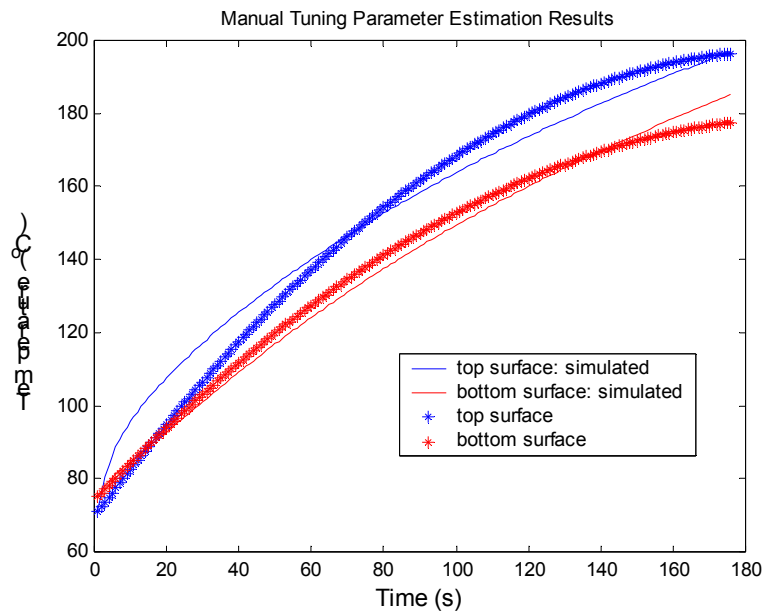
Figure 3.26: *manual tuning parameter estimation results*

73

3.4.2.4 Future Modeling Improvements

Due to the originality of this project, the modeling work on sheet heating presented in this report was only a first attempt. A number of improvements are possible. To begin, a database of temperature dependent material properties is necessary. Some thermoplastic materials exhibit highly nonlinear, temperature dependent behavior characterized by varying specific heat, density, and emissivity values. Using temperature dependent material properties in the sheet heating model will greatly improve performance.

Performance can also be significantly improved by using time-varying values for sheet thickness and radiation view factors, which would better account for the effects of sheet sag. These values would need to be found using the IMI thermoforming simulation software. At the time of completion of this project, the time-varying radiation view factors could not be extracted from the simulation software. A few minor programming modifications were required first.

Finally, improvements could be made by studying some of the unmodelled dynamics including the effects from reflected radiation within the oven and volumetric absorption of radiation energy by the sheet. Proper examination of these topics would, however, require expert knowledge of thermal radiation heat transfer.

4. Controller Development

4.1 Introduction

The definition of controller objectives for this project was an iterative process. Because there is virtually no documented work on in-cycle control of thermoforming, a lot of time was spent on determining the exact role of an in-cycle control design within the overall thermoforming control strategy. The problem was basically treated as a tracking problem where the responsibilities of the in-cycle controller include setpoint tracking, disturbance rejection, and maintaining stability and robustness.

One major assumption was made prior to commencing controller design. It was assumed that the optimal setpoint trajectory was known. In effect, the problems of in-cycle control and setpoint generation were separated from one another. This is important because the setpoint generation problem is beyond the scope of this project, as it would require someone with expert knowledge of thermoforming. It involves determining the appropriate temperature distribution within the sheet such that the desired material distribution of the formed part is met.

The next phase in the controller development was to settle upon an appropriate control strategy that would meet the control objectives. Two strategies were considered. The first involves controlling the sheet centerline temperature directly, which would require the use of a fully functional soft sensor design to estimate the sheet centerline temperatures. This approach was eventually not considered because of the overall complexity of the design. Furthermore, it would not have been possible to fully test this control strategy until the completion of both an in-cycle control design as well as a soft sensor, which would ultimately slow the progress of the project.

The chosen control strategy is much simpler to implement and test. It involves direct control of sheet surface temperatures and indirect control of sheet centerline temperatures. With this approach, the in-cycle control and soft sensor designs are separated. The role of the in-cycle controller is to track the ideal setpoint (figure 4.1) while maintaining stability and rejecting disturbances. The role of the soft sensor is to provide an estimate of sheet centerline temperatures and indicate when the sheet should

be removed from the oven. The idea is that the sheet surface temperature is brought up to its maximum allowable temperature as quickly as possible. The surface temperature is then maintained and the sheet is removed from the oven when the soft sensor detects that the desired sheet centerline temperature is reached. This scheme results in minimal sheet heating time.
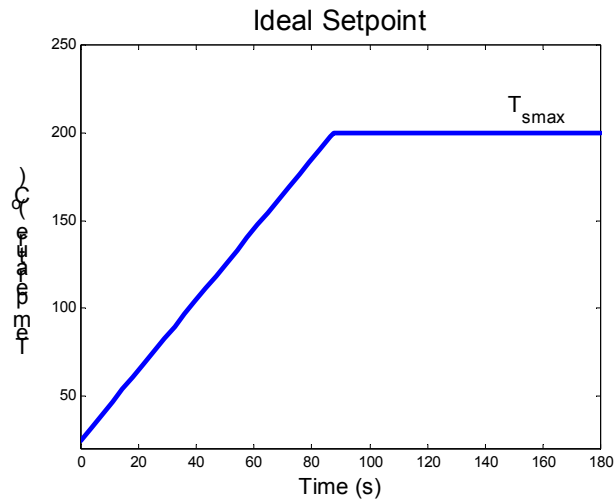
Figure 4.1: *Ideal sheet surface temperature setpoint trajectory. Note that the actual surface temperature trajectory that is obtained will change depending on sheet material, sheet thickness, and heater type.*

The leading designs for in-cycle control are robust H_∞ and model predictive control (MPC) designs. Both of these designs are well suited for multi-input, multi-output (MIMO) processes. PID control was not considered however. Even though PID control is an industry workhorse, it is not directly applicable to MIMO systems. A few other designs were only briefly considered. These included possible artificial neural network designs as well as a feedforward-feedback design similar to the controller structures used for many RTP applications as documented in [13], [19], and [21].

Before discussing the details of the H_∞ and MPC control designs it is interesting to note some of the challenges that make this a difficult control problem. First, the high level of uncertainty of the material properties and radiation heat transfer is a problem. Second, the thermoforming process is highly nonlinear. This may limit the effectiveness of a linear design. Sheet sag also presents challenges. Because sag results in a time varying process, a time invariant control design may also prove to be ineffective. Finally,

76

the uncertainty in the heater surface temperatures presents the most difficult challenge. It is never easy to control a process with poor actuators.

4.2 H_∞ Optimal Controller Design

4.2.1 H_∞ Optimal Control Theory

H_∞ optimal control theory has developed considerably since the early work of Zames. Only the basic design concepts will be presented here however. Full coverage of the subject is given in [8], [11], and [7]. The H_∞ control problem is basically an optimization problem whereby the H_∞ norm of a linear system is minimized using feedback. Before describing the design procedure, a number of definitions are required.

H_∞ Space: This is the vector space of all stable, causal systems with finite H_∞ norms.

H_∞ Norm: Vector and matrix norms typically quantify the "size" of signals and systems. The H_∞ norm of a system gives the maximum gain of the frequency response of the system and is written as:

$$\|H\|_\infty = \sup_{\omega \in \Re} |H(j\omega)| \tag{4.1}$$

The H_∞ norm of a system can be easily calculated in Matlab using the *hinfnorm* command. A few alternative definitions of the H_∞ norm may help to explain its significance. The H_∞ norm of a system's input-output transfer matrix gives the maximum gain of the system from the $\mathcal{L}_2$ norm (size) of its input signal, $x(t)$, to the $\mathcal{L}_2$ norm of its output signal, $y(t)$. Similarly, the H_∞ norm of a system can also be thought of as the maximum power gain of the system.

***μ*-synthesis:** *μ*-synthesis is a control design technique that uses a structured "norm" similar to the H_∞ norm of the system for the controller design. The *D-K* Iteration is the name of the algorithm that is used to calculate the actual optimal controller, K, in Matlab.

Linear Fractional Transformation (LFT): The LFT is a convenient tool that is used to represent the interconnection of feedback control system components in a very general structure. LFT's are not absolutely necessary for SISO systems but they are very useful for MIMO systems, and as such, the LFT is used with Matlab's H_∞ design toolboxes. Detailed information on how to construct an LFT is given in [7] and [10]. The LFT notation is given in figure 4.2. The structure in figure 4.2 is a lower LFT structure (denoted by $\mathcal{F}_\mathrm{L}[P(s),\ K(s)]$) where *P(s)* is the generalized plant.[6] *K(s)* is the feedback controller. *u* is the controller output. The measured error between a subset of the system inputs, *w*, and outputs, *z,* is represented by the *e* signal.
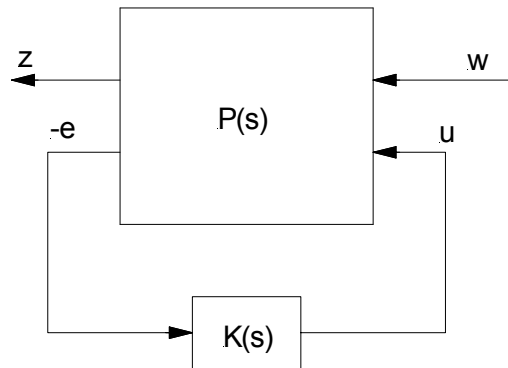
Figure 4.2: *Basic LFT notation for H_∞ control design.*

Design Problem

Using the LFT notation, the standard H_∞ problem is written as:

$$\min_{K \in S} \ \left\| T_{zw} \right\|_\infty \tag{4.2}$$

This is a minimization problem that involves calculating the optimal controller *K*, such that the transfer matrix, T_{zw}, is stabilized and its H_∞ norm is minimized. Referring to

---

[6] *P(s)* is also an LFT structure that can be constructed using Matlab's *sysic* command.

figure 4.2, the transfer matrix, T_{zw}, is the closed loop transfer matrix from the exogenous inputs, w, to the output, z, where $T_{zw} = \mathcal{F}_L[P(s),\ K(s)]$. Unfortunately, this is an extremely difficult problem to solve. As a compromise, the sub-optimal H_∞ problem is most often considered. The sub-optimal problem is stated as:

Given $\gamma > 0$, find an admissible controller (if one exists) such that $\|T_{zw}\|_\infty < \gamma$, given the generalized plant model, P(s), and the performance level, γ.

The sub-optimal controller can be calculated directly using the Matlab command *hinfsyn*. The details of exactly how the sub-optimal controller is found is not too important for this discussion. It is important, however, to mention the assumptions that must be verified before the *hinfsysn* command is utilized. To begin, suppose that a stable state-space realization of the generalized plant, *P(s)*, is given by:

$$P(s) = \begin{bmatrix} A & B_1 & B_2 \\ C_1 & 0 & D_{12} \\ C_2 & D_{21} & 0 \end{bmatrix} \tag{4.3}$$

The following assumptions[7] are then made before computing the sub-optimal controller:

A1: The pair (A, B_1) is stabilizable and the pair (A, C_1) is detectable

A2: The pair (A, B_2) is stabilizable and the pair (A, C_2) is detectable

A3: $D_{12}^T \begin{bmatrix} C_1 & D_{12} \end{bmatrix} = \begin{bmatrix} 0 & I \end{bmatrix}$

A4: $\begin{bmatrix} B_1 \\ D_{12} \end{bmatrix} D_{21}^T = \begin{bmatrix} 0 \\ I \end{bmatrix}$

Uncertainty Modeling and Robustness

The most significant aspect of the H_∞ control theory is its ability to accommodate model uncertainties. A certain level of model uncertainty will always exist since the mathematical models used for the control design are only approximations of the actual physical processes. Modeling errors, or uncertainty, can result from any combination of

---

[7] Consult the *h_inf_build_model_unstruc.m* file in the Appendix for details on how to check these assumptions. More details can be found in [7].

unmodeled process dynamics including nonlinearities, variations in the model parameters, uncertainty in the actuator and sensor dynamics, and model order reduction. The H_∞ control theory allows one to design robust controllers that will remain stable in the presence of model uncertainty. In other words, an H_∞ controller will ensure stability even though the mathematical models may not accurately describe the actual process.

There are two ways of representing uncertainty: *structured and unstructured* model uncertainty. The latter will be considered first. Unstructured uncertainty can be used to lump a number of modeling errors into a single perturbation. Additive and multiplicative uncertainty are the two basic forms of unstructured uncertainty. Additive uncertainty is represented by equation (4.4) and figure 4.3.

$$G_p(s) = G(s) + \Delta_a(s)$$
$$\text{where } \left\| \Delta_a(j\omega) \right\|_\infty < \delta_a(\omega), \forall \omega$$

(4.4)
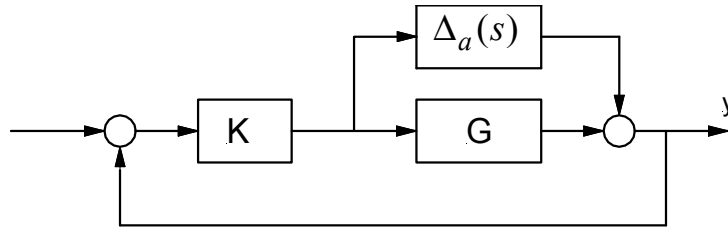
Figure 4.3: *additive uncertainty*

Equation (4.4) is saying that the actual physical process is represented by the nominal plant, *G(s)*, plus the lumped perturbation, $\Delta_a(s)$. The second line in equation (4.4) states that only the size of the perturbation, not its structure, is known, and that the upper bound of the perturbation will be less than $\delta_a(\omega)$ for all ω.

One form of multiplicative uncertainty is given by equation (4.5). The structure is shown in figure 4.4.

$$G_p(s) = \left(I_p + \Delta_m(s) \right) G(s)$$
$$\text{where } \left\| \Delta_m(j\omega) \right\|_\infty < \delta_m(\omega), \forall \omega$$

(4.5)
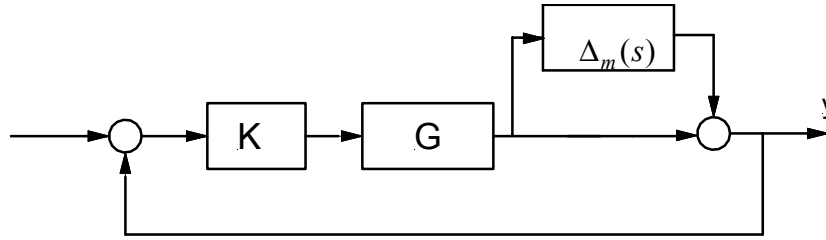
Figure 4.4: *output multiplicative uncertainty*

Equation (4.5) is stating that the actual plant is represented by the nominal plant, *G(s)*, plus the scaling of the nominal plant by the perturbation, $\Delta_m(s)$. The second line in equation (4.5) gives the upper bound of the perturbation $\Delta_m(s)$.

Since the structures in figures 4.3 and 4.4 can be represented by an LFT structure, the conditions for robust stability will only be given for the LFT uncertainty structure shown in figure 4.5.

Conditions for robust stability with the LFT structure are:

$$\| \mathcal{F}_{\mathrm{L}}[P(s), K(s)] \|_\infty \leq 1 \tag{4.6a}$$

$$\text{with } \Delta(s) = W(s)\tilde{\Delta}(s) \tag{4.6b}$$

$$\left\| \tilde{\Delta}(s) \right\|_\infty < 1 \tag{4.6c}$$

Figure 4.5: *LFT uncertainty structure*

Equation (4.6a) states that closed loop stability will be ensured for a family of plants represented by the combination of the nominal plant, *P(s)*, and the perturbation, $\Delta(s)$.

81

The weighting function, *W(s)*, in equation (4.6b) is a design parameter. As was the case for the δ's in equations 4.4 and 4.5, *W(s)* represents the frequency dependent upper bound on the perturbation, Δ(s). Finally, equation (4.6c) indicates that the standard H_∞ control theory (which requires that $\|\Delta(s)\|_\infty < 1$) can be used for controller design by letting $\Delta(s) = W(s)\tilde{\Delta}(s)$ and then bringing *W(s)* "inside" of the generalized plant P(s).

As mentioned earlier, unstructured uncertainty can be used to lump a number of uncertainties into one perturbation block. Sometimes it may be desirable to represent the uncertainty due to the variation of individual model parameters. 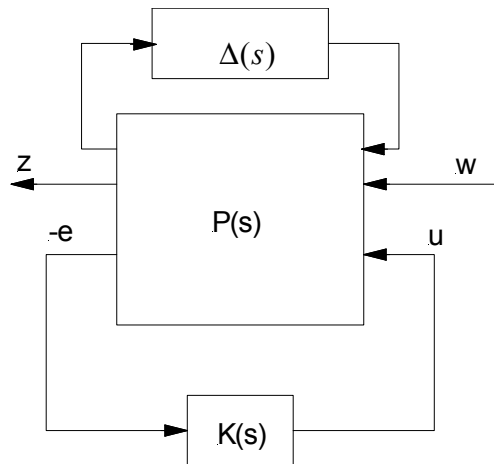This type of uncertainty is best represented using the structured uncertainty approach. The basic idea of structured uncertainty modeling is that each uncertain parameter will have its own individual Δ block within the LFT diagram. Structured uncertainty modeling will be discussed in more detail in section 4.2.2

Performance Specifications

The H_∞ control theory is a powerful tool for the design of robust, stable controllers; however, stability is only the most basic requirement in feedback control systems. Closed loop feedback control designs must also offer a certain level of performance. Performance specifications for the H_∞ design are achieved via the concept of mixed-sensitivity robust H_∞ control design. The mixed-sensitivity design involves adding fictitious uncertainty blocks to the LFT structure to accommodate performance specifications. The diagram shown in figure 4.6 will be used to identify the most common performance specifications used for H_∞ controller design. The *h_inf_build_model_unstruc.m* file in the Appendix can be used as a reference on how to build the LFT structure used for the mixed-sensitivity design. The *P* block in the figure represents, in LFT format, the generalized plant with uncertainty. The *K* block represents the controller. The remaining "*W*" blocks are used to represent various performance specification weighting functions. These weighting functions are tuning parameters that are chosen by the designer to achieve the best compromise between conflicting objectives. The weighting functions are also used for normalization of signals for the case when different units are involved. Similarly, the weighting functions can be used to

place a lesser or greater importance on a particular signal. Table 4.1 summarizes the "W" blocks found in figure 4.6.
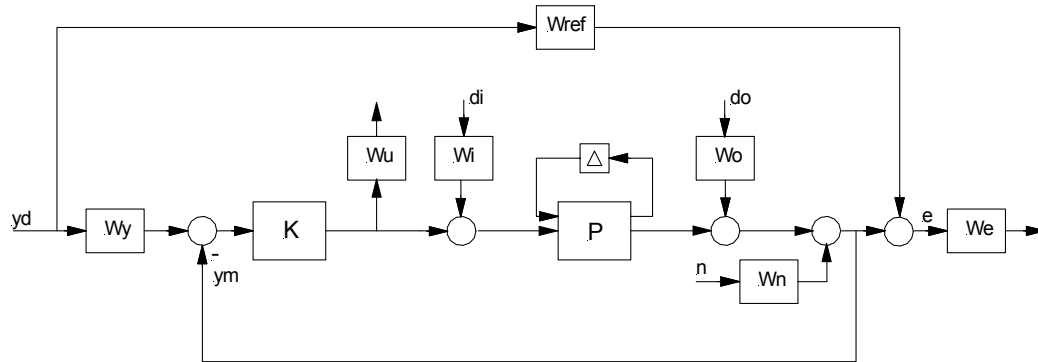
Figure 4.6: *mixed-sensitivity H$_\infty$ design structure*

Table 4.1: *H$_\infty$ design performance weighting functions*

Weighting Function	Description
W_y	is used in problems requring tracking of a reference signal. It describes the magnitude and frequency dependance of the reference signal.
W_{ref}	is used in model matching design problems. It represents the desired closed loop performance.
W_u	is used to constrain the actuators so that they operate within their normal operating range.
W_i	represents the frequency content and magnitude of exogenous disturbances at the plant input.
W_o	represents the frequency content and magnitude of exogenous disturbances at the plant output.
W_n	represents the frequency content of the measurement noise.
W_e	is used to weight and shape the frequency dependant sensitivity function

4.2.2 H$_\infty$ Controller Design

The *H$_\infty$* controller design procedure will be outlined with reference to the interconnection structure shown in figure 4.7 and the information in tables 4.2 and 4.3.
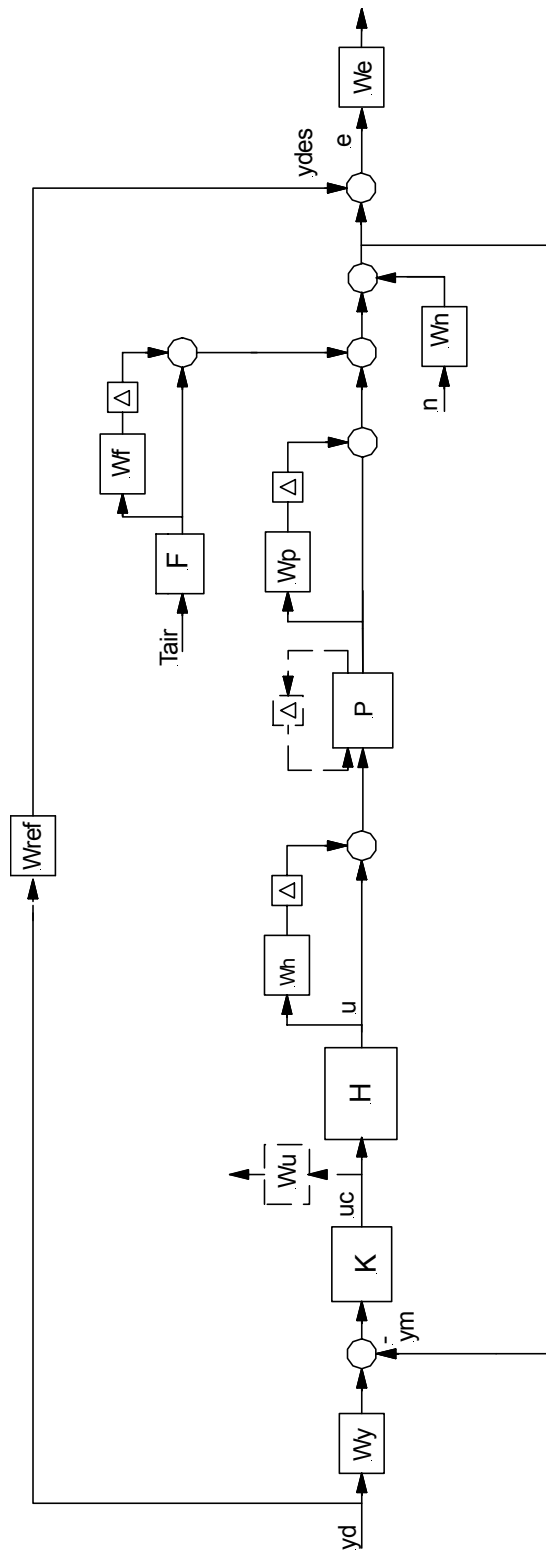
Figure 4.7: H_∞ controller design interconnection

Table 4.2: *signal definitions for H_∞ control design*

Signal	Definition
y_d	desired sheet surface temperature setpoint
e	measured error between the desired and actual sheet surface temperature
u_c	controller output: embedded heater setpoint temperature
u	heater surface temperature
T_{air}	oven air temperature
y_m	measured sheet surface temperature
n	measurement noise
y_{des}	desired sheet surface temperature for model matching design

Table 4.3: *block definitions for H_∞ controller design*

| Block Name	Definition
W_y	setpoint weighting function
W_{des}	desired closed loop transfer function for model matching design
K	controller
W_u	weighting function for control moves
H	linearized heater model
W_h	heater uncertainty weighting function
P	linearized sheet heating model
W_p	sheet heating model uncertainty weighting function
F	linearized oven air temperature model
W_f	oven air temperature uncertainty weighting function
W_n	measurement noise weighting function

The *F* block in figure 4.7 is unfamiliar at this point. This block represents the linearized transfer function from the oven air temperature to the sheet surface temperature. The *F* block represents the convection heat transfer dynamics, and it is separated from the sheet model as a result of the linearization. Since the oven air temperature cannot be directly controlled, T_{air}, is treated as a measureable disturbance with known dynamics acting on the system rather than a controlled input into the sheet model. The second feature in figure 4.7 that is not immediately clear is the inclusion of the dashed components. These components simply represent the location of blocks that were used for alternative

designs.   All solid lines represent the system interconnection for the primary H_∞ controller design.

The first controller design step was uncertainty modeling for the heater, sheet, and air disturbance models. The air disturbance model, F, is considered first. For the 4-input, 2-output design, with two oven air temperature measurements (one above and one below the sheet) F becomes:

$$F = \begin{bmatrix} \dfrac{Ah_{upper}}{\rho V C_p} & 0 \\[3ex] 0 & \dfrac{Ah_{lower}}{\rho V C_p} \end{bmatrix} \tag{4.7}$$

where h_{upper} and h_{lower} are the upper and lower convection heat transfer coefficients respectively. V is the volume of the sheet surface layers (i.e. the volume of nodes 1 and N). Now, it is known that the upper heat transfer coefficient ranges from about 5 to 30, and the lower heat transfer coefficient ranges from about 3 to 5. The multiplicative uncertainty weighting function for the air disturbance model, W_f, then becomes:

$$W_f = \begin{bmatrix} \dfrac{\Delta h_{upper}}{h_{upper}} & 0 \\[3ex] 0 & \dfrac{\Delta h_{lower}}{h_{lower}} \end{bmatrix} \tag{4.8}$$

The Δh terms are simply found by taking the absolute difference between the nominal heat transfer coefficients and the chosen maximum value (e.g. $\Delta h_{upper} = \left| h_{upper} - 30 \right|$).

The heater model uncertainty is also conveniently represented using the multiplicative uncertainty structure.   The results from the heater identification experiments indicate that there is about a 40 $^{\circ}$C variation in temperature across the heater surface. At nominal heater operating temperatures of around 625 K, this translates into an uncertainty of about +/- 3 percent. A slightly less conservative estimate of 2 percent was used for the actual design. The W_h block is written as:

$$
W_h = \begin{bmatrix} 0.02 & 0 & 0 & 0 \\ 0 & 0.02 & 0 & 0 \\ 0 & 0 & 0.02 & 0 \\ 0 & 0 & 0 & 0.02 \end{bmatrix}
\tag{4.9}
$$

The uncertainty modeling for the sheet heating model is slightly more complicated because there are far more sources of uncertainty. Both structured and unstructured uncertainty designs were evaluated. Structured, parametric uncertainty was considered first. The possible range in value for each uncertain sheet model parameter is given below in table 4.4.

Table 4.4: *parameter uncertainty levels for sheet heating model*

Parameter	Level of Uncertainty
delay	4 to 7 seconds
heater surface temperature	2 % to 5 %
convection heat transfer coefficient	values range from 2 to 5 for bottom and 5 to 30 for top
effective emissivity	values range from 0.5 to 0.9
thermal conductivity[*]	10 %
density[*]	5 %
specific heat[*]	5 %
radiation view factors	average < 30 %
sheet thickness[**]	not well known

* Only an estimate. Will be higher if constant value is used in model.
** *Very little uncertainty if varying thickness is used, otherwise uncertainty depends on material and original sheet thickness.*

Before proceeding with the structured uncertainty design a sensitivity analysis was performed in order to identify the key model parameters. The sensitivity analysis results also helped in the tuning of the model parameters during the model validation procedure. The results will be presented in [26].

The parametric uncertainty modeling was implemented as follows:

The uncertain state space system is represented as:

$$
\begin{bmatrix} \dot{x}(t) \\ y(t) \end{bmatrix} = \left(\begin{bmatrix} A_0 & B_0 \\ C_0 & D_0 \end{bmatrix} + \sum_{i=1}^{m} \delta_i \begin{bmatrix} A_i & B_i \\ C_i & D_i \end{bmatrix} \right) \begin{bmatrix} x(t) \\ u(t) \end{bmatrix}
\tag{4.10}
$$

where A_0, B_0, C_0, and D_0 are the original state space matrices. For each of the *m* uncertain parameters within the model a new set of perturbed matrices is generated.

now let $r_i = rank \begin{bmatrix} A_i & B_i \\ C_i & D_i \end{bmatrix}$ (4.11)

and then factor each matrix using singular value decomposition as:

$$\begin{bmatrix} A_i & B_i \\ C_i & D_i \end{bmatrix} = \begin{bmatrix} E_i \\ F_i \end{bmatrix} [G_i \quad H_i]$$ (4.12)

where $\begin{bmatrix} E_i \\ F_i \end{bmatrix} \in R^{(n+ny)\times r_i}$, $[G_i \quad H_i] \in R^{r_i \times (n+ny)}$

Now define a new generalized plant with the added inputs and outputs:

$$\begin{bmatrix} \dot{x} \\ y \\ z_1 \\ \vdots \\ z_m \end{bmatrix} = \begin{bmatrix} A_0 & B_0 & E_1 & \cdots & E_m \\ C_0 & D_0 & F_1 & \cdots & F_m \\ G_1 & H_1 & 0 & \cdots & 0 \\ \vdots & \vdots & \vdots & \ddots & \vdots \\ G_m & G_m & 0 & \cdots & 0 \end{bmatrix} \begin{bmatrix} x \\ u \\ w_1 \\ \vdots \\ w_m \end{bmatrix}$$ (4.13)

The *h_inf_build_model_struc.m* file in the Appendix can be consulted for more details on the parametric uncertainty modeling procedure.

An unstructured output multiplicative uncertainty modeling approach was also considered. The results shown in figure 4.8 were obtained by performing a Monte Carlo type analysis, which involved comparing the frequency response of various perturbed models with a nominal response. As can be seen from the figure, the level of uncertainty is very high even at low frequencies, where the uncertainty is nearly 125 percent. Fortunately, the bandwidth of the system is very low (aprox. 0.001 rads/sec for the sheet heating model), which means that the very high uncertainty at higher frequencies can be ignored.
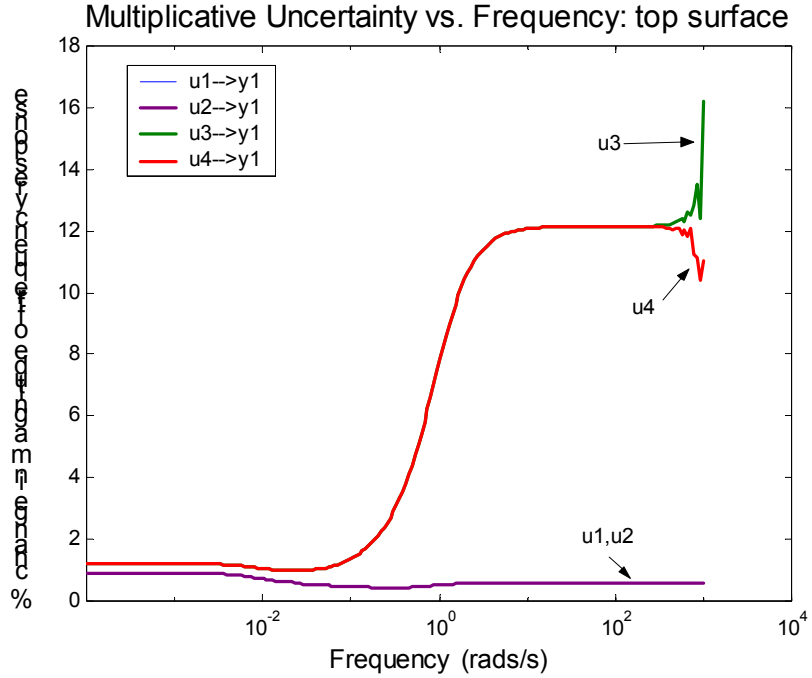
Figure 4.8: *H_∞ multiplicative uncertainty results*

The form of the multiplicative uncertainty weighting function, W_p, that was used is:

$$W_p = \begin{bmatrix} \dfrac{a_0}{\left(w_b s + 1\right)^2} & 0 \\ 0 & \dfrac{a_0}{\left(w_b s + 1\right)^2} \end{bmatrix} \tag{4.14}$$

where a_0 and w_b were chosen to reflect the desired level of uncertainty.

After comparing the results from both uncertainty designs it was decided that the multiplicative uncertainty was the best approach mainly because of its simplicity. It seems that the very large system matrices that resulted from the structured uncertainty design led to more conservative controller designs. In fact, the D-K iteration for the structured uncertainty design, which considers only three parameters, resulted in larger μ values than for the unstructured design, which considers all uncertain parameters.

Performance Specifications

The performance specifications will now be discussed with reference to the design structure from figure 4.7.

Measurement Noise

Measurement noise is not a major concern for the Raytek IR sensors used on the IMI machine because the measurements are pre-filtered and quite stable. A low weighted W_n was chosen as:

$$W_n = \begin{bmatrix} 1e-5 & 0 \\ 0 & 1e-5 \end{bmatrix} \qquad (4.15)$$

Setpoint

A weighting function on the setpoint reference signal was used for some designs to account for the fact that the reference signal, y_d, will never contain any high frequency content. The use of W_y allowed for a more aggressive weighting on the error function W_e. W_y was chosen as:

$$W_y = \begin{bmatrix} \dfrac{1}{500s+1} & 0 \\ 0 & \dfrac{1}{500s+1} \end{bmatrix} \qquad (4.16)$$

Model Matching Design

The model matching design shown in figure 4.7 was used in an attempt to "slow" the control action and reduce some of the overshoot that was observed in some of the early simulations. The form for W_{des} is that of a 2nd order transfer function:

$$W_{des} = \begin{bmatrix} \dfrac{\omega_n^2}{s^2 + 2\zeta\omega_n s + \omega_n^2} & 0 \\[4mm] 0 & \dfrac{\omega_n^2}{s^2 + 2\zeta\omega_n s + \omega_n^2} \end{bmatrix} \qquad (4.17)$$

Values for ω_n were chosen to be around 0.001 and the damping ratio, ζ, was chosen to be around 0.8.

Control Moves

The control moves were constrained with the use of W_u. The desired shape of this weighting function is shown below in figure 4.9. The larger weighting at higher frequencies is used to prevent the actuators from responding to any higher frequency content in the error signal; therefore, W_u constrains the heaters to operate within their natural bandwidth (aprox. 0.05 rads/sec). This prevents unnecessary wear and tear on the actuators.

The form of W_u is:

$$W_u = \begin{bmatrix} k\dfrac{50000s+1}{s+10} & 0 & 0 & 0 \\[4mm] 0 & k\dfrac{50000s+1}{s+10} & 0 & 0 \\[4mm] 0 & 0 & k\dfrac{50000s+1}{s+10} & 0 \\[4mm] 0 & 0 & 0 & k\dfrac{50000s+1}{s+10} \end{bmatrix} \qquad (4.18)$$

The k term was used to scale the numerator of W_u to prevent heater saturation. Values for k were anywhere between 0.1 and 0.000 001 depending on the simulation conditions.

Error

The weight on the error signal, W_e, was the primary controller design parameter. The ideal shape of the frequency response for W_e is that of a 1st or 2nd order frequency
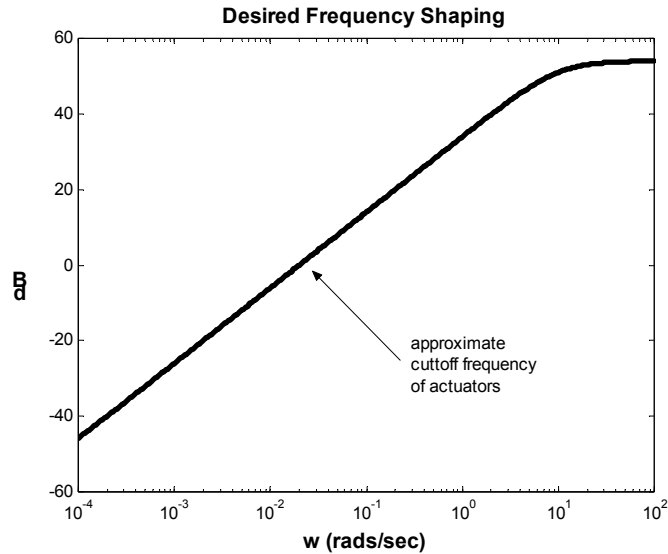
Figure 4.9: *desired shape of control moves weighting function*

response with a steady roll off beginning near the bandwidth of the plant. Ideally, one wants the error weighting function to have a large DC gain (large *k*) and a large bandwidth (small *a*) so that the controller will respond as quickly as possible with a minimum amount of steady state error. The form of W_e is given as:

$$W_e = \begin{bmatrix} \dfrac{k}{(as+1)^2} & 0 \\ 0 & \dfrac{k}{(as+1)^2} \end{bmatrix} \tag{4.19}$$

The values of *k* and *a* used for controller testing are given in the Matlab *h_inf_build_model_unstruc.m* in the Appendix.

It is interesting to note that the performance specifications, most notably W_u and W_e, had the greatest effects on the calculation of μ. As a result, the level of controller performance was less than what was originally hoped for. This was unexpected given the high level of uncertainty. An increase in the level of performance had a larger effect on μ than did an increase in uncertainty.

4.2.3 Simulation Results

The effectiveness of several H_∞ controller designs was evaluated based on simulation results. The linear controllers were tested using the full nonlinear Simulink model given in the Appendix. Early controller designs were unsuccessful because of the very high uncertainty level. With full uncertainty, the level of performance was so small that the controller effectively did not respond to reasonably sized error signals. To compensate, the level of uncertainty was reduced in order to achieve a higher level of robust performance. The fact that the uncertainty level was actually reduced by more than 50 percent and no stability problems were observed, suggests that the original level of uncertainty was a very conservative estimate.

The simulated responses for two different setpoints are of interest. The first setpoint is simply the step response of a simple first order system as seen in figure 4.11. The reason why this type of setpoint trajectory was used instead of an actual step is because a step setpoint would never be applied in a real application. The first order response setpoint is then much more realistic. The simulations for this setpoint will be referred to as "long-cycle" simulations in this discussion. The long-cycle simulations were performed in order to evaluate stability, overshoot, and steady state error. No disturbances or model perturbations were introduced for the long-cycle simulations.

Figure 4.10 shows the long-cycle simulation results. The controller used for this simulation was the model matching design, which results in relatively slow control action as can be seen by the lagging response early on in the cycle time. The steady state error performance is quite good (less than 5 $^{\circ}$C) and there is no significant overshoot. A large overshoot will occur, however, if the initial heater band temperatures were set too high. For example, if the initial heater temperatures were set such that the natural steady state sheet surface temperatures were near 300 $^{\circ}$C, and the final setpoint value was 200 $^{\circ}$C, significant overshoot would result. This is because the controller expects the heaters to cool as fast as they will heat up, but the heaters can only cool at their very slow, natural rate. When the heaters are called upon to operate in "cooling mode" the performance of the control system suffers greatly and overshoot becomes a major problem since the system is effectively operated in open loop until a "heating mode" is resumed.
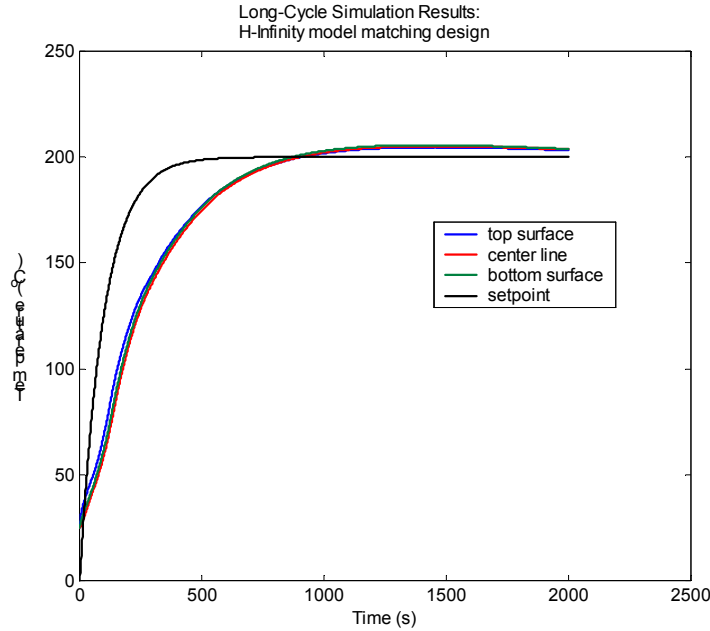
Figure 4.10: *long-cycle H∞ simulation results: sheet surface temperatures*

The simulations for the second setpoint will be referred to as the "short-cycle" simulations. The setpoint for the short-cycle simulations was the actual open loop temperature response for the IMI machine. The data was recorded during the sheet heating model system identification experiments. External disturbances and model parameter perturbations were introduced for the short-cycle simulations in order to examine closed loop stability, robustness, and disturbance rejection.

The model matching design that was used in the long-cycle simulation was also tried with the short-cycle simulation; however, the results were not good. Because the cycle time was much shorter, the controller did not have much time to respond to the error signal, and as a result, the controller had very little impact on the response. This suggests the need for a more aggressive controller design that will respond more quickly and have a greater impact on sheet temperatures for short-cycle applications. A new controller was then designed for the short-cycle simulations. The new design was a regular design without model matching (see figure 4.7 for placement of W_e). The weight on the error was increased at all frequencies which resulted in more aggressive control. The results of the short-cycle simulations are shown below in figures 4.11a and 4.11b.

94
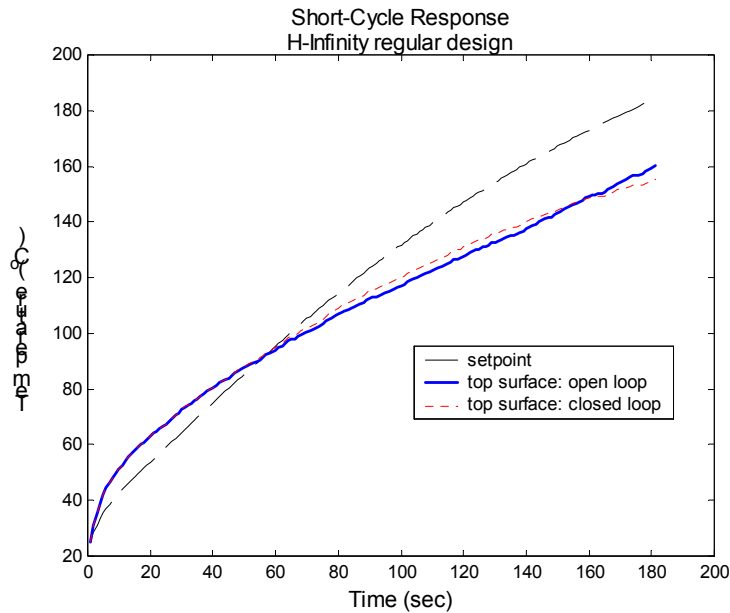
Figure 4.11a: *short-cycle H∞ simulation results: sheet surface temperatures*
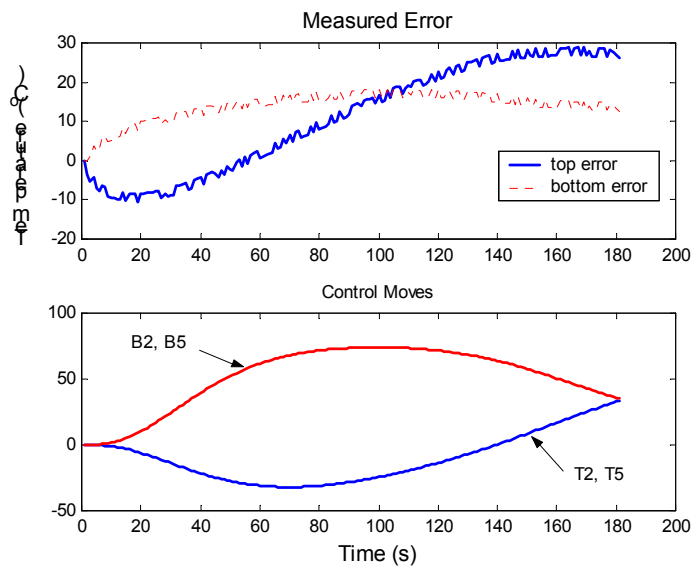
Figure 4.11b: *short-cycle H∞ simulation results: error signal and control moves*

The plot for the control moves in figure 4.11b indicates that the controller remained stable in the presence of disturbances and model perturbations. The control moves were constrained to be within the bandwidth and saturation limits of the heaters. The plot also indicates that the controller did not respond to the high frequency noise in the error signal. This is good news. The bad news is that the closed loop response is not

95

significantly different than the open loop response, even with the use of the rather aggressive controller design. This being said, it is safe to say that in-cycle control for short-cycle applications will have a limited effectiveness at best. This is because the system cannot be pushed very far beyond its natural bandwidth.

The H_∞ control simulation results suggest that dual mode control may be necessary. This means that a single controller design is not suitable for both short-cycle (thin sheet) and long-cycle (thick sheet) applications. Slow control action is required for thick sheet applications in order to avoid overshoot and more aggressive control action is required for thin sheet applications. It has already been stated that the slower model matching design did not perform well in the short-cycle simulation. Conversely, the more aggressive control design did not perform well in the long-cycle simulation as can be seen from the massive overshoot exhibited in figure 4.12.
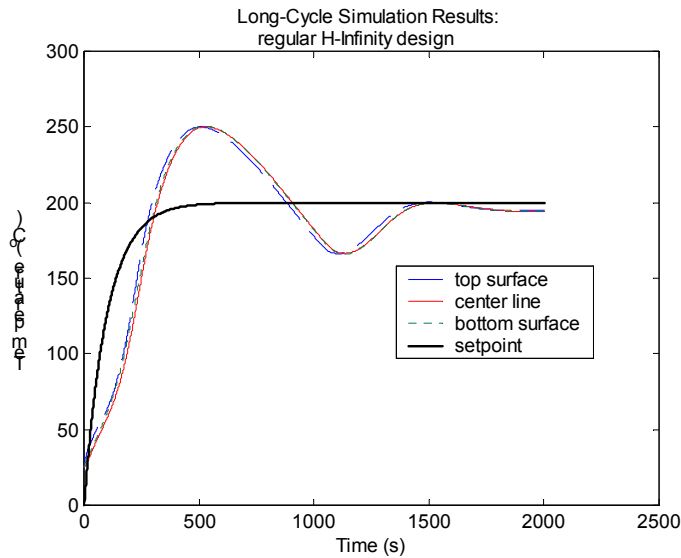
Figure 4.12: *long-cycle H_∞ simulation results with aggressive controller design*

The discussion so far has been centered around the closed loop simulation results of a simplified, low order, 2-input, 4-output controller design. A few simulations were also performed for a full order, 10-input, 12-output controller design. In this design, all twelve heater zones are considered as well as five sheet zones. The long-cycle simulation results are shown in figure 4.13. Although the sheet temperatures come quite close to the

final setpoint value of 200 °C, there is a much larger steady state offset than for the low order case.
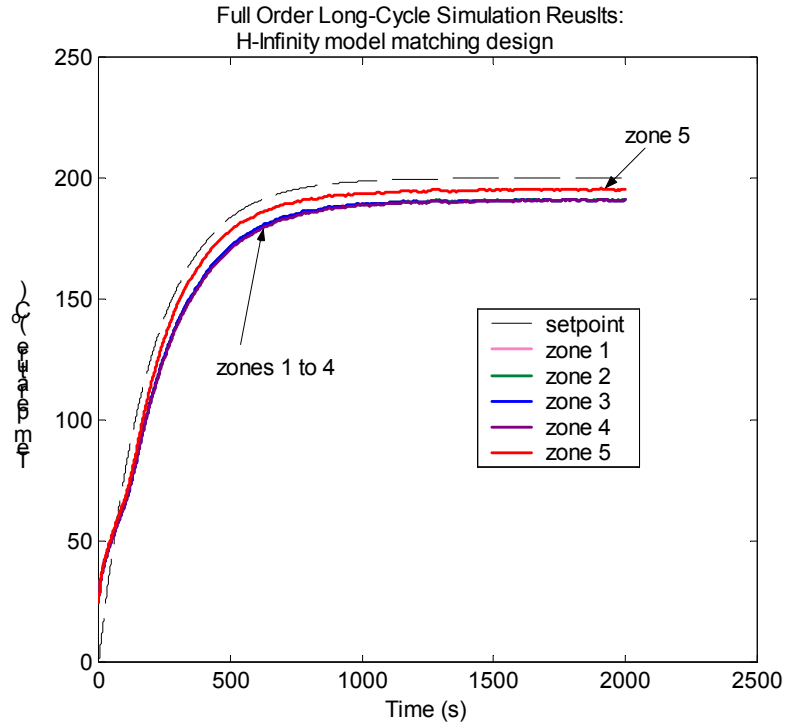
Figure 4.13: *long-cycle H_∞ simulation results for full order controller*

4.2.4 Stability Analysis

The H_∞ controller designs were evaluated by examining the results of the mixed sensitivity closed loop μ calculations. Since stability is the most basic requirement, the closed loop robust stability was evaluated by considering the closed loop μ calculations for interconnection structures without any performance specifications. The mixed sensitivity closed loop μ results for the more aggressive, high performance, controller design used for the short-cycle simulations is shown below in figure 4.14.

As can be seen from the figure, the controller design does not ensure robust stability and robust performance. One can live with the possibility of reduced robust performance due to model uncertainties; however, robust stability is more critical. The

robust stability of this controller design was assessed by observing the closed loop μ calculations for various levels of uncertainty shown below in figure 4.15.
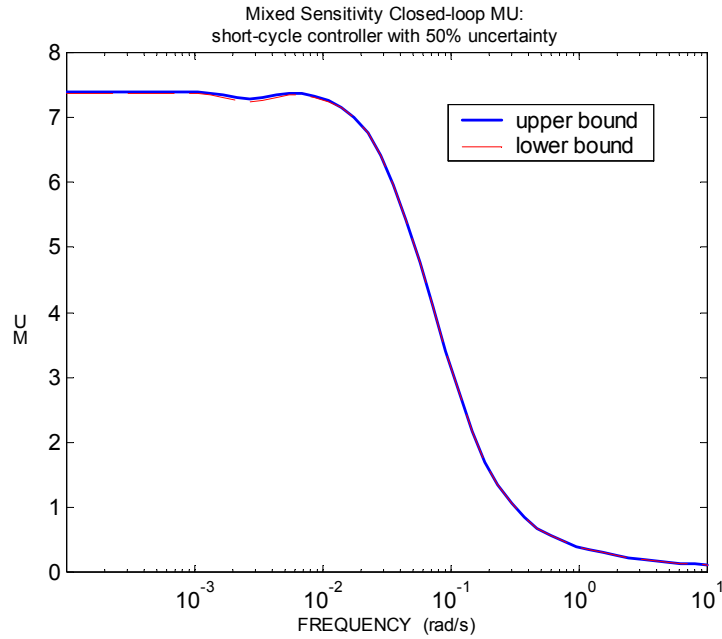

Figure 4.14: *mixed-sensitivity closed loop μ results for short-cycle controller design*
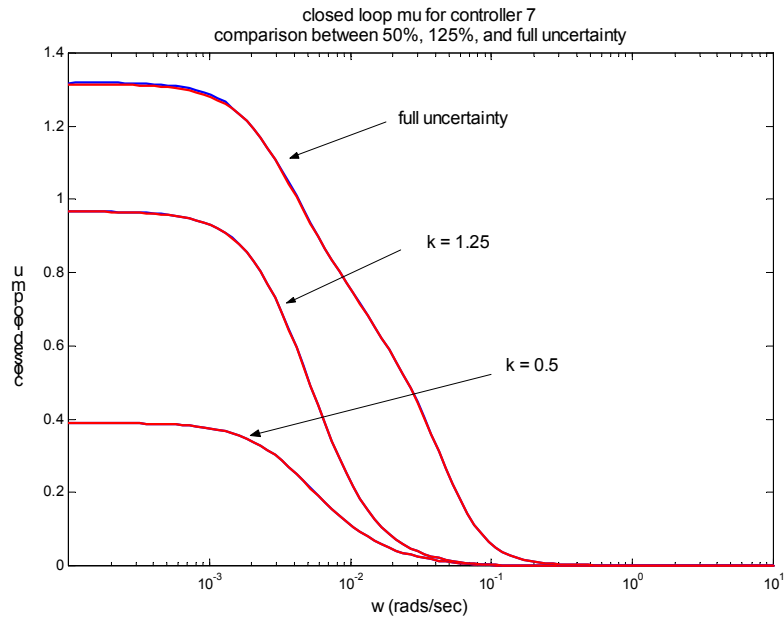

Figure 4.15: *closed loop μ results for short-cycle controller design: no performance specifications*

The upper curve indicates that robust stability is not ensured for full sheet model multiplicative uncertainty (see figure 4.8). This is not necessarily bad news because the very high uncertainty that appears well above the system bandwidth can be ignored as mentioned earlier. The middle curve represents the closed loop μ for a more realistic level of uncertainty represented by:

$$\frac{k}{(200s+1)^2} \qquad (4.20)$$

where k represents the level of uncertainty (k x 100%) at low frequencies. A k value of 1.25 represents 125 percent uncertainty at lower frequencies. The middle curve indicates that the closed loop system will remain stable for this realistic level of uncertainty. This is good news since the full level of uncertainty of the overall system was more likely overestimated rather than under estimated. The lower curve shows the closed loop μ for the 50 percent level uncertainty that was used for the controller designs.

4.3 MPC Design

4.3.1 Introduction

The model predictive control (MPC) design methodology is based on a relatively few number of basic concepts. As its name suggests, the concept of using future predictions from a process model is at the heart of the MPC design. MPC is basically an optimization problem which involves the minimization of a cost function of the form:

$$
\begin{aligned}
J = \min_{\Delta u} \sum_{i=1}^{Np} & \left[\hat{y}(t+i)-y_r(t+i)\right] Q_i \left[\hat{y}(t+i)-y_r(t+i)\right]^T \\
& + \sum_{i=0}^{N_u-1}\left[\Delta u(t+i)^T R_i \Delta u(t+i)\right]
\end{aligned}
\qquad (4.21)
$$

From the equation it is clear that MPC operates in discrete time. The MPC controller calculates the control moves by solving (4.21) at each sampling instant. The first term in equation (4.21) corresponds to the minimization of the predicted errors, $\hat{y}-y_r$, over a

future time period known as the prediction horizon, N_p. The second term in the equation corresponds to the minimization of the overall size of the control moves, Δu, over a time period known as the control horizon, N_u. The Q and R terms are simply scaling terms that can be used as tuning parameters to shape the weight of the cost function over the prediction and control horizons respectively.

The general MPC control algorithm involves the following basic steps which are taken at each sampling instant:

1) sample the process

2) calculate the future outputs, $\hat{y}$, over the prediction horizon using the process model

3) calculate the set of control moves over the control horizon by solving the cost function

4) update the process by sending only the first control move (i.e. $\Delta u(t+0)$) to the process, all other future control moves are discarded.

The MPC design methodology actually covers a wide range of controllers; however, they all follow the same basic algorithm presented above. The primary differences between designs are the form of the process models that are used to calculate the predicted outputs and the way in which disturbances are handled. The various MPC designs will not be discussed here since they are well documented in the literature (see [8]).

4.3.2 MPC Controller Design

Many MPC applications utilize linear models for prediction of future plant outputs. This can be done if the process is operating in a relatively small region around a steady state operating point. The use of linear models also greatly simplifies the minimization of the cost function since the minimization problem can be put into the form of a standard quadratic programming problem in which a solution is easily attainable.

Unfortunately, thermoforming does not fall into this category. The process model is highly nonlinear, and the operating range is wide (25 to 200 ^{o}C). As such, it is not

possible for a single linear model to accurately predict sheet temperatures over the entire prediction horizon. It is also not feasible to use multiple models, or gain scheduling, because even though you will have a new model or operating point at each sampling instant, the actual sheet temperatures will be far away from this operating point towards the end of the prediction horizon resulting in significant prediction errors. It now appears that some form of nonlinear MPC must be considered.

Nonlinear MPC is a relatively new and growing field of research. The research seeks solutions to a number of problems surrounding the application of nonlinear MPC controller designs. One of these problems is the availability of appropriate nonlinear models for systems. Fortunately, this is not an issue here since a first principles approach was used to develop a nonlinear state space model. The other major problem with nonlinear MPC is the actual solution of the minimization of the cost function. Advanced nonlinear programming algorithms could be used for the minimization; however, the speed and accuracy of the solution is not guaranteed. In some cases, it is possible to transform the nonlinear model into a linear model using appropriate linearization, or transformation, techniques. Although this type of transformation may have been possible for this particular application, a simpler solution was sought.

The simplified nonlinear MPC design that is used involves a modification of the calculation of the predicted profile, $\hat{y}$. The predicted profile is calculated as the sum of a nonlinear, $\hat{y}_{nl}$, and linear, $\hat{y}_l$, components as:

$$\hat{y} = \hat{y}_{nl} + \hat{y}_l \tag{4.22}$$

The nonlinear response is the response of the full nonlinear state space model over the prediction horizon when the control input values, u, are kept constant and equal to the values from the previous sampling instant, $u(t-1)$. The linear response is the response of the linearized system to the sequence of future incremental control moves, $\Delta u(t+i)$ for $i=0$ to N_u-1, that are calculated by the control algorithm.

Using this convention, the problem can be recast into the standard quadratic programming form as shown in [11]:

$$J = \min_{\Delta u} \frac{1}{2} \Delta u^T H \Delta u + f^T \Delta u \qquad (4.23)$$

where: $H = G^T Q G + R$ is the Hessian

$f = -G^T Q(y_r - \hat{y})$ is the gradient

G is the step response matrix

The G step response matrix is also used in dynamic matrix control (DMC), a form of MPC and is formed for the multi-variable case as:

$$G = \begin{bmatrix} \boxed{\begin{array}{c} \text{ouput 1} \\ \text{input 1} \end{array}} & \cdots & \boxed{\begin{array}{c} \text{output 1} \\ \text{input m} \end{array}} \\ \vdots & \boxed{\begin{array}{c} \text{output i} \\ \text{input j} \end{array}} & \vdots \\ \boxed{\begin{array}{c} \text{output n} \\ \text{input 1} \end{array}} & \cdots & \boxed{\begin{array}{c} \text{output n} \\ \text{input m} \end{array}} \end{bmatrix} \qquad (4.24)$$

Where each block in (4.24) contains the step response data in the format shown in (4.25) below. The notation $y_{i,j}$ represents the response for the ith output to a step at the jth input. The capability of this design with, $\hat{y} = \hat{y}_{nl} + \hat{y}_l$, is not perfect, but it is much better than that for the purely linear MPC design.

$$G = \begin{bmatrix} y_{i,j}(t+1) & 0 & 0 \\ y_{i,j}(t+2) & y_{i,j}(t+1) & 0 \\ \vdots & y_{i,j}(t+2) & \cdots & \vdots \\ \vdots & \vdots & & \\ y_{i,j}(t+N_p) & y_{i,j}(t+N_p-1) & y_{i,j}(t+N_p-(N_u-1)) \end{bmatrix} \qquad (4.25)$$

Problems can arise, however, due to the fact that this simplified design uses the principle of superposition, which does not hold for nonlinear systems. The prediction accuracy will deteriorate as the process strays further from the operating point used for linearization. This usually results in larger than required future control moves. One way to help remedy this problem is to make the following changes to the general design.

First, consider the control input variable to be the sum of a base control sequence, $u_b(t+i)$, and a sequence of incremental control moves, $u_i(t+i)$ which gives:

$$u(t+i) = u_b(t+i) + u_i(t+i) \qquad\qquad (4.26)$$

The predicted output, $\hat{y}_{nl}$, becomes the response of the nonlinear model for the base control sequence, $u_b(t+i)$. If, at each sampling instant, the calculated future incremental control moves are not close to zero, then the base control sequence is updated to become the sum of the previous base control sequence and the current control increments found by solving the minimization problem.

This modification was actually not implemented for this project because it was believed that it would not significantly improve the performance of the design since only a short control horizon was used. This modification may be implemented at a later date.

MPC Algorithm

The main MPC algorithm is outlined here for pedagogical purposes. The actual Matlab function that was used to implement the MPC controller is given in the Appendix.

Before Control Loop

1. Initialize Parameters

    1. build the G matrix from step response values
    2. generate the reference trajectory
    3. initialize the predicted profile
    4. initialize all remaining controller variables

Main Control Loop

2. Sample Process

    1. record the process measurements
    2. perform measurement conditioning if necessary

3. Adjust Prediction Horizon

    1. perform any adjustments according to the measured error between the predicted process values and the measured process values

4. Calculate Optimal Control Moves

    1. first calculate the predicted error
    2. solve the minimization problem to find the control moves

5. Send Control Moves

    1. constrain control moves if necessary
    2. send control moves to the process

6. Generate Predicted Profile

    1. calculate the new predicted profile as a result of the new control moves

7. Update Variables

    1. advance the predicted horizon by one sampling time increment
    2. update the control move variables

8. Delay For One Sampling Instant

End of Control Loop

MPC Robustness

One of the problems with MPC is that it is generally not very robust. Performance will deteriorate in the presence of modeling errors and external disturbances acting on the system. Two modifications were made in order to improve the robustness of the nonlinear MPC design. Both of these modifications occur within step 3 in the MPC algorithm presented above.

The first modification is a polynomial filtering approach and involves the following basic steps as suggested in [11]:

1. The error between the measured output, $y_m(t)$, and the predicted output, $\hat{y}(t)$, is structured as a polynomial of the form:

$$error(t) = e_0 + e_1 t + e_2 t^2 + ... + e_M t^M \qquad (4.27)$$

where M is the order of the polynomial and a controller design parameter.

2. The coefficients of the polynomial in (4.27) are found using a least squares approach with measured error data over a past finite horizon. The length of this horizon is another tuning parameter.

3. The future predicted errors over the prediction horizon are found using the estimated coefficients.

4. The predicted profile is then adjusted by adding the predicted errors from step 3 as a correction term.

The authors in [11] state that this approach has been successfully applied in industrial applications to remove the steady state offset resulting from model mismatch. I had great difficulties, however, tuning the parameters of the polynomial filter. The order of the polynomial was eventually chosen to be zero. In effect, the entire prediction profile is shifted either up or down depending on past error values. The length of the time horizon over which past error data was collected was chosen to be equal to the prediction horizon.

The second modification for robustness improvement was the addition of an integration term in the algorithm. The integration term was not added to the error signal, $y_r - \hat{y}$. It was instead added to another error signal, the difference between the value of the desired setpoint, y_r, and the measured process output, y_m. This error is integrated over time and added to a fictitious reference trajectory that is used for calculating the predicted error profile. In effect, the fictitious reference trajectory is continuously shifted until the actual measured output matches the true reference trajectory. The integration is implemented in the discrete time MPC controller by adding the following lines of code:

$$
\begin{aligned}
error\_sum &= error\_sum + [y_r(t+0) - y_m] \times ki \\
y_r(t+i) &= y_r(t+i) + error\_sum \quad \text{for } i = 0 \text{ to } N_p
\end{aligned}
\tag{4.28}
$$

where ki is the integration constant and a tuning parameter. This technique works quite well for "step-like" reference trajectories and even ramp reference signals even though

linear systems theory states that a system type of 2 (i.e. double integration) is required for zero steady state error to ramp signals. An attempt was made to use double integration in the design, but the tuning of the two integration constants proved to be very difficult.

MPC Tuning

It is worthwhile to discuss how some of the tuning parameters affect the performance of the MPC controller. Aside from the tuning difficulties mentioned for the polynomial error fitting and integration, the MPC tuning process is generally quite intuitive and not all that difficult. The most important tuning parameters are the lengths of the prediction and control horizons (N_p and N_u respectively) and the weights on the individual predicted errors and control moves terms in the cost function (Q_i's and R_i's respectively). As a general rule, the length of the prediction horizon should be long enough such that the step response of the system reaches 99 percent of its steady state value. Shorter prediction horizons can also be used if desired, but one must remember that this will diminish the predictive capabilities of the controller. The length of the control horizon can be set as desired. A longer control horizon results in more aggressive control action as well as a more computationally demanding design. The Simplified MPC (SMPC) controller (i.e. $N_u = 1$) is quite often an effective controller design.

The choice of the weights used in the cost functions are much more arbitrary. The MPC design developed in this project used constant R values to place an equal weight on all actuators. The values for the Q terms were generally constant although, at times, heavier weights were used for earlier or later portions of the predicted error profile.

4.3.3 Simulation Results

The MPC controller design was evaluated by considering the same simulation conditions and performance criteria that were used with the H_∞ design. Figure 4.16 shows the results of the long-cycle simulation. It is clear from the results that the MPC design fairs much better than the H_∞ design when applied to the long-cycle setpoint. The initial dynamic tracking behavior during the rising portion of the setpoint is quite good.

The steady state behavior is also quite good, but this was expected since the nonlinear model used for the simulation and the prediction of $\hat{y}_{nl}$ are the same, and only very small disturbances were introduced into the simulation. The most promising aspect of the response is the fact that there is very little overshoot. Overshoot could be avoided even when the initial heater band settings were quite high, which was not the case for the H_∞ design.
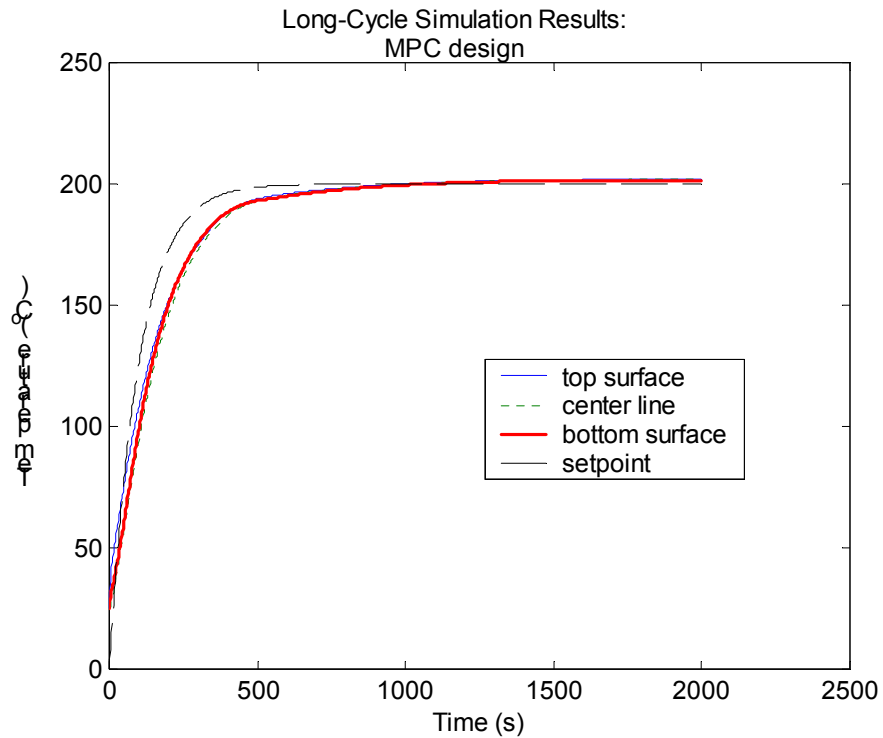
Figure 4.16: *long-cycle MPC simulation results: sheet surface temperatures*

The short-cycle results are shown in figures 4.17a and 4.17b. As can be seen from figure 4.17a the MPC controller performed better for this simulation as well. The more aggressive control action that is required for the shorter cycle time was achieved by reducing the prediction horizon, increasing the control horizon, and by placing a greater emphasis on the earlier portion of the predicted error profile.
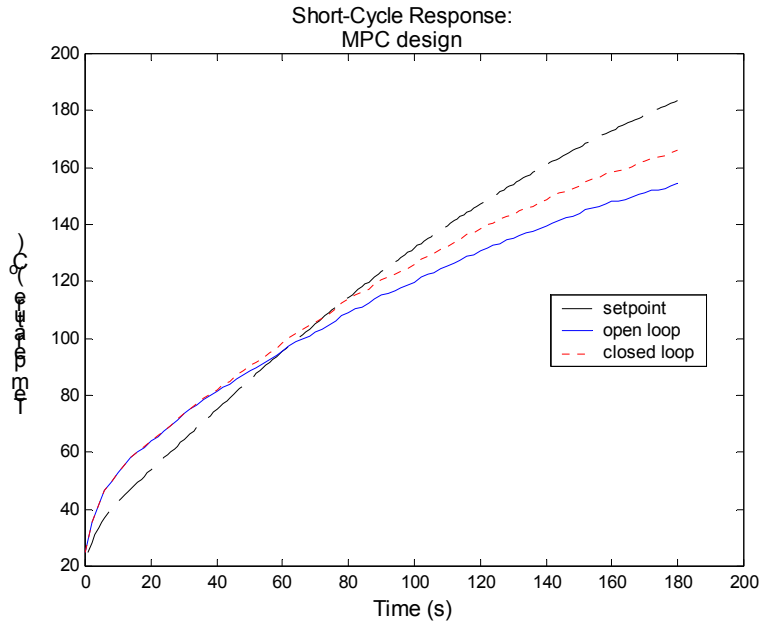
Figure 4.17a: *short-cycle MPC simulation results: sheet surface temperatures*
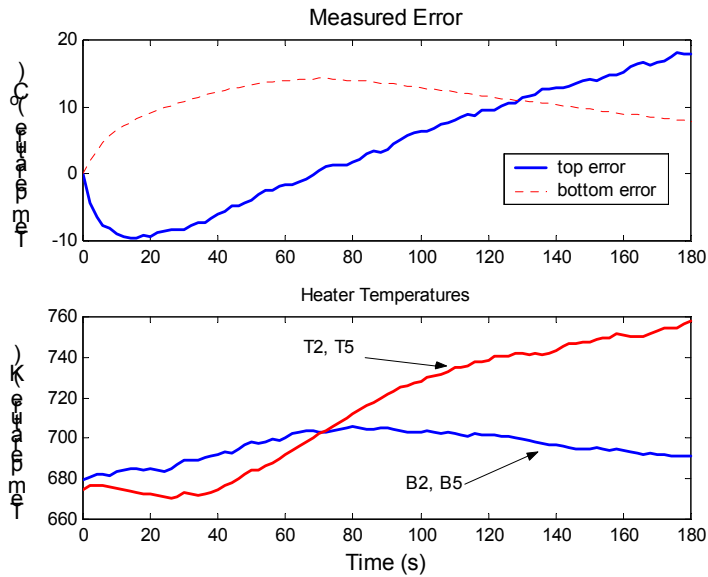
Figure 4.17b: *short-cycle MPC simulation results: error and control moves*

Figure 4.17b shows the error signal and the heater temperatures for the short cycle simulation. It is clear from the figure that the controller is more or less sending equal control moves to each of the two heaters for both the upper and lower heater banks. This is due to the symmetry of the oven-sheet zone configuration. It is important to point out that the behavior of the heaters will be quite different if the minimization of the control

moves is not included in the cost function. Initially, only the predicted error terms were included in the cost function. The simulation results appeared quite good; however, there was a problem with heater temperature divergence, meaning that one (out of two) heater zones in both the upper and lower heater banks would tend to saturate while the other zone would cool to an appropriate level. For example, heater zone T2 (B2) would saturate and zone T5 (B5) would cool down. Although this results in a good simulated response, this type of behavior would be unacceptable in practice since the result would be severe uneven temperature distribution across the sheet. The conclusion was that the control moves must be included in the cost function.

A full order MPC controller was also designed and tested with the long-cycle setpoint. The results are shown below in figure 4.18. The predictive behavior of the controller is evident here. The initial tracking during the slow, rising section of the curve is quite poor. This is because the controller is compensating for future predicted errors. The behavior during the steady state portion of the setpoint curve is also interesting. The response of sheet zones 1 to 4 is very good with no overshoot, and good tracking. Also, the symmetry of the sheet zone configuration is emphasized here as all four of the zones
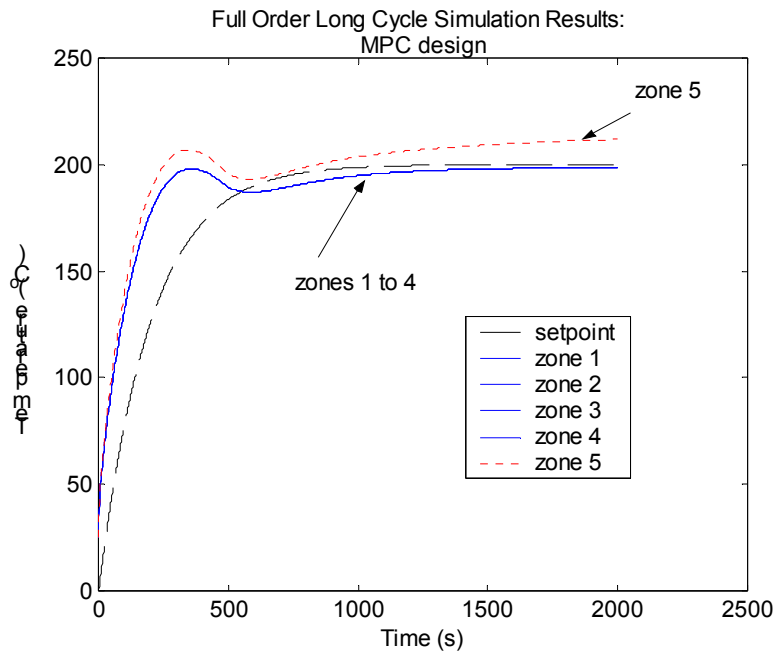

Figure 4.18: *long-cycle MPC simulation results for full order controller*

have identical responses. The response of sheet zone 5, the middle of the sheet, is not quite so good. The temperature for zone 5 rises above the steady state setpoint of 200 ^{o}C, and it does not appear that the temperature will begin to fall back down towards the setpoint.

4.4 Comparison Between Designs

Each of the control designs that were tested have their own distinct advantages and disadvantages. Based entirely upon the simulation results, the MPC design appears to be the clear winner. Neither design can claim victory, however, without first being tested on a real machine. Nevertheless, it is still worthwhile to discuss the possible effectiveness of each design here.

The H_∞ design has the advantages of ease of implementation, and being a less computationally demanding controller. The H_∞ design procedure also allows for the treatment of robust performance and stability analysis. One of the main disadvantages is the overall complexity of the design procedure. Proper controller maintenance and tuning will require personnel with knowledge of advanced control concepts, which could be considered a disadvantage for some. The overshoot issue surrounding the H_∞ controller design is a result of the fact that it is a frequency domain design. This presents a challenging problem since the desired performance characteristics for thermoforming are specified in the time domain. A solution to the overshoot problem may be some form of anti-overshoot protection as mentioned in [12] or possibly some form of "setpoint tuning". It was demonstrated that less aggressive control action gives acceptable overshoot performance; however, there is still room for improvement. Loop shaping techniques and/or gain scheduling could significantly improve performance. Integration could also be incorporated into the design to improve tracking and steady state performance.

The MPC design has the advantage of being a simpler design. It is easier to understand conceptually, and as such, it also offers the advantage of being easier to tune and maintain. It is, however, a much more computationally demanding design, and

stability and real-time performance is difficult to assess. The most significant advantage of the design is the fact that the performance specifications are given in the time domain. This allows for aggressive control action without significant overshoot. The other significant advantage of the MPC design is that it is easily re-configurable for the implementation of a fault tolerant design. The steady state performance of the MPC controller was not as good as hoped. Some simulations resulted in slow oscillations about the steady state setpoint with a magnitude of about +/- 5 ^{o}C. In practice, one could live with this type of behavior given the level of uncertainty of the process including the IR sensor measurements. In principle, however, this type of oscillatory behavior is not desirable. The nonlinear model is believed to be the culprit of these oscillations. One possible solution would be to implement a switching design that would involve switching to a purely linear design once the system outputs closely approach the steady state value of the reference trajectory. The linear MPC design should offer much smoother steady state behavior.

There is still an issue common to both designs that has yet to be discussed. The full order, long-cycle simulations for both designs suggest that there is an effective controllability problem. Even though the linear model is completely controllable, all of the nonlinear simulations resulted in obvious steady state offsets toward the end of the cycle times. Temperatures for sheet zones 1 to 4 would more or less follow the same trajectory whereas sheet zone 5 (center of the sheet) would follow a noticeably different trajectory. A significant amount of time was spent trying to correct the problem. Unfortunately, the problem could not be resolved. More work may be required to address this issue depending on how the controller designs perform on an actual machine.

5. Summary and Conclusions

This thesis documents the early development of a control strategy for the thermoforming reheat process. The application of in-cycle control to sheet reheat was considered in detail. The work was carried out with the primary objective of improved material distribution via better pre-forming sheet temperature control in mind. In Section 1 the problem was defined and the possible benefits of closed loop control were identified. A number of works that are relevant to the sheet reheat problem were cited. Section 2 included a detailed description of the overall thermoforming process with specific attention being given to the processing parameters that directly affect the sheet reheat stage.

The process model that was used for in-cycle controller design was developed in Section 3. It was found that a purely black box modeling approach was not appropriate due to the difficulties in applying standard system identification techniques as well as the large number of required system identification experiments. A first principles sheet modeling approach along with a black box heater modeling approach proved to be more practical. The nonlinear state space equations were presented as well as a number of recommendations for model improvements, of which the most significant was better representation of dynamic material properties.

Section 4 presented the details of H_∞ and MPC in-cycle controller designs. Simulation results indicate that the slow cooling dynamics of the ceramic heating elements pose a major problem for the H_∞ design. Without any time domain predictive abilities, the H_∞ controller is susceptible to significant overshoot as a result of the nonlinear heater dynamics. The MPC simulation results are somewhat more promising in that the overshoot problem is not a factor in the MPC design; however, further study into real-time and stability issues is required. In conclusion, the performance of any in-cycle control design will be dependant upon the reheat cycle time. Shorter cycle time applications will have to rely more on adaptive cycle-to-cycle control and soft sensor prediction since in-cycle control performance will be limited. That being said, it is believed that in-cycle control has great potential for medium to long cycle thermoforming

applications. Hopefully, closed loop reheat control will eventually become mainstream within the thermoforming industry.

Unfortunately, due to length restrictions, not all discussions could be included in this thesis. Full detailed discussions of this work will be available in a future CIM report, [26]. The CIM report will document the results of experimental testing of the controller designs. It will also contain discussions on future recommendations and the integration of this work with other thermoforming research work currently underway at McGill and IMI.

Acknowledgements

Bibliography

[1]   James L. Throne. "Technology of Thermoforming", Hanser Publishers, 1996

[2]   Adolf Illig. "Thermoforming: A Practical Guide", Hanser Publishers, 2001

[3]   John Florian. "Practical Thermoforming, Principles and Applications, Second Edition", Marcel Dekker Inc., 1996

[4]   J.P. Holman. "Heat Transfer, 8th Edition", McGraw-Hill, 1997

[5]   Robert Siegel, John R. Howell. "Thermal Radiation Heat Transfer, 3rd Edition", Hemisphere Publishing, 1992

 [6]   D.G. Baird, D.I. Collais. "Polymer Processing Principles and Design", Butterworth-Heinemann, 1995

[7]   K. Zhou, J.C. Doyle. "Essentials of Robust Control", Prentice Hall, 1998

[8]   Benoit Boulet. "Robust Industrial Control, Course Notes Part 1: Model Predictive Control", Coronado Systems, 2000

[9]   Benoit Boulet. "Robust Industrial Control, Course Notes Part 2: Robust and Optimal Control", Coronado Systems, 2000

[10]   Gary J. Balas, John C. Doyle, Keith Glover, Andy Packard, Roy Smith. "Matlab User's Guide: μ-Analysis and Synthesis Toolbox, Version 3", The Math Works, 1998

[11]   Murali Gopinathan, Raman K. Mehra, Joseph C. Runkle. "Hot Isostatic Pressing Furnaces, Their Modeling and Predictive Fault-Tolerant Control", in IEEE Control Systems Magazine, pp. 67-82, December 2000

[12]   Charles Schaper, Mehrdad Moslehi, Krishna Saraswat, Thomas Kailath. "Control of MMST RTP: Repeatability, Uniformity, and Integration for Flexible Manufacturing", in IEEE Transactions on Semiconductor Manufacturing, Vol 7, No. 2, May 1994

[13]   Poogyeon Park, Charles Schaper, Thomas Kailath. "Control Strategy for Temperature Tracking in Rapid Thermal Processing of Semiconductor Wafers", in Proceedings of the 31st Conference on Decision and Control, pp. 2568-2572, December 1992

[14] Young Man Cho, Thomas Kailath. "Model Identification in Rapid Thermal Processing Systems", in IEEE Transactions on Semiconductor Manufacturing, Vol 6, No. 3, August 1993

[15]   A. Yousefi, A. Bendada, R. DiRaddo. "Improved Modeling for the Reheat Phase in Thermoforming Through an Uncertainty Treatment of the Key Parameters", in SPE ANTEC, May 2001

[16]   W. Michaeli, J. van Marwick. "Automation of the Thermoforming Process by a Wall Thickness Closed-Loop Control", in SPE ANTEC, 1996

[17]   Rickey Dubay, Yash P. Gupta, Adam C. Bell. "Predictive Control of Plastic Melt in Heated Zones With Insulation", in Journal of Injection Molding Technology, Vol. 2, No. 1, pp. 37-45, March 1998

[18] Suman Banerjee, J. Vernon Cole, Klavs F. Jensen. " Nonlinear Model Reduction Strategies for Rapid Thermal Processing Systems", in IEEE Transactions on Semiconductor Manufacturing, Vol. 11, No. 2, May 1998

[19] Jalil Kamali, Robert L. Kosut. "Time-Varying Optimal Controller for Rapid Thermal Processing (RTP) Reactors", in Proceedings of the 36th Conference on Decision and Control, pp. 2541-2542, December 1997

[20] Robin DeKeyser, James Donald III. "Model Based Predictive Control n RTP Semiconductor Manufacturing", in Proceedings of the 1999 IEEE International Conference on Control Applications, pp. 1636-1641, August 1999

[21] Arvind Srinivasan, Celal Batur, Robert Veillette, Bruce N. Rosenthal, Walter M.B. Duval. "Projective Control Design for Muli-Zone Crystal Growth Furnace", in IEEE Transactions on Control Systems Technology, Vol. 2, No. 2, June 1994

[22] Mukul Agarwal. " A Systematic Classification of Neural-Network-Based Control", in The 3rd IEEE Conference on Control Applications, August 1994

[23] Sang Kyung Lee, Jong Hae Kim, Oh Do Chang, Hong Bae Park. "Robust Controller Design for RTP using Structured Uncertainty Approach", in SICE, July 1999

[24] Tarek Alaeddine, Haris Doumanidis. " Distributed Parameter Thermal Controllability – the Inverse Heat Conduction Problem in Materials Processing, in ACC, 2002

[25] R. W. DiRaddo, A. Garcia-Rejon. "In-cycle Deterministic and Stochastic Dynamics of Extrusion Blow Molding", in Intern. Polymer Processing VII, pp. 257-266, 1992

[26] CIM report No. CIM-TR02-01

Appendix

```
%%%%%%%%%%%%%%%%%%%%%%%%%%%%%%%%%%%%%%%%%%%%%%%%%%%%%%%%%%%%%%%%%%%%%%%%%%%%
% C:\Bens Folder\McGill\thesis\matlab\h infinity\h_inf_build_model_unstruc.m
% Author: Ben Moore
% Date: November 13, 2001    last revision:  February 23, 2002
%
% This script is used to build the interconnections for the H-infinity control
% design. Unstructured uncertainty is used here.  Note that this code is used with
% a 4 input, 2 output plant model.  Changes can easily be made to incorporate a
% full order system.
%
%%%%%%%%%%%%%%%%%%%%%%%%%%%%%%%%%%%%%%%%%%%%%%%%%%%%%%%%%%%%%%%%%%%%%%%%%%%%

% initialize the nominal model parameters
clear all;
simulation_parameters_h_inf;
global N        %total number of nodes used in simulation
global delta_h  %delta_h is the distance between nodes (m)
global l        %length of square section (m)
global p        %density (kg/m^3)
global k        %thermal conductivity (W/m.K)
global Cp       %specific heat (J/kg.K)
global E_heater %emissivity of the heater (unitless dimension)
global E_sheet  %emissivity of the sheet (unitless dimension)
global sigma    %Stefan_Boltzman constant (W/m^2K^4)
global h_u      %convective heat transfer coefficient for upper side of the
                %sheet (W/m^2.K)
global h_l      %convective heat transfer coefficient for lower side of the sheet
                %(W/m^2.K)
global F_view   %the view vactors used to calculate the radiation heat transfer

%delta_h = (3.17e-3 - 0.000457e-3*t)/N;  %time varying thickness if necessary
V = l^2*delta_h;

% build nominal model
for i = 1:4
   u_star(i) = 350;    %initialize heater temperatures in degrees Celcius
end
x_star = 100*ones(1,N);                %make the operating point at 100 degrees
P = h_inf_lin_model(u_star,x_star);   %obtain the linearized model

% build the multiplicative uncertainty weighting function
%load mult_uncrt_sys; %mult_uncrt_sys was found using the h_inf_mult_uncrt script
%Wp = daug(mult_uncrt_sys,mult_uncrt_sys);   %create the diagonal matrix Wp
tmp = tf(0.5,conv([200 1],[200 1])); %the uncertainty at low frequencies
[a,b,c,d]=ssdata(tmp);         %create state space model from transfer function
tmp = pck(a,b,c,d);            %convert to mu toolbox model format
Wp = daug(tmp,tmp);            %create the diagonal matrix Wp

% build the heater model

% the time delay
t_lag = 5;                         %the lag time of the heater response in seconds
num_d,den_d] = pade(t_lag,1);        %approximate the time delay with a 1st order
                        %Pade approximation
%the first order embedded dynamics
tc = 25;                           %the time constant of the embedded response
num_e = 1;
den_e = [tc 1];

%the second order surface dynamics found using matlabs system identification %toolbox
k = 1/1.023;
num_s = k*[0 0.123355 0.000302];   den_s = [1 0.085266  0.000295];

%obtain the linearized gain of the surface offset
k_upper = (u_star(1) + 31.51 + 0.0662*u_star(1))/u_star(1);
k_lower = (u_star(3) + 35.51 + 0.0452*u_star(3))/u_star(3);

%build the overall transfer matrix
num_heater = conv(num_s,conv(num_d,num_e));
den_heater = conv(den_s,conv(den_d,den_e));
tmp1 = tf(k_upper*num_heater,den_heater);
```

```
tmp2 = tf(k_lower*num_heater,den_heater);

%convert to mu toolbox model format and create overall heater model
[a,b,c,d]=ssdata(tmp1);  tmp1=pck(a,b,c,d);
[a,b,c,d]=ssdata(tmp2);  tmp2=pck(a,b,c,d);
H = daug(tmp1,tmp1,tmp2,tmp2);

%consider a 2% uncertainty in the heater surface temperature
tmp = 0.02;
Wh = diag([tmp tmp tmp tmp]);        %create the diagonal matrix Wh

% build the oven air temperature distrubance matrix F
F = diag([l^2*h_u/(p*V*Cp/2) l^2*h_l/(p*V*Cp/2)]);

% specifiy the necessary weights
tmp = tf(20,conv([40 1],[40 1]));     %the error weight
[a,b,c,d]=ssdata(tmp);   tmp = pck(a,b,c,d);
We = daug(tmp,tmp);                   %create the diagonal matrix We

tmp = tf(0.08*[50000 1],[1 10]);      %the control weight ----> good performance
[a,b,c,d]=ssdata(tmp);   tmp = pck(a,b,c,d);
Wu = daug(tmp,tmp,tmp,tmp);           %create the diagonal matrix Wu

tmp = 0.000001;                       %the sensor noise weight
Wn = diag([tmp tmp]);                 %create the diagonal matrix Wn

pert_h_u = 15;        %the expected variation in upper heat transfer coefficient
pert_h_l = 2;         %the expected variation in lower heat transfer coefficient
tmp1 = pert_h_u/h_u;  %the upper air temperature uncertainty
tmp2 = pert_h_l/h_l;  %the lower air temperature uncertainty

Wf = diag([tmp1 tmp2]);       %create the diagonal matrix Wf

% specify Wref
wn = 0.001;  zeta = 0.707;  num = wn^2;  den = [1 2*zeta*wn wn^2];
tmp = tf(num,den);  [a,b,c,d]=ssdata(tmp);  tmp = pck(a,b,c,d);
Wref = daug(tmp,tmp);         %create the diagonal matrix Wref

% specify Wy
num = 1;  den = [500 1];  tmp = tf(num,den);
[a,b,c,d]=ssdata(tmp);  tmp = pck(a,b,c,d);
Wy = daug(tmp,tmp);           %create the diagonal matrix Wy

% make the system interconnections
%regular design without model mathcing
%systemnames = 'We Wu H Wh P F Wn Wf Wp Wy';
%inputvar = '[wp{2};wh{4};wf{2};wn{2};yd{2};t_air{2};u{4}]';
%outputvar = '[Wp;Wh;Wf;We;Wu;Wy - P - wp - F - wf - Wn]';

%design with model matching
systemnames = 'We Wu H Wh P F Wn Wf Wp Wy Wref';
inputvar = '[wp{2};wh{4};wf(2);wn{2};yd{2};t_air{2};u{4}]';
outputvar = '[Wp;Wh;Wf;We;Wu;Wref - P - wp - F - wf - Wn]';
input_to_Wref = '[yd]';
input_to_Wy = '[yd]';
input_to_Wp = '[P]';
input_to_Wu = '[u]';
input_to_H = '[u]';
input_to_Wh = '[H]';
input_to_P = '[H + wh]';
input_to_F = '[t_air]';
input_to_Wf = '[F]';
input_to_Wn ='[wn]';
%input_to_We = '[Wy - P - wp - F - wf - Wn]';        %regular design
input_to_We = '[Wref - P - wp - F - wf - Wn]';       %design with model matching
sysoutname = 'P';
cleanupsysic = 'yes';
sysic;


% get a minimal balanced realization of P
```

```
[P,sig]=sysbal(P,1e-10);

% must check stabilizability of (AP,BP2) and(AP,BP1)
% PBH test: [[-AP +sI] must not loose rank at closed RHP eigenvalues of AP
% extract partitioned state-space matrices
[AP,BP,CP,DP]=unpck(P);
BP1 = BP(:,1:14);
BP2 = BP(:,15:18);
CP1 = CP(1:14,:);
CP2 = CP(15:16,:);
DP11 = DP(1:14,1:14);
DP12 = DP(1:14,15:18);
DP21 = DP(15:16,1:14);
DP22 = DP(15:16,15:18);


rhpeigs = [];  [v,eigs] = eig(AP);  eigs = diag(eigs);

for i = 1:length(AP)
   if real(eigs(i)) >= 0
      rhpeigs = [rhpeigs; eigs(i)];            %extract the RPH eigenvalues
   end
end
p = length(rhpeigs);
if p > 0 %check for stabilizability and detectability if there are RHP eigenvalues
   r = length(AP);
      rkb1=[];        %ranks at RHP eigenvalues
      rkb2=[];        %ranks at RHP eigenvalues
      for j = 1:p
         rkb1=[rkb1; rank([(rhpeigs(j)*eye(length(AP))) - AP BP1])];
         rkb2=[rkb2; rank([(rhpeigs(j)*eye(length(AP))) - AP BP2])];
      end
      if min(rkb1) < length(AP)
         fprintf('PROBLEM: (AP,BP1) IS NOT STABILIZABLE')
         stop
      end
      if min(rkb2) < length(AP)
         fprintf('PROBLEM: (AP,BP2) IS NOT STABILIZABLE')
         stop
       end

      %must check detectability of (CP2,AP) and (CP1,AP)
      %PHB test: [(sI - AP)' CP2']' must not lose rank at closed RHP eigenvalues
      %of AP
      rkc1=[];        %ranks at RHP eigenvalues
      rkc2=[];        %ranks at RHP eigenvalues
      for j = 1:p
         rkc1=[rkc1; rank([(rhpeigs(j)*eye(length(AP))) - AP; CP1])];
         rkc2=[rkc2; rank([(rhpeigs(j)*eye(length(AP))) - AP; CP2])];
      end
      if min(rkc1) < length(AP)
         fprintf('PROBLEM: (CP1,AP) IS NOT DETECTABLE')
         break
      end
      if min(rkc2) < length(AP)
         fprintf('PROBLEM: (CP2,AP) IS NOT DETECTABLE')
      break
   end
  end

% A check must be made to see if the generalized plant is well possed.
% This is done by checking to see if the matrices [AP - jwI BP2; CP1 DP12] and
% [AP - jwI BP1; CP2 DP21] must have full column and row rank respectively for all % w.

ww =logspace(-4,3,200);        %set the grid of frequency test points
for i = 1:200
   rk = rank([sqrt(-1)*ww(i)*eye(length(AP))-AP BP2; CP1 DP12]);
   if rk < (length(AP)+length(BP2(1,:)))
      fprintf('PROBLEM: MATRIX [AP -jw BP2; CP1 DP12] IS RANK DEFICIENT AT FREQ =
%g',ww(i));
      break
```

120

```
      end
end

for i = 1:200
    rk = rank([sqrt(-1)*ww(i)*eye(length(AP))-AP BP1; CP2 DP21]);
    if rk < (length(AP)+length(CP2(:,1)))
        fprintf('PROBLEM: MATRIX [AP -jw BP1; CP2 DP21] IS RANK DEFICIENT AT FREQ =
%g',ww(i));
        break
    end
end


% compute the H-infinity solution to the control problem
nmeas = 2;                      %the number of measurements
ncon = 4;                       %the number of control inputs
tol = 1e-3;                     %specifiy the tolerance
[K,Tzw,norms,X,Y,hamx,hamy] = hinfsyn(P,nmeas,ncon,1,1e3,tol);

% perform a d-k iteration
DK_DEF_NAME = 'h_inf_dkdef_unstruc';
dkit
[a,b,c,d]=unpck(k_dk1);
controller = ss(a,b,c,d);
%save controller# controller




function [sys,x0,str,ts] = mpc_controller_nl(t,x,u,flag,heat_flag)

%%%%%%%%%%%%%%%%%%%%%%%%%%%%%%%%%%%%%%%%%%%%%%%%%%%%%%%%%%%%%%%%%%%%%%%%%%%%%%%%
C:\Bens Folder\McGill\thesis\matlab\mpc\mpc_controller_nl.m
% Author: Ben Moore
% Date: November 29, 2001    last revision:  February 5, 2002
%
% This Sfunction implements the nonlinear MPC control algorithm.
% Note that this control algorithm is designed for a 4 input, two output system.
% (i.e. heater zones T2 T5 B2 B5, and sheet zone 5)
%
% INPUTS:   t = time
%           x = states
%           u(1:6) = upper heater zone temperatures in degrees Kelvin
%           u(7:12) = lower heater zone temperatures in degrees Kelvin
%           u(13:17) = upper oven air temperatures in degrees Kelvin
%           u(18:22) = lower oven air temperatures in degrees Kelvin
%           flag = variable used by the solver
%           heat_flag(1:12) = used to indicate whether a particular heater zone is
%                             considered in the simulation.  Set to 0 if heater
%                             zone is unused, otherwise set to 1. heat_flag(1:6)
%                             corresponds to the upper heater zones 1 to 6
%                             respectively and heat_flag(7:12)correspond to the
%                             lower heater zones 1 to 6 respectively.
%
%%%%%%%%%%%%%%%%%%%%%%%%%%%%%%%%%%%%%%%%%%%%%%%%%%%%%%%%%%%%%%%%%%%%%%%%%%%%%%%%

switch flag,

  case 0,
    [sys,x0,str,ts]=mdlInitializeSizes;  %initialize
  case 1,                                     %do nothing
  case 2,                                     %do nothing
  case 3,                                     %do nothing
    sys=mdlOutputs(t,x,u,flag,heat_flag);     %calculate the control moves
  case 4,                                     %do nothing
  case 9,
    sys=mdlTerminate(t,x,u);  % put necessary clean up procedures here
```

```matlab
   otherwise
      error(['Unhandled flag = ',num2str(flag)]); %unexpected flags
end


%===============================================================================
% mdlInitializeSizes
% Return the sizes, initial conditions, and sample times for the S-function.
%===============================================================================

function [sys,x0,str,ts]=mdlInitializeSizes

sizes = simsizes;

sizes.NumContStates  = 0;
sizes.NumDiscStates  = 0;
sizes.NumOutputs     = 4;
sizes.NumInputs      = 27;  % 12 heater, 10 oven air, and 5 state variables
sizes.DirFeedthrough = 1;
sizes.NumSampleTimes = 1;   % at least one sample time is needed

sys = simsizes(sizes);
x0  = [];       %initialize the initial conditions
str = [];       %str is always an empty matrix
ts  = [0 0];   %initialize the array of sample times


%===============================================================================
% mdlOutputs
% Calculate the control moves using the MPC algorithm
%===============================================================================

function sys=mdlOutputs(t,x,u,flag,heat_flag)

% first initialize all the proper variables

global y_hat;          %y_hat is the predicted profile of the outputs
global x_hat_nl;       %x_hat_nl is the predicted profile of all state variables
global count;          %count is the iteration number
global setpoint        %setpoint is the desired trajectory data that is loaded in
                       %"mpc_simulation_parameters.m"
global error;          %error is the measured error (i.e. ym - y_hat)
global error_sum1;     %error_sum1 is a running sum that is used to implement
                       %integration
global error_sum2;     %error_sum2 is a running sum that is used to implement
                       %double integration
global N;              %N is the number of layers in the sheet
global heater_out_old; %heater_out_old is the heater setpoint temperatures from
                       %the previous iteration
global heater_out      %heater_out is the current heater setpoints
global time_data       %time_data is a vector holding time data over a finite
                       %horizon (used with error)

tmp_count = 1;
for i = 1:12
   if heat_flag(i) ~= 0
      u_star(tmp_count) = u(i);            %extract the heater operating points,
      tmp_count = tmp_count + 1;           %used for mpc_lin_model
   end
end

x_star = u(23:23+N-1); %extract the sheet operating point (NOTE: this would be
                       %found using the soft sensor in a real application)
input = u(1:22);       %extract the inputs, used for mpc_sim
Ts = 2;                %set the sampling period for the control algorithm
Np = 80;               %set the prediction horizon
Nu = 1;                %set the control horizon
n = 2;                 %the number of ououts
m = 4;                 %the number of inputs
ysp = [1 1];           %the desired final sheet surface temperatures in degrees C
```

```
len = Np;                %len is the length of the error prediction horizon
M = 0;                   %M is the order of the polynomial fit for the error data
Ki1 = 1e-4;              %this is the first integration constant
Ki2 = 5e-2;              %this is the second integration constant

if t == 0                %% initialization of necessary control algorithm variables

    error = zeros(n*Np,1);      %initialize the measured error (i.e. ym - y_hat)
    time_data = zeros(len,1);   %initialize the time data
    error_sum1 = zeros(2,1);    %initialize the integration running error
    error_sum2 = error_sum1;    %initialize the integration running error
    heater_out_old = u_star - 273;    %intialize the heater setpoints

    %initialize the heater_out variable (this one gets sent as the heater
    %setpoints)
    for i = 1:2
        %remove the embedded to surface offset for upper heaters
        heater_out(i) = (heater_out_old(i) - 31.5)/(1 + 0.0662);
    end
    for i = 3:4
        %remove the embedded to surface offset for lower heaters
        heater_out(i) = (heater_out_old(i) - 35.5)/(1 + 0.0425);
    end

    %initialize the predicted profile for all state variables
    %Note that the predicted profile starts at time t = 0 seconds.
    %x_star  = Tamb*ones(N,1) at t = 0
    x_hat_nl = mpc_sim_nl(x_star,input,Ts,Np,heat_flag);
    y_hat = [x_hat_nl(:,1); x_hat_nl(:,N)];

else if t >= Ts*count  %%%%  enter this portion of the code every sampling instant

    %  build the G step response matrix
    lsys = mpc_lin_model(u_star,x_star);    %linearize about the operating point
    dsys = samhld(lsys,Ts);                 %discretize the plant
    [A,B,C,D]=unpck(dsys);                   %unpack the system matricies
    T_step = Ts*Np;                          %set the step time
    tmp = ss2step(A,B,C,D,T_step,Ts,[],n);  %obtain the step response data

    %build the G matrix from the tmp data that is in step model format
     G = zeros(n*Np,m*Nu);
     for j = 1:m
        for k = 1:Nu
            for r = 1:n
               G(k+(r-1)*Np:r*Np,k+(j-1)*Nu) = tmp(r:n:(n*(Np-k+1)-(n-r)),j);
            end
        end
     end

     % sample the process

    count = count + 1;                 %upadate the iteration counter
    ym = [x_star(1)  x_star(N)];       %sample the process

    % Adjust the prediction horizon according to the measured error.  In this
    % control algorithm a polynomial filter approach is used to adjust the
    % prediction horizon according to error data over a past finite horizon. (i.e.
    % y_meas(t) - y_hat(t) = error(t) = e_0 + e_1*t + e_2*t^2 + .... + e_N*t^N).
    % At each sampling instant, the predicted error is evaluated using the
    % estimated coefficients for the polynomial and added as a correction term to
    % the predicted profile.  The design parameters are the order of the polynomial
    % fit and the length of the horizon in which the error polynomial coefficients
    % are estimated. NOTE: This approach did not work as well as planned so a
    % slightly different approach was used.  At each sampling instant the initial
    % states for the prediction simulation were obtained from the actual
    % measurement values. In a real application the initial states would be found
    % via the soft sensor.  In effect the predicted  y_hat values get shifted up or
    % down at each sampling instant according to the measured error.  This scheme
    % works well with linear MPC control, and it also seems to work quite well
    % with this particular nonlinear MPC algorithm.
```

```
%update the error prediction vector
if count > len
    for i = 1:len-1
        error(i) = error(i+1);
    end
    for i = len+1:n*len-1
        error(i) = error(i+1);
    end
    for i = 1:len-1
        time_data(i) = time_data(i+1);
    end
    error(len) = ym(1) - y_hat(1);
    error(2*len) = ym(2) - y_hat(Np+2);
    time_data(len) = Ts*count;
else
    error(count) = ym(1) - y_hat(1);
    error(count + len) = ym(2) - y_hat(Np+2);
    time_data(count) = Ts*count;
end

%now fit the error
%obtain the coefficients for the upper sheet surface
coef11 = polyfit(time_data,error(1:len),M);
%obtain the coefficients for the lower sheet surface
coef22 = polyfit(time_data,error(len+1:2*len),M);

%now generate the predicted error over the new prediction horizon
time_data_fit = Ts*(count+1):Ts:Ts*(count+n*Np);
error_fit1 = polyval(coef11,time_data_fit);
error_fit2 = polyval(coef22,time_data_fit);

%Now add the predicted error to the predicted profile.  As mentioned above this
%approach did not work.
for i = 2:Np+1
    y_hat(i) = y_hat(i) + error_fit1(i-1);
    y_hat(i+Np+1) = y_hat(i+Np+1) + error_fit2(i-1);
end

% generate the setpoint trajectory

for i = 1:Np+1
    y(i) = ysp(1)*setpoint(Ts*(count+i-1),2);
    y(i+Np+1) = ysp(2)*setpoint(Ts*(count+i-1),2);
end

%Integration can be implemented by adjusting a virtual setpoint trajectory that
%is used in the calculation of the optimal control moves.  The idea is that an
%integration term is added to this virtual setpoint trajectory until the process
%tracks the actual setpoint trajectory.

error_sum1(1) = error_sum1(1) + ((ym(1) - 273) - y(1))*Ki1;
error_sum1(2) = error_sum1(2) + ((ym(2) - 273) - y(Np+2))*Ki1;

%Note that double integration was finally not used since it was very difficult
%to find the right combination of integration constants that gave a smooth
%response.  In theory double integration should be used to track ramp inputs.
%Zero steady state error for ramp inputs requires a system type number of 2.
%This is not easy to implement here though.

error_sum2(1) = error_sum2(1) + error_sum1(1)*Ki2;
error_sum2(2) = error_sum2(2) + error_sum1(2)*Ki2;

for i = 1:Np+1
    y(i) = y(i) - error_sum1(1);    %for double integration add error_sum2
    y(i+Np+1) = y(i) - error_sum1(2);
end

%  calculate the optimal control moves

%generate the predicted error
pred_error = zeros(2*Np,1);
```

```
for i = 1:Np
    pred_error(i) = y(i+1) - (y_hat(i+1) - 273);
end
for i = Np+1:n*Np
    pred_error(i) = y(i+2) - (y_hat(i+2) - 273);
end

%Q is a diagonal matrix containing the weights on the individual error terms
Q = 1e-4*eye(length(G(:,1)));
 for i = 1:Np
    Q(i,i) = 1e-4*i^4;      %put a heavier weight on the later time steps
    Q(i + Np,i + Np) = Q(i,i);
 end

R = 1e-4*eye(m*Nu);          %also put a weight on each individual heater zone

H = G'*Q*G + R;              %H is the hessian
f = -G'*Q*pred_error;        %f is the gradient
A = [eye(m*Nu); -eye(m*Nu)];%A is used in the quadprog call
delta_u_max = 1*Ts*ones(m*Nu,1);   %constrain the positive control moves
delta_u_min = 0.35*Ts*ones(m*Nu,1);%constrain the negative control moves
b = [delta_u_max; delta_u_min];    %b is used in the quadprog call
delta_u = quadprog(H,f,A,b);       %solve the quadratic programming problem
y_lin = G*delta_u;                 %calculate the response of the linear plant

%update the heater outputs by adding the control moves
dummy = delta_u(1:Nu:m*Nu);
for i = 1:m
    heater_out(i) = heater_out_old(i) + dummy(i);
    if heater_out(i) > 550
        heater_out(i) = 550; %constrain the heater temperatures if necessary
    end
end
heater_out_old = heater_out;       %update the heater_out_old variable

%the heater surface temperature offset must be removed first
for i = 1:2
    heater_out(i) = (heater_out_old(i) - 31.5)/(1 + 0.0662);
end
for i = 3:4
    heater_out(i) = (heater_out_old(i) - 35.5)/(1 + 0.0425);
 end

% generate the predicted profile
 Xo = x_star;                %the initial states for the current prediction are
                             %the states that are predicted by the soft sensor
 input(2) = heater_out_old(1)+273; %Changed on Feb. 3  Before the
                                   %heater_out_old variable was obtained from
                                   %measured heater temperatures. Without
 input(5) = heater_out_old(2)+273; %change there was significant ocsil
                                   % about the setpoint at steady state.
 input(2+6) = heater_out_old(3)+273;   input(5+6) = heater_out_old(4)+273;

 x_hat_nl = mpc_sim_nl(Xo,input,Ts,Np,heat_flag); %simulate non linear response
 y_hat = [x_hat_nl(:,1); x_hat_nl(:,N)];          %extract surface temperatures

%add the linear response
 for i = 2:(Np+1)
    y_hat(i) = y_hat(i) + y_lin(i-1);
    x_hat_nl(i,1) = y_hat(i);
 end
 for i = (Np+3):(n*Np+n)
    y_hat(i) = y_hat(i) + y_lin(i-2);
    x_hat_nl(i,N) = y_hat(i);
 end

% adjust the prediction horizon by one sampling instant
y_hat(Np+1) = y_hat(Np);
 for i = 1:(Np)
     y_hat(i) = y_hat(i+1);
 end
```

```
      y_hat(n*Np+n) = y_hat(n*Np+n-1);
      for i = (Np+2):(n*Np+n-1)
          y_hat(i) = y_hat(i+1);
      end

      else

    %%%%%%%%%%%%%%%%%        delay for one sampling period    %%%%%%%%%%%%%%%%%

      end

end

sys = heater_out;                  %send the control moves to the plant




%===============================================================================
% mdlTerminate
% Perform any end of simulation tasks.
%===============================================================================
%
function sys=mdlTerminate(t,x,u)

global count; count = 0;                        %reset the count variable
sys = [];
```
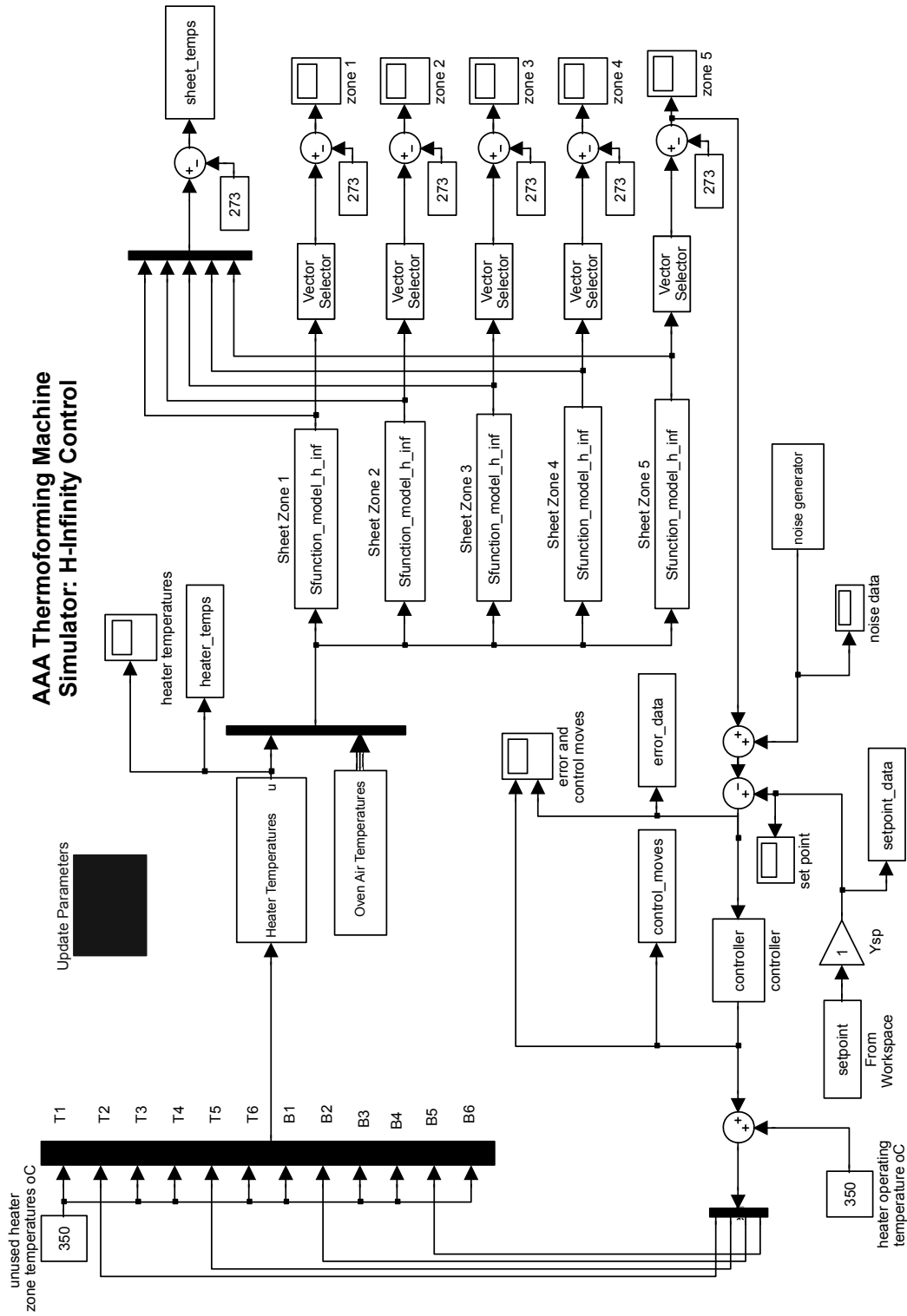
Figure A.1: *H-Infinity controller Simulink simulation model*
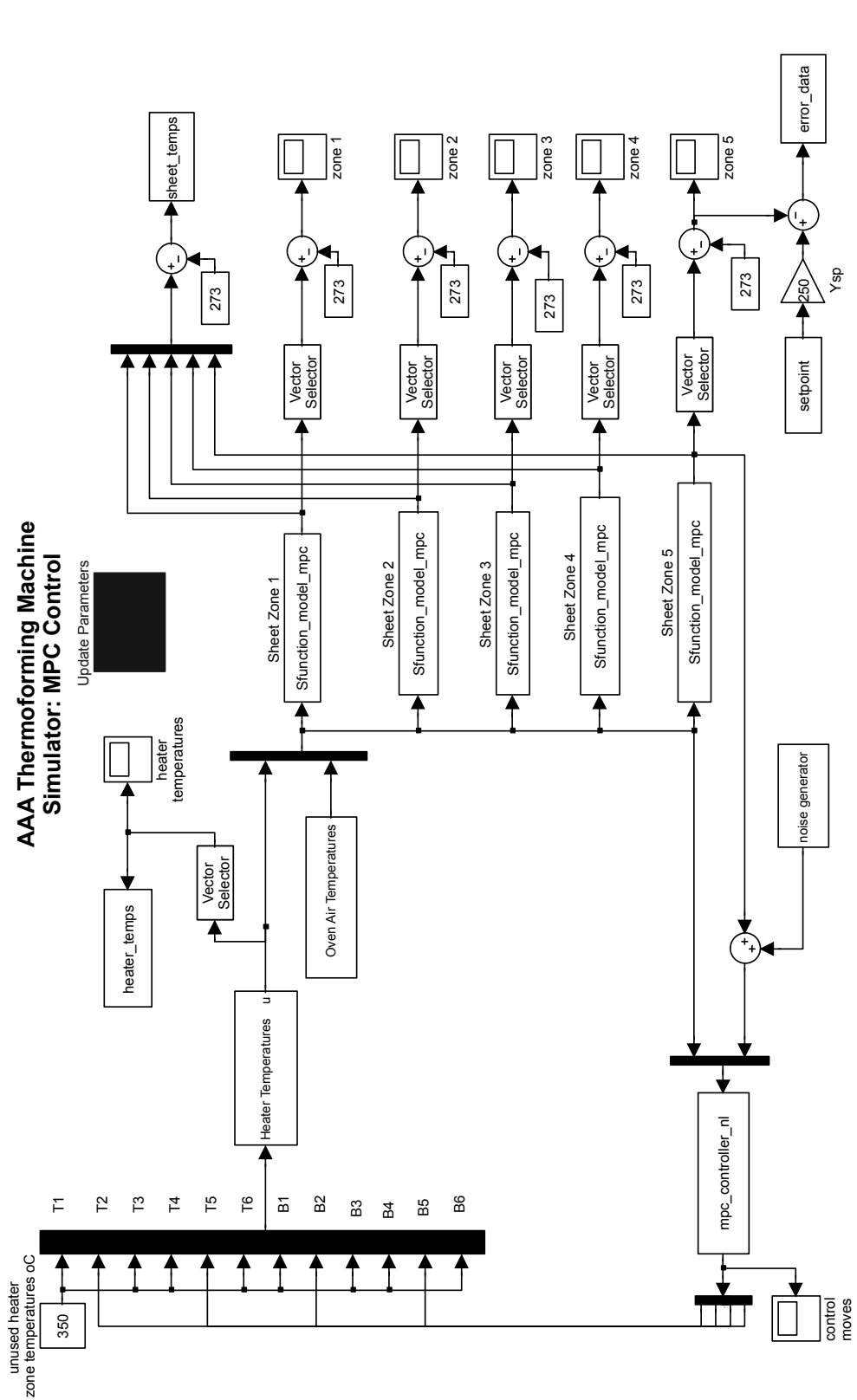
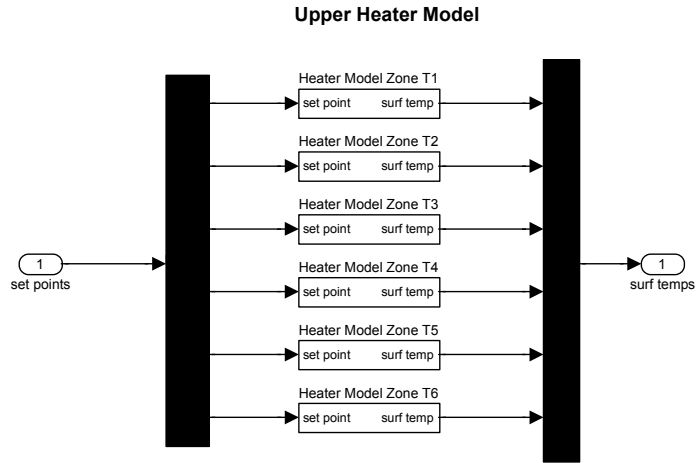*Figure A.2:* MPC controller Simulink simulation model
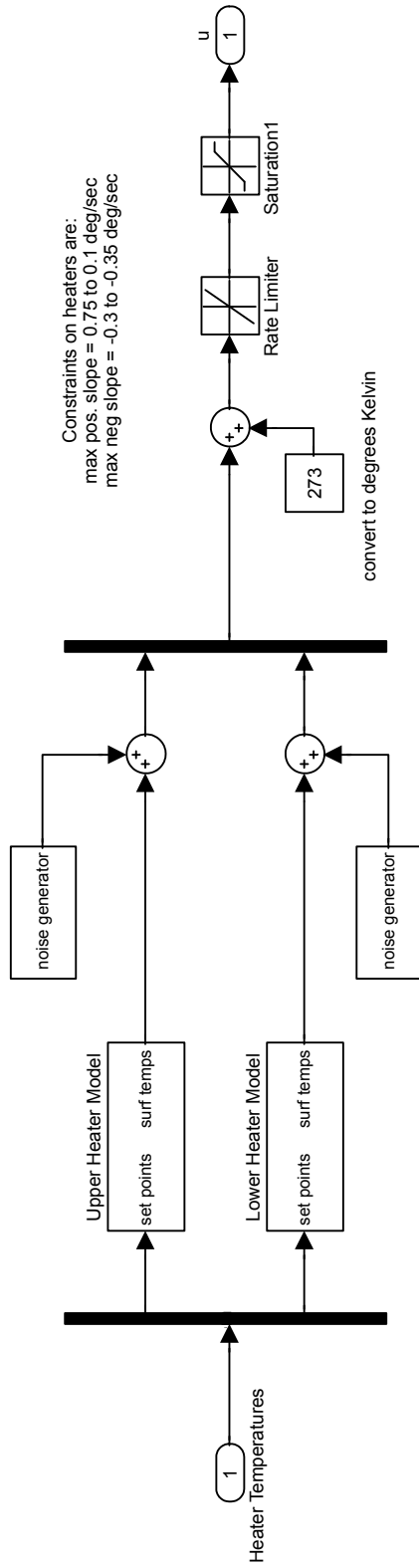
Figure A.3: *Heater Temperatures block from main Simulink controller simulation models*

Upper Heater Model

Figure A.4: Upper Heater Model block in Simulink Diagram
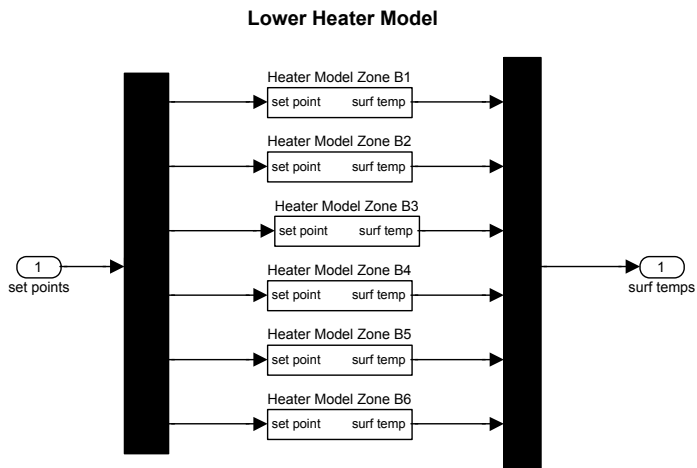
Lower Heater Model

Figure A.5: Lower Heater Model block in Simulink Diagram
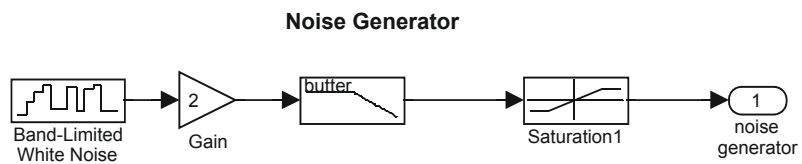
Noise Generator

Figure A.6: Noise Generator block

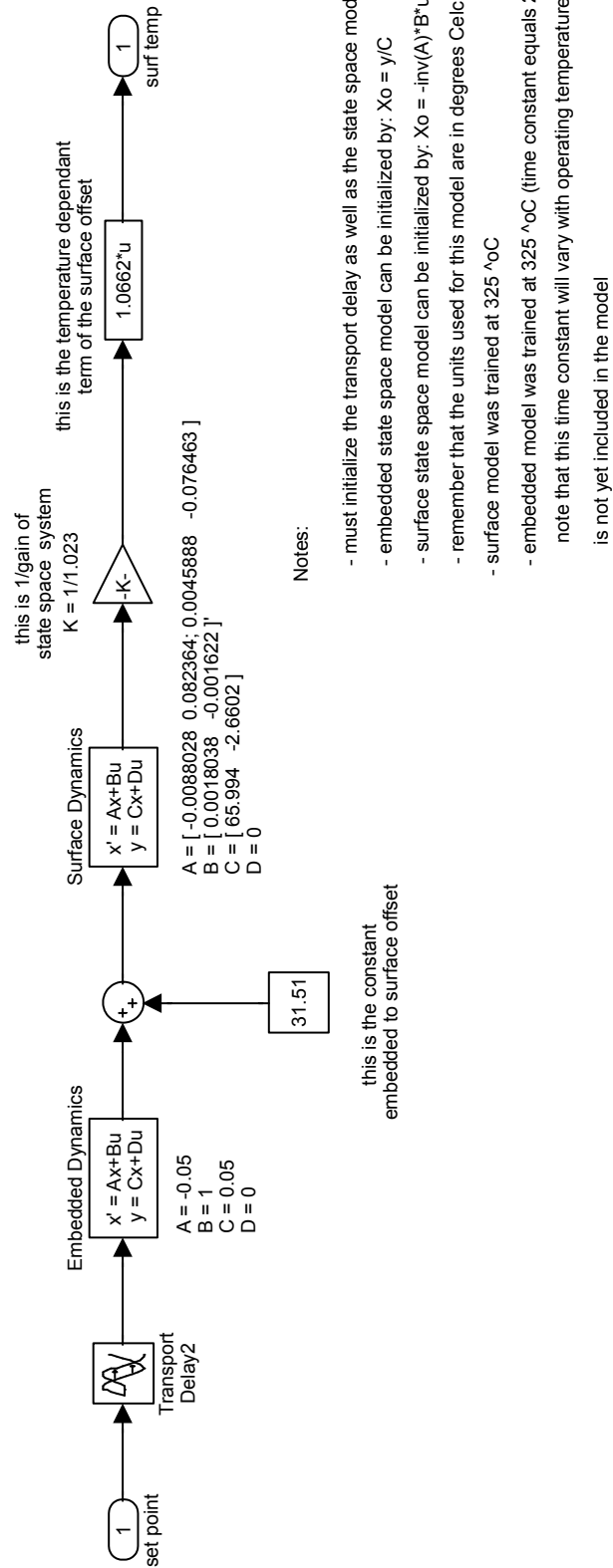**Simulation model of a single heater zone T1**

Figure A.7: *Simulink model for a single heater zone*
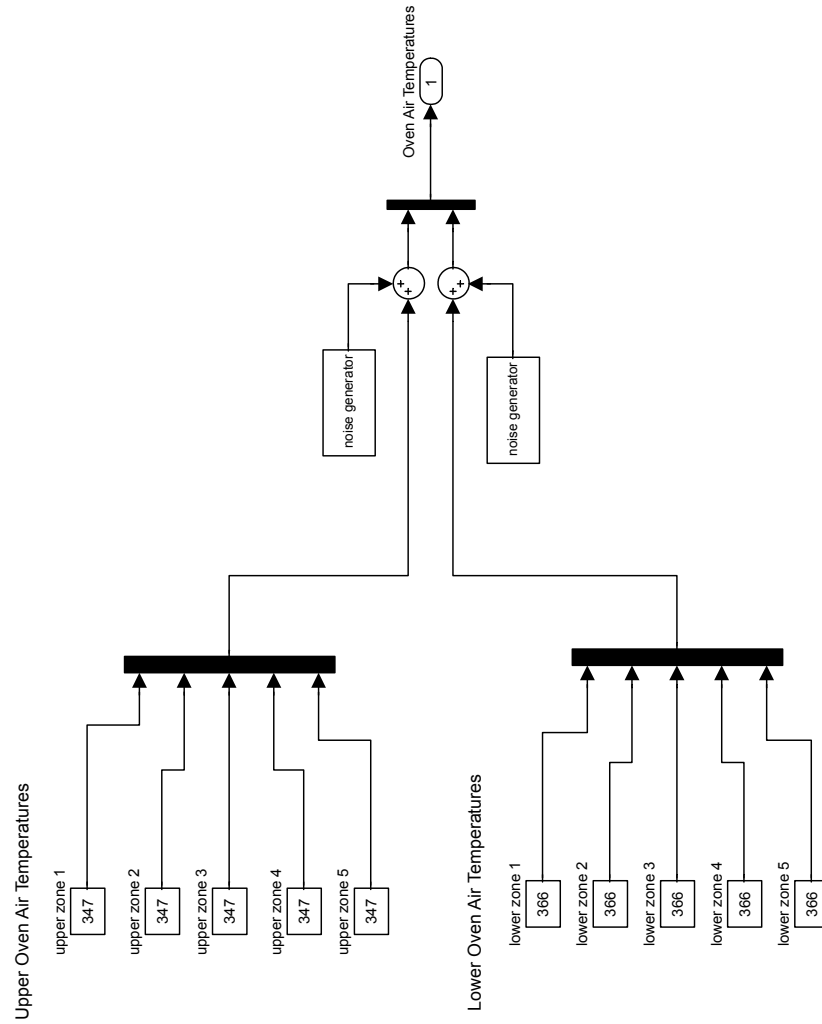
Oven Air Temperatures

Figure A.8: Oven Air Temperatures block from main Simulink controller simulation models

Linearized State Space Equations

for all sheet zones:

$$\dot{\theta}^{(zn\times 1)} = A^{(zn\times n)}\theta^{(zn\times 1)} + B^{(zn\times m)}u^{(m\times 1)} + F^{(zn\times 2z)}d^{(2z\times 1)}$$

$$y^{(2z\times 1)} = C^{(2z\times nz)}\theta^{(zn\times 1)}$$

where: θ represents the sheet temperatures
u represents the heater temperatures
d represents the oven air temperatures
n is the number of states (i.e. the number of layers)
m is the number of inputs (i.e. the number of inputs)
z is the number of sheet zones

$$
A = \begin{bmatrix}
A_1 & 0 & \cdots & & 0 \\
0 & \ddots & & & \\
\vdots & & A_i & & \vdots \\
& & & \ddots & 0 \\
0 & & \cdots & 0 & A_z
\end{bmatrix}
\quad
B = \begin{bmatrix}
B_1 \\
\vdots \\
B_i \\
\vdots \\
B_z
\end{bmatrix}
\quad
C = \begin{bmatrix}
C_1 & 0 & \cdots & & 0 \\
0 & \ddots & & & \\
\vdots & & C_i & & \vdots \\
& & & \ddots & 0 \\
0 & & \cdots & 0 & C_z
\end{bmatrix}
\quad
F = \begin{bmatrix}
F_1 & 0 & \cdots & & 0 \\
0 & \ddots & & & \\
\vdots & & F_i & & \vdots \\
& & & \ddots & 0 \\
0 & & \cdots & 0 & F_z
\end{bmatrix}
$$

for a single sheet zone:

$$\dot{\theta}^{(n\times 1)} = A^{(n\times n)}\theta^{(n\times 1)} + B^{(n\times m)}u^{(m\times 1)} + F^{(n\times 2)}d^{(2\times 1)}$$

$$y^{(2\times 1)} = C^{(2\times n)}\theta^{(n\times 1)}$$

where: θ represents the sheet temperatures
u represents the heater temperatures
d represents the oven air temperatures
n is the number of states (i.e. the number of layers)
m is the number of inputs (i.e. the number of inputs)

$$
A = \begin{bmatrix}
\dfrac{df_1}{d\theta_1} & \dfrac{df_1}{d\theta_2} & 0\cdots & & & 0 \\
& \ddots & & & & \\
0\cdots & \dfrac{df_i}{d\theta_{i-1}} & \dfrac{df_i}{d\theta_i} & \dfrac{df_i}{d\theta_{i+1}} & \cdots 0 \\
& & & \ddots & & \\
0\cdots & & & 0 & \dfrac{df_N}{d\theta_{N-1}} & \dfrac{df_N}{d\theta_N}
\end{bmatrix}
$$

$$
B = \begin{bmatrix}
\dfrac{df_1}{d\theta_{H_1}} & \cdots & \dfrac{df_1}{d\theta_{Hi}} & \cdots & \dfrac{df_1}{d\theta_{H_N}} \\
0 & \cdots & 0 & \cdots & 0 \\
\vdots & \ddots & \vdots & \ddots & \vdots \\
0 & \cdots & 0 & \cdots & 0 \\
\dfrac{df_N}{d\theta_{H_1}} & \cdots & \dfrac{df_N}{d\theta_{Hi}} & \cdots & \dfrac{df_N}{d\theta_{H_N}}
\end{bmatrix}
$$

$$
C = \begin{bmatrix}
1 & 0 & \cdots & 0 \\
0 & \cdots & 0 & 1
\end{bmatrix}
\qquad
F = \begin{bmatrix}
\dfrac{df_1}{d\theta_{\infty_u}} & 0 \\
0 & \vdots \\
\vdots & 0 \\
0 & \dfrac{df_N}{d\theta_{\infty_l}}
\end{bmatrix}
$$

133

Exterior Nodes:

$$f_1 := \frac{d\theta_1}{dt} = \frac{1}{\rho V C_p}\left[Q_{rad} + Q_{conv} - \frac{kA}{\Delta h}(\theta_1 - \theta_2)\right]$$

$$Q_{rad} = A\sigma\mathcal{E}_{eff}\left(r_1 + r_2\theta_1\right)\sum_{i=1}^{6}\left(\theta_{H_i}^4 - \theta_1^4\right)F_i$$

$$Q_{conv} = Ah\left(\theta_\infty - \theta_1\right)$$

where:

$$\frac{df_1}{d\theta_1} = \frac{1}{\rho V C_p}\left(\frac{dQ_{rad}}{d\theta_1} + \frac{dQ_{conv}}{d\theta_1} + \frac{d}{d\theta_1}\left[-\frac{kA}{\Delta h}(\theta_1 - \theta_2)\right]\right)$$

$$= \frac{1}{\rho V C_p}\left(A\sigma\mathcal{E}_{eff}\left[r_1\theta_1^3\sum_{i=1}^{6}F_i - 5r_2\theta_1^4\sum_{i=1}^{6}F_i + r_2\sum_{i=1}^{6}\theta_{H_i}^4 F_i\right] - Ah - \frac{kA}{\Delta h}\right)$$

$$\frac{df_1}{d\theta_2} = \frac{1}{\rho V C_p}\left(\frac{kA}{\Delta h}\right)$$

$$\frac{df_1}{d\theta_i} = 0 \quad \text{for } i = 3 \text{ to N-1}$$

$$\frac{df_1}{d\theta_{H_i}} = \frac{1}{\rho V C_p}4A\sigma\mathcal{E}_{eff}\left(r_1 + r_2\theta_1\right)F_i\theta_{H_i}^3$$

$$\frac{df_1}{d\theta_\infty} = \frac{Ah}{\rho V C_p}$$

Interior Nodes:

$$f_i := \frac{d\theta_i}{dt} = \frac{1}{\rho V C_p}\left[\frac{kA}{\Delta h}\theta_{i-1} - \frac{2kA}{\Delta h}\theta_i + \frac{kA}{\Delta h}\theta_{i+1}\right]$$

$$\frac{df_i}{d\theta_{i-1}} = \frac{1}{\rho V C_p}\frac{kA}{\Delta h}$$

$$\frac{df_i}{d\theta_i} = -\frac{1}{\rho V C_p}\frac{2kA}{\Delta h}$$

$$\frac{df_i}{d\theta_{i+1}} = \frac{1}{\rho V C_p}\frac{kA}{\Delta h}$$

for i = 2 to N-1